

QUANTIFYING THE WATER-ATMOSPHERE FLUX OF AMMONIA FOR THE
ESTUARIES OF THE TEXAS COASTAL BEND

A Thesis

by

WARREN DUNEGAN

BS, Indiana University of Pennsylvania, 2004

Submitted in Partial Fulfillment of the Requirements for the Degree of

MASTER OF SCIENCE

in

ENVIRONMENTAL SCIENCE

Texas A&M University-Corpus Christi
Corpus Christi, Texas

May 2020

© Warren Lee Dunegan

All Rights Reserved

May 2020

QUANTIFYING THE WATER-ATMOSPHERE FLUX OF AMMONIA FOR THE
ESTUARIES OF THE TEXAS COASTAL BEND

A Thesis

by

WARREN DUNEGAN

This thesis meets the standards for scope and quality of
Texas A&M University-Corpus Christi and is hereby approved.

J. David Felix, PhD
Chair

Hussain A.N. Abdulla, PhD
Committee Member

Xinping Hu, PhD
Committee Member

May 2020

ABSTRACT

In the United States urbanization and agricultural activities within coastal watersheds have greatly contributed to excessive nutrient loading in downstream waters. As a result, a gross majority of U.S. estuaries are now considered to be ecologically impaired. Nitrogen (N) is often a limiting nutrient to primary production in estuarine waters and as such, excessive contributions have been linked to eutrophication, hypoxic events, and the emergence of harmful algal blooms (HABs). Such indicators of nutrient pollution have occurred in the surface waters of the Texas Coastal Bend, a coastal region of southeastern Texas, USA that borders the northwest Gulf of Mexico. Within that region, hypoxic episodes in areas of Corpus Christi Bay and persistent HABs in Baffin Bay have both been observed. Ammonium (NH_4^+) is an inorganic N species that in great enough concentrations, can directly influence such conditions as it is immediately bioavailable to primary producers. Total ammonia (NH_x) refers to the combined concentration of both NH_4^+ and its complementary gaseous compound, ammonia (NH_3). In water, NH_x is partitioned between NH_4^+ and NH_3 by the chemical and physical conditions which are present there. Further, when such aqueous concentrations of NH_3 are great enough and favorable water quality and meteorological conditions exist, NH_3 may be emitted from surface waters into the lower atmosphere. This water-atmosphere exchange process is bidirectional, allowing for both NH_3 emission to the atmosphere, and atmospheric NH_3 invasion into surface waters. Due to the two-way nature of this process, the determination of net NH_3 deposition in coastal regions must factor local surface water NH_3 emissions as well as ambient air NH_3 concentrations to produce accurate estimates. Quantifying water-atmosphere NH_3 flux was the primary objective of this study, where ten sites throughout the Coastal Bend were observed regularly during regional and local campaigns of eight and twelve months, respectively. Surface water NH_4^+ concentrations,

atmospheric NH₃ concentrations and a collection of supporting surface water and meteorological parameters were obtained to determine resulting rates of water-atmosphere NH₃ flux. Across the entire Coastal Bend, a NH₃ flux of $2.52 \pm 3.57 \text{ ng m}^{-2} \text{ s}^{-1}$ was calculated, denoting net NH₃ emission during the period of September 2018 - April 2019. Specific to the Corpus Christi area, a similarly upward water-atmosphere NH₃ flux of $2.54 \pm 1.23 \text{ ng m}^{-2} \text{ s}^{-1}$ was determined for the period of May 2018 - April 2019. Seasonal trends in water-atmosphere NH₃ flux were evident as generally the late summer and fall months featured NH₃ emission events from surface waters while winter and early spring months saw the deposition of atmospheric NH₃. Individual locations displayed characteristic water-atmosphere NH₃ flux signatures, including a site at San Antonio Bay where it is believed that a host of conditions unique to that estuary resulted in NH₃ emission in two months during which all nearby bays displayed deposition. Within the Corpus Christi area, the NH₃ fluxes of Corpus Christi Bay, the Upper Laguna Madre and the nearshore Gulf of Mexico appear to have been influenced by a collection of factors including the wet deposition of NH₄⁺, surface water inflow and transport, and the transfer of NH₄⁺ enriched sediment pore water into the overlying water column. Additionally, water-atmosphere NH₃ emission events from the Gulf of Mexico periodically coincided with deposition at the Upper Laguna Madre, indicating a potentially important transport pathway for NH₃ between coastal marine waters and a neighboring coastal lagoon. Bulk water-atmosphere NH₃ estimates derived from the Corpus Christi area fluxes revealed an annual magnitude of NH₃ emission that amounted to more than 30% of an earlier quantification of total N deposition to area surface waters. As a potentially substantial contributor to local ambient air NH₃ concentrations, the water-atmosphere flux of NH₃ requires comprehensive quantification across varying estuary

systems to help guide mitigation efforts if NH₃ emissions in the U.S. are ever subject to regulations similar to those set forth in European countries.

ACKNOWLEDGEMENTS

I would like to thank committee chair Dr. J. David Felix for conceiving this project and offering hours of guidance and support throughout. Committee members Dr. Hussain Abdulla and Dr. Xinping Hu are greatly appreciated for the time and service they have dedicated to this endeavor as well. Further thanks go to Dr. Jennifer Smith-Engle for all her efforts to secure me assistantships over the past two years, and to Dr. Blair Sterba-Boatwright for creating and sharing very helpful R scripts. Students of the Felix lab, both past and present, are also appreciated for their support throughout this project. This work would not have been possible without the contributions of everyone just mentioned.

TABLE OF CONTENTS

CONTENTS	PAGE
ABSTRACT	v
ACKNOWLEDGEMENTS	viii
TABLE OF CONTENTS	ix
LIST OF FIGURES	xii
LIST OF TABLES	xiv
1. Introduction	1
2. Methods	6
2.1. Study area	6
2.2. Meteorological measurements and condensate collection	9
2.3. Surface water measurements and sample collection	9
2.4. NH_4^+ concentration analysis	10
2.5. Determining atmospheric NH_3 from condensate	11
2.6. Determining water-atmosphere NH_3 flux	14
2.7. Statistical analyses	16
3.Results	16

3.1. NH ₃ flux parameters of all Coastal Bend sites	16
3.1.1. Surface water NH ₄ ⁺ concentrations	17
3.1.2. Atmospheric NH ₃ concentrations	19
3.1.3. Additional measurements for determining water-atmosphere NH ₃ flux	20
3.1.4. NH _{3(eq)} values	22
3.2. Water-atmosphere NH ₃ fluxes of all Coastal Bend sites	24
3.3. NH ₃ flux parameters of Corpus Christi area sites	27
3.4. Water-atmosphere NH ₃ fluxes of Corpus Christi area sites	31
4. Discussion	33
4.1. Temporal analysis of Coastal Bend water-atmosphere NH ₃ fluxes	33
4.1.1. Fall months (September 2018 - November 2018)	35
4.1.2. Winter months (December 2018 - February 2019)	42
4.1.3. Spring months (March 2019 - April 2019)	47
4.2. Spatial analysis of Coastal Bend water-atmosphere NH ₃ fluxes	52
4.2.1 Water-atmosphere NH ₃ flux characteristics of San Antonio Bay	54
4.2.2. Water-atmosphere NH ₃ flux characteristics of two Coastal Bend primary- secondary bay estuary systems	60
4.3. Temporal analysis of Corpus Christi area water-atmosphere NH ₃ fluxes	64
4.4. Spatial analysis of Corpus Christi area water-atmosphere NH ₃ fluxes	72

4.4.1. Atmospheric NH ₃ dynamics of Corpus Christi area	72
4.4.2. Surface water transport and NH ₄ ⁺ concentrations of Corpus Christi area ...	77
4.4.3. Surface water NH ₄ ⁺ responses to rain events in Corpus Christi area	80
4.5. Implications for Coastal Bend NH ₃ budget	85
5. Conclusions	88
REFERENCES	92
LIST OF APPENDICES	98
Appendix A	99
Appendix B	100
Appendix C	101

LIST OF FIGURES

FIGURES	PAGE
Figure 1. Map of all Coastal Bend study sites.	7
Figure 2. Boxplot of monthly $\text{NH}_{3(\text{eq})}$ values for all Coastal Bend sites, September 2018 - April 2019.	24
Figure 3. Map displaying site water-atmosphere NH_3 fluxes by specified ranges of mean values in $\text{ng m}^{-2} \text{s}^{-1}$, September 2018 - April 2019.	27
Figure 4. Boxplot of monthly water-atmosphere NH_3 fluxes of Corpus Christi area sites, May 2018 - April 2019.	32
Figure 5. Boxplot of seasonal water-atmosphere NH_3 flux values for all Coastal Bend sites, September 2018 - April 2019.	34
Figure 6. Boxplot of monthly water-atmosphere NH_3 flux values for all Coastal Bend sites, September 2018 - April 2019.	35
Figure 7. Map of Corpus Christi area sites with mean atmospheric NH_3 concentrations in $\mu\text{g}/\text{m}^3$ and standard deviations (in parentheses). Arrow represents the path of SSE wind through the region.	45
Figure 8. Boxplot of monthly water-atmosphere NH_3 flux values for all northern subregion sites, September 2018 - April 2019.	55
Figure 9. Map of San Antonio Bay displaying the mouth of the Guadalupe River and the SAB study site.	57

Figure 10. Map displaying the Lavaca-Colorado and Mission-Aransas estuaries, their respective bays and the study sites of the northern subregion. 61

Figure 11. Graph of weekly atmospheric NH₃ concentrations in µg/m³ at CCB, May 4 - July 27, 2018. 74

Figure 12. Map showing Oso Bay relative to Corpus Christi Bay and CCB site. 76

Figure 13. Photo of condensate collecting device with ice-filled test tubes and collection vials visible inside modified 5-gallon bucket. 98

LIST OF TABLES

TABLES	PAGE
Table 1. Previously reported water-atmosphere NH ₃ flux values.	3
Table 2. Coastal Bend study sites, location information and associated water bodies.	8
Table 3. Description of the parameters utilized in Farmer and Dawson's (1982) equation for determining atmospheric NH ₃ concentration from condensate.	12
Table 4. Constant values applied to Farmer and Dawson's (1982) equation for determining atmospheric NH ₃ concentration from condensate.	12
Table 5. Monthly mean water NH ₄ ⁺ concentrations and standard deviations (in parentheses) in μM for all Coastal Bend sites, September 2018 - April 2019.	18
Table 6. Monthly atmospheric NH ₃ concentrations in μg/m ³ with standard deviations (in parentheses, for mean values) from September 2018 - April 2019.	20
Table 7. Additional measurements for calculating water-atmosphere NH ₃ flux reported by monthly mean with standard deviations (in parentheses) for all Coastal Bend sites, September 2018 - April 2019.	21
Table 8. Additional measurements for calculating water-atmosphere NH ₃ flux reported by site mean with standard deviations (in parentheses) for all Coastal Bend sites, September 2018 - April 2019.	22
Table 9. Monthly mean NH _{3(eq)} values and standard deviations (in parentheses) in μg/m ³ for all Coastal Bend sites, September 2018 - April 2019.	23

Table 10. Monthly mean water-atmosphere NH₃ flux values and standard deviations (in parentheses) in ng m⁻² s⁻¹ for all Coastal Bend sites, September 2018 - April 2019. 25

Table 11. Monthly mean water NH₄⁺ concentrations and standard deviations (in parentheses) in μM for Corpus Christi area sites, May 2018 - April 2019. 28

Table 12. Monthly mean atmospheric NH₃ concentrations and standard deviations (in parentheses) in μg/m³ for Corpus Christi area sites, May 2018 - April 2019. 29

Table 13. Additional parameters for calculating water-atmosphere NH₃ flux reported by site mean with standard deviations (in parentheses) for Corpus Christi area sites, May 2018 - April 2019. 30

Table 14. Monthly mean NH_{3(eq)} values and standard deviations (in parentheses) in μg/m³ for Corpus Christi area sites, May 2018 - April 2019. 31

Table 15. Monthly mean water-atmosphere NH₃ flux values and standard deviations (in parentheses) in ng m⁻² s⁻¹ for Corpus Christi area sites, May 2018 - April 2019. 32

Table 16. Monthly and seasonal mean water-atmosphere NH₃ flux values, atmospheric NH₃ concentrations, NH_{3(eq)} values and surface water NH₄⁺ concentrations of all Coastal Bend sites, September 2018 - April 2019. Standard deviations are displayed (in parentheses). 34

Table 17. Site mean water-atmosphere NH₃ flux values, atmospheric NH₃ concentrations, NH_{3(eq)} values and surface water NH₄⁺ concentrations of all Coastal Bend sites, November 2018. Standard deviations are displayed (in parentheses). 40

Table 18. Site mean water-atmosphere NH₃ flux values, atmospheric NH₃ concentrations, NH_{3(eq)} values and surface water NH₄⁺ concentrations of all Coastal Bend sites, December 2018. Standard deviations are displayed (in parentheses). 43

Table 19. Site mean water-atmosphere NH₃ flux values and surface water NH₄⁺ concentrations of all Coastal Bend sites, March - April 2019. Standard deviations are displayed (in parentheses). 49

Table 20. Monthly mean water NH₄⁺ concentrations, NH_{3(eq)} values, atmospheric NH₃ concentrations and NH₃ water-atmosphere flux values of the northern and southern subregions of the Coastal Bend, September 2018 - April 2019. Standard deviations are displayed (in parentheses). 53

Table 21. Mean water NH₄⁺ concentrations, NH_{3(eq)} values, atmospheric NH₃ concentrations and NH₃ water-atmosphere flux values of the northern subregion sites, September 2018 - April 2019. Standard deviations are displayed (in parentheses). 55

Table 22. Mean water NH₄⁺ concentrations of the northern subregion sites, August 2018 - October 2018. Values in bottom row represent the mean monthly NH₄⁺ concentrations of MB, AB and CB only. Standard deviations are displayed (in parentheses). 58

Table 23. Measured DO % of saturation of the northern subregion sites, September 2018 - October 2018. 59

Table 24. Monthly mean NH₃ water-atmosphere flux values, water NH₄⁺ concentrations, pH values, salinity values, NH_{3(eq)} values and atmospheric NH₃ concentrations of individual sites within the Lavaca-Colorado and Mission-Aransas estuary systems. Standard deviations are displayed (in parentheses). 62

Table 25. Monthly and seasonal mean water-atmosphere NH₃ flux values, atmospheric NH₃ concentrations, NH_{3(eq)} values and surface water NH₄⁺ concentrations of Corpus Christi area sites, May 2018 - April 2019. Standard deviations are displayed (in parentheses). 65

Table 26. Individual monthly mean water-atmosphere NH₃ flux values, atmospheric NH₃ concentrations, NH_{3(eq)} values and surface water NH₄⁺ concentrations of Corpus Christi area sites, August 2018 - October 2018. Standard deviations are displayed (in parentheses). 67

Table 27. Individual monthly mean water-atmosphere NH₃ flux values, atmospheric NH₃ concentrations, NH_{3(eq)} values and surface water NH₄⁺ concentrations of Corpus Christi area sites for June and December 2018. Standard deviations are displayed (in parentheses). 68

Table 28. Individual monthly mean water-atmosphere NH₃ flux values, atmospheric NH₃ concentrations and surface water NH₄⁺ concentrations of CCB, May 25 - July 6, 2018. Standard deviations are displayed (in parentheses). 75

Table 29. Surface water NH₄⁺ concentrations of CCB and UL in μM, October 20, 2018. Standard deviations are displayed (in parentheses). 78

Table 30. Weekly mean surface water NH₄⁺ concentrations of Corpus Christi area sites in μM, May 4 - July 6, 2018. Standard deviations are displayed (in parentheses). 81

Table 31. Weekly salinity measurements of Corpus Christi area sites, May 25 - July 6, 2018. ... 83

Table 32. Weekly mean water-atmosphere NH₃ fluxes of GM and UL, June 22 - July 13, 2018. Standard deviations are displayed (in parentheses). 84

Table 33. Monthly calculated NH₃ flux totals in mT for Coastal Bend bays and estuaries, September 2018 - April 2019. 86

Table 34. Monthly calculated NH₃ flux totals in mT for Corpus Christi Bay and the Upper Laguna Madre, May 2018 - April 2019. 87

Table 35. Comparison of annual atmospheric inorganic N loads estimated by Meyers et al. (2000), with values adjusted by this study’s annual NH₃ emission estimates for Corpus Christi Bay and the Upper Laguna Madre. 88

Table 36. Previously reported watershed characteristics data of the Coastal Bend estuary systems. 99

Table 37. Previously reported meteorological and hydrological measurements of the Coastal Bend estuary systems. 100

Table 38. Previously reported surface water and watershed measurements of the Coastal Bend estuary systems. 100

1. Introduction

Worldwide, coastal ecosystems have endured significant increases in eutrophication, hypoxic events, harmful algal blooms, biodiversity loss and other environmental degradation due to excess nutrient loading (Howarth, 2008; Castro et al., 2003). In the United States, two thirds of coastal systems were considered moderately to severely impaired by 2012, with that percentage expected to increase (Davidson et al., 2012). Nitrogen (N), commonly the limiting nutrient to estuarine primary production, is now being delivered to these systems in concentrations far exceeding biological demand. Anthropogenic activities are responsible for nearly all the additional N, with agriculture and sewage treatment being the greatest contributing sources (Castro et al., 2003). Excessive N is then delivered to coastal systems by point source discharges and non-point mechanisms such as surface runoff, groundwater discharge and atmospheric deposition (Castro et al., 2003).

Nitrate (NO_3^-) and ammonium (NH_4^+) are important inorganic species to the N cycles of coastal ecosystems and are of great concern due to their potential to fuel excessive primary production. In such forms these N species are immediately bioavailable, requiring no chemical or biological transformation for assimilation into aquatic food webs. NO_3^- concentrations typically exceed NH_4^+ in estuarine waters by three times or more, due to the preferential uptake of NH_4^+ by phytoplankton and because of the oxidation of NH_4^+ to NO_3^- by nitrification (Gruber, 2008). As such, NH_4^+ pools are predominantly maintained by atmospheric deposition and by regeneration processes within the water column (Gruber, 2008). Several processes contribute to the in-situ production of NH_4^+ , including the photolysis of dissolved organic nitrogen (DON), flux from the underlying sediment, excretion of zooplankton and the remineralization of organic matter (OM), among others. (Mesfioui et al., 2015; Bange, 2008). The ammonia (NH_3) produced

by these processes partitions in water between NH_4^+ ions and aqueous NH_3 , with the resulting proportions of each being dependent largely on the chemical composition of the water (Johnson et al., 2008).

The species duality exists in the overlying atmosphere as well, where ammonia is present both as a gas (NH_3) and as ammonium (NH_4^+) aerosols. NH_3 is the primary alkaline gas in the atmosphere and as such, plays a part in numerous physical and chemical processes which influence air quality (Bange, 2008; Norman and Leck, 2005). NH_3 reacts with available acidic species and partially neutralizes them through the formation of new particles (Norman and Leck, 2005). Such particles may contribute to cloud formation by serving as cloud condensation nuclei (CCN) (Quinn et al., 1988). Chemical reactions between NH_3 and sulfuric (H_2SO_4) and nitric (HNO_3) acids produce $(\text{NH}_4)_2\text{SO}_4$ and NH_4NO_3 aerosols, respectively. The resulting particles measure less than $2.5 \mu\text{m}$ in diameter, and thus contribute to fine particulate matter ($\text{PM}_{2.5}$) in the lower atmosphere. $\text{PM}_{2.5}$ is noteworthy as it poses a serious threat to human health; prolonged exposure to the fine particles can result in respiratory damage (Pope and Dockery, 2006).

As a gas, NH_3 can transport between surface water and its overlying atmospheric layer. Depending on the concentration and partial pressures of each, and the physical and chemical conditions present, a transfer of NH_3 across the water-atmosphere boundary will occur (Asman et al., 1994). As a bidirectional process, NH_3 may enter the atmosphere from surface waters by emission or be deposited from the atmosphere into the water. Upward NH_3 air-sea exchanges have only been directly observed in the last thirty or so years, beginning with the work of Quinn et al. (1988). Since then, bidirectional water-atmosphere NH_3 fluxes have been observed or modeled over numerous marine waters across the globe (Table 1). From such studies, low latitude and coastal waters have been most frequently observed to display NH_3 emission (Paulot

et al., 2015; Johnson et al., 2008). Among those same works, multiple factors have been identified as contributing to NH₃ emission, including warm water temperatures, high water NH₄⁺ concentrations and low atmospheric NH₃ concentrations. Although such favorable conditions for NH₃ emission exist in the comparatively nutrient-rich surface waters of estuaries, very few studies have attempted to quantify the water-atmosphere fluxes of those systems. Of U.S. estuaries, only the Chesapeake Bay has received observation for water-atmosphere NH₃ flux (Larsen et al., 2001).

Table 1. Previously reported water-atmosphere NH₃ flux values.

Study	Location and details	Minimum (ng NH ₃ m ⁻² s ⁻¹)	Maximum (ng NH ₃ m ⁻² s ⁻¹)	Mean/net (ng NH ₃ m ⁻² s ⁻¹)
Asman et al. (1994)	North Sea, Southern Bight	-14.80	8.51	
Gibb et al. (1999)	Arabian Sea, Aug. to Oct.			-0.31
	Arabian Sea, Nov. to Dec.			0.46
Johnson et al. (2008)	Atlantic Ocean	-4.76	3.46	
Larsen et al. (2001)	Chesapeake Bay	-26.04	52.08	
Quinn et al. (1988)	NE Pacific Ocean	0.51	3.10	
Quinn et al. (1990)	NE and central Pacific Ocean			1.40
Quinn et al. (1996)	Caribbean Sea	-3.00	-2.20	
	Sargasso Sea	-6.81	-1.52	
	Bermuda	-2.60	-1.16	
	North Sea	-15.02	8.61	
Sorensen et al. (2003)	North Sea	-7.10	5.60	-1.01

The observation of NH₃ emissions from water to atmosphere raises an important consideration; earlier deposition estimates for NH₃ and total nitrogen had not always accounted for NH₃ returning to the atmosphere (Asman et al., 1994). Therefore, it is very possible that for previously observed locations that featured even periodic marine emission of NH₃, deposition quantities may have been overestimated. Work conducted by Asman et al. (1994), which observed water-atmosphere NH₃ flux over the Southern Bight of the North Sea, determined annual total NH₃ deposition quantities 50% lower than those reported in an earlier study which did not account for emission. Later, Sorensen et al. (2003) proposed that previous NH₃ dry deposition estimates for a coastal area of the North Sea may have been overestimated by 100%

or more. More recent analysis by Li et al. (2016) displayed that annual NH_3 dry deposition estimates produced by the Multilayer Model (MLM) - a single-direction, dry deposition inferential model - were a factor of 1.9 greater than estimates produced by a model that accounted for bidirectional NH_3 exchange between land surface and atmosphere.

Factoring bidirectional exchange into NH_3 deposition models is not the only opportunity to improve dry deposition estimates. Li et al. (2016) reported that when bidirectional deposition models were fitted with site-specific NH_3 flux parameterizations, their predictions generally agreed ($\pm 30\%$) with direct NH_3 flux measurements. That finding supported their claim that significant uncertainties in the estimates produced by their own bidirectional model resulted from the use of generalized parameters. Often, a simple lack of available observations has made it necessary to apply generalized data to NH_3 flux models (Wentworth et al., 2016; Paulot et al., 2015). Zhao et al. (2015) utilized satellite measurements to simulate lower level atmospheric columns of NH_3 . They cited uncertainty in their model's predictions of NH_3 over the NW Pacific due to a lack of in-situ observations of both the dry deposition of NH_3 and surface water NH_4^+ concentrations. Earlier, GEOS-Chem model projections of atmospheric NH_3 concentrations over the Midwest U.S. were found to be underestimated, resulting from data from the eastern U.S. being extrapolated across the Midwest due to a lack of prior regional NH_3 observations (Zhang et al., 2012). Additionally, Heald et al. (2012) found GEOS-Chem model predictions of atmospheric NH_3 in California to be underestimated and identified the need for yearlong NH_3 emission observations in that region. As a coastal state, the accurate inventorying of NH_3 emissions in California would have to consider the contribution of marine sources.

Quantifying the water-atmosphere flux of NH_3 by direct observation presents the opportunity to produce more precise dry deposition estimates for NH_3 by factoring periods of

emission. Such predictions can be further refined with the inclusion of site-specific and directly observed parameterizations for the water-atmosphere flux of NH_3 . Furthermore, by having this data available to validate their predictions, the accuracy of regional and global scale atmospheric transport models can be improved. Such advantages reveal the utility of directly observed data to the modeling community and highlight a current need for accurate and localized NH_3 flux data.

To date, the water-atmosphere flux of NH_3 has not been quantified for the Texas Coastal Bend; a coastal region of southeastern Texas that borders the northwest Gulf of Mexico between the latitudes of 26.1 to 28.8 N. In the Coastal Bend, southeastern winds dominate much of the year, moving relatively clean marine air from the Gulf over the Texas coast and inland (Larkin and Bomar, 1983). The estuaries of the region are protected by a nearly continuous barrier island and have waters that are generally shallow, warm, and feature chemical characteristics that when paired with air masses originating from the Gulf, can favor the emission of NH_3 . The quantification of water-atmosphere NH_3 flux is then a crucial component of future dry deposition and emission estimates for the Texas Coastal Bend and may serve as a useful reference for NH_3 transport models in other low latitude coastal regions.

In this study, the direction and magnitude of water-atmosphere NH_3 fluxes were determined from direct observations of surface water NH_4^+ and ambient air NH_3 concentrations, and a collection of meteorological and water measurements taken weekly to biweekly across three sites local to the Corpus Christi, TX metropolitan area from May 2018 to April 2019. The same observations were made monthly for seven additional sites spanning the greater Coastal Bend region from August 2018 to April 2019. In total, nine bays/lagoons of six estuary systems and the Gulf of Mexico are represented here.

2. Methods

2.1. Study area

The Texas Coastal Bend as defined in this study includes the south Texas Gulf coast from Matagorda Bay southward to the Lower Laguna Madre. The city of Corpus Christi sits near the geographical center of the Coastal Bend, along the southern shore of Corpus Christi Bay. As the only major city in the Coastal Bend, Corpus Christi (pop. 326,554) serves as the economic and cultural hub of the region (U.S. Census Bureau, 2019). Fishing villages and tourist destinations dot the mainland coast and barrier islands, with expanses of the Upper and Lower Laguna Madre shores bordered by private ranches (Tunnell and Judd, 2002). Large areas of the region's barrier islands are state or federally owned, including Padre Island National Seashore, about 15 km south of Corpus Christi. Industry is prevalent along Corpus Christi Bay and Aransas Bay, and farther north along San Antonio Bay and Lavaca Bay, where fuel refining and petrochemical processing are the major activities (Hardebeck et al., 1997). Agriculture is prevalent throughout the Coastal Bend with rangeland predominant in the southern reaches and cropland in the north (Bricker et al., 2007).

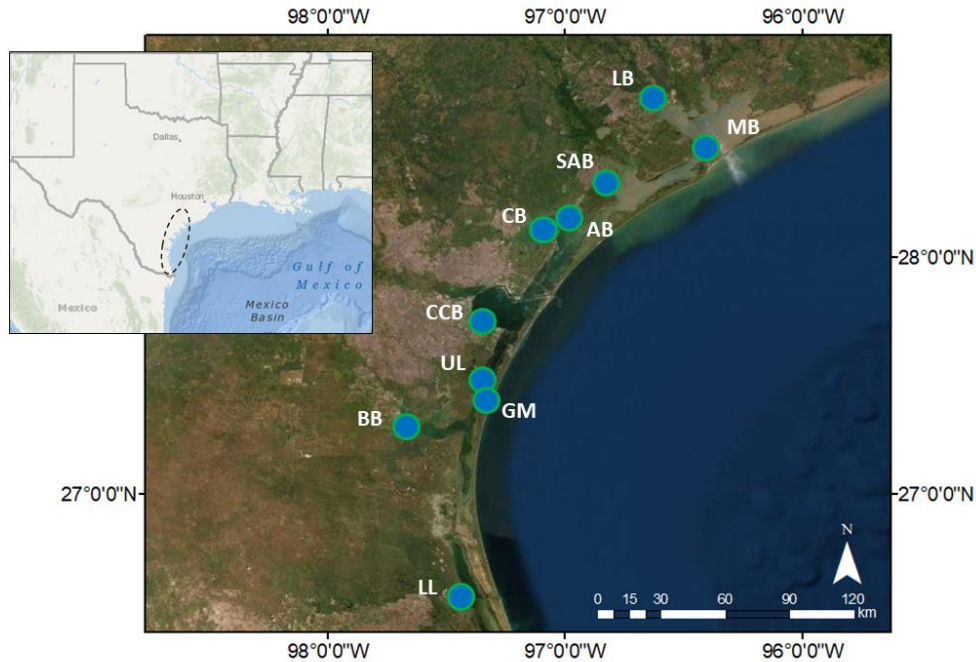


Figure 1. Map of all Coastal Bend study sites.

The climate of the Texas Coastal Bend features a severe latitudinal precipitation gradient. Annual rainfall totals nearly double from 66 cm/yr in the southern end of the region to more than 112 cm/yr in the northern reaches (Larkin and Bomar, 1983). The relatively higher temperatures and less frequent precipitation in the south lead to very high evaporation rates for the area's surface waters, including the Laguna Madre and Baffin Bay. As a result of evaporation exceeding freshwater recharge, these expansive yet shallow water bodies are hypersaline and considered negative estuaries (Montagna et al., 2018). Conversely, the estuary waters from Corpus Christi Bay northward receive substantial freshwater inflow from five major river systems which drain over 25% of the land area of Texas (Bricker et al., 2007).

Sampling sites for this study span the Texas Coastal Bend north to south from Lavaca Bay to the Lower Laguna Madre. Sites were chosen with the goal of obtaining an even latitudinal distribution along the Coastal Bend, and to best represent the great variability in

precipitation, hydrology and land usage along the coast. To allow for comparison, multiple bays within estuary systems were sampled when possible (Matagorda Bay - Lavaca Bay and Aransas Bay - Copano Bay), as were waters on opposing shores of North Padre Island (Upper Laguna Madre and Gulf of Mexico). The North Padre Island sites, along with the Corpus Christi Bay site comprised the weekly/biweekly sampling sites of the Corpus Christi area from May 2018 to April 2019, while all others were included in regionwide sampling which took place from August 2018 to April 2019. In total, 10 sites were sampled from and are listed in Table 2 and mapped on Figure 1.

Table 2. Coastal Bend study sites, coordinates, location information and associated water bodies.

Site Code	Coordinates	Location	Associated water body
LB	28.6393, -96.6097	Port Lavaca – Fishing Pier Park	Lavaca Bay
MB	28.4544, -96.4033	Port O’Connor – King Fisher Beach	Matagorda Bay
SAB	28.2916, -96.8085	Aransas National Wildlife Refuge	San Antonio Bay
AB	28.1248, -96.9836	Goose Island State Park	Aransas Bay
CB	28.0954, -97.0533	Copano Village – Murph Park	Copano Bay
CCB	27.7157, -97.3204	Texas A&M – CC - University Beach	Corpus Christi Bay
UL	27.4698, -97.3135	Bird Island Basin – Padre Island N.S.	Upper Laguna Madre
GM	27.3807, -97.3146	South Beach – Padre Island N.S.	Gulf of Mexico
BB	27.2851, -97.6634	Riviera public fishing pier	Baffin Bay
LM	26.5695, -97.4275	Port Mansfield – Fred Stone Park	Lower Laguna Madre

To contribute to this investigation of water-atmosphere NH₃ flux across the Coastal Bend region, two subregions are defined here and will be referenced throughout: The “northern” subregion begins with the CB site and extends northward to include AB, SAB, MB and LB. The “southern” subregion begins at CCB and expands southward to include UL, GM, BB and LL. Herein, any mention of “northern” and/or “southern” sites will be made in reference to the associated sites of each, as listed above. The distinction bounds the five most northern and five most southern sites, evenly dividing the ten total study sites between the two subregions. While these groups diverge latitudinally, and to an extent by hydrologic and biogeochemical

characteristics, they were defined solely for the purpose of aiding in the comparison of numerous sites and no other factors were considered in their classification.

2.2. Meteorological measurements and condensate collection

Measurements of ambient air temperature, relative humidity, wind speed and wind direction were taken with a Kestrel 5000 environmental meter. Condensate was created from ambient water vapor and collected for NH_4^+ concentration analysis in the lab. A collection device consisting of a modified plastic 5-gallon bucket, four 25x250 mm glass test tubes, four plastic funnels and four 50 ml polyethylene centrifuge vials was positioned out of direct sunlight and shielded from wind contact (Appendix A). The four test tubes were packed with ice and placed immediately within the collection device. Condensate would form and eventually stream off the tubes, drip onto the funnels and run into the centrifuge vials. Following 40 minutes of deployment, the collection device was disassembled and the contents of the four centrifuge vials were combined. 15 mL of the condensate was then passed through a 0.2 μm syringe filter into a clean 15 mL polyethylene centrifuge vial. The sample vial was sealed in a plastic bag and stored in a cooler at $\sim 3^\circ\text{C}$ for transport to the lab.

2.3. Surface water measurements and sample collection

A YSI Pro 2030 multiparameter probe was utilized to obtain in-situ measurements of temperature, dissolved oxygen (DO) concentration, and specific conductivity of surface waters. The probe was deployed at a depth of approximately 10 cm and held away from any disturbed sediments. An Extech pH-220 handheld pH meter and electrode was used to obtain a simultaneous measure of water pH. Both instruments were calibrated per their respective manufacturer's recommendations. Before, during and following the parameter measurements -

approximately five minutes apart - three discrete surface water samples were collected for lab analysis of their NH_4^+ concentrations. For each sample, 125 mL of water was collected in a clean wide-mouthed polypropylene bottle from an area over undisturbed sediment at a depth of approximately 5 cm. 15 mL of that sample was then filtered, stored and transported to the lab by the same procedure as the condensate samples.

2.4. NH_4^+ concentration analysis

Surface water NH_x concentrations indicate the total ammonia ($\text{NH}_3 + \text{NH}_4^+$) concentration of the sampled water body. Due to the preservation of water samples prior to analysis and the immediate addition of reagent during aliquot preparation in the lab, it is assumed that the resulting NH_4^+ concentration of the measured aliquot accurately represents the NH_x from which the water was sampled. To maintain consistency with previous literature, all surface water NH_x concentrations will herein be reported in $\mu\text{M NH}_4^+$.

Water and condensate samples collected during field work were analyzed for NH_4^+ by the ortho-phthalaldehyde (OPA) method as detailed by Holmes et al. (1999). The OPA method is a fluorometric analysis method for determining the NH_4^+ concentrations of surface water samples. The method was chosen for this study as it allows for a precise analysis of a wide range of NH_4^+ concentrations, including the detection of very low concentrations. Solutions of sodium sulfite (Na_2SO_3), OPA, and sodium tetraborate were first prepared as detailed by Holmes et al. (1999). 0.5 mL of the Na_2SO_3 solution, 5.0 mL of the OPA solution and 94.5 mL of the borate buffer were combined to create a working reagent. Once prepared, the working reagent was refrigerated at approximately 2°C in the dark for 24 hours before use.

To cover the range of anticipated NH_4^+ concentrations in surface water and condensate samples, NH_4^+ standards were prepared of ammonium chloride (NH_4Cl) and milli-Q ultrapure water at 0.1, 0.5, 1.0, 2.5, 5.0, 10.0 and 20.0 μM NH_4^+ concentrations. 0.25 mL of each standard, water sample and condensate sample were combined with 1.0 mL of the working reagent and stored in the dark for 3 hours (Holmes et al., 1999). Following storage, the standards and samples were analyzed using a Trilogy Laboratory Fluorometer to obtain fluorescence values. The measured fluorescence of the NH_4^+ standards were used to create a standard curve, which allowed for the determination of NH_4^+ concentrations from the measured fluorescence values of the water and condensate samples.

2.5. Determining atmospheric NH_3 from condensate

Farmer and Dawson (1982) present a method for obtaining ambient air concentrations for trace gases by collecting and analyzing condensate. Being that water vapor makes up approximately 1% of the lower atmosphere, its theoretically possible that an analyte collected in condensate could be at an aqueous concentration 100 times greater than its concentration in the ambient air (Farmer and Dawson, 1982). For that reason, and particular to this study, it was necessary to convert the measured NH_4^+ concentration of the collected condensate to an atmospheric NH_3 concentration:

$$C_{\text{NH}_3\text{-AIR}} = C_{\text{NH}_4\text{-COND}} \times [(D_{\text{H}_2\text{O}}/D_{\text{NH}_3}) \times (B_{\text{NH}_3}/B_{\text{H}_2\text{O}})] \times (V_{\text{AIR}} - V_{\text{TUBE}})$$

Table 3. Description of the parameters utilized in Farmer and Dawson’s (1982) equation for determining atmospheric NH₃ concentration from condensate.

Parameter	Description
C _{NH3-AIR}	Concentration of NH ₃ in ambient air (g/mL)
C _{NH4+COND}	Concentration of NH ₄ ⁺ in condensate (g/mL)
D _{H2O}	Diffusion coefficient for water vapor in air (m ² /s)
D _{NH3}	Diffusion coefficient for NH ₃ in air (m ² /s)
B _{NH3}	NH ₃ boundary layer thickness
B _{H2O}	Water vapor boundary layer thickness
V _{AIR}	Water vapor density of ambient air (g/cm ³)
V _{TUBE}	Water vapor density at tube surface (g/cm ³)

Table 4. Constant values applied to Farmer and Dawson’s (1982) equation for determining atmospheric NH₃ concentration from condensate.

	Value
(D _{H2O} /D _{NH3})	1.065
(B _{NH3} /B _{H2O})	1.000
V _{TUBE}	4.855x10 ⁻⁶ g/cm ³

D_{H2O}/D_{NH3} is the quotient of the diffusion coefficients for water vapor and NH₃ in air (Table 3). Few values for the diffusion coefficient for NH₃ in air were found in the literature. Of the five that were available, only two were determined for air temperatures that could be expected to be measured during this study. At those temperatures (16°C and 36°C) the reported NH₃-air diffusion coefficients are 22.667 m²/s and 26.176 m²/s, respectively (Tang et al., 2015). When divided into the corresponding water vapor-air diffusion coefficients, values of 1.07 and 1.06 are determined. As the two values are very close and span a range of air temperatures within which nearly all atmospheric sampling had taken place; a simple average of the values (1.065) was utilized (Table 4).

B_{NH3}/B_{H2O} represents the quotient of the boundary layer thicknesses of NH₃ and water vapor. In their work, Farmer and Dawson (1982) present nearly identical equations for each of those independent factors. The only disparity is the use of a specific Schmidt number for NH₃

and for water vapor (Farmer and Dawson, 1982). The Schmidt number for a gas can be found by dividing the kinematic viscosity by the diffusion coefficient of that gas at a specific temperature. Being that only two diffusion coefficients for NH₃ were reported at temperatures measured of the ambient air during this study, only two relevant Schmidt numbers can be determined for the gas: at both 16°C and 36°C the Schmidt number for NH₃ is 0.600. Conversely, a wide range of diffusion coefficient values have been reported for water vapor in air. Using the diffusion coefficient and kinematic viscosity values reported by Tucker and Nelken (1982), Schmidt numbers were determined for water vapor within the same temperature range (16°C - 36°C). The resulting Schmidt numbers for water vapor ranged from 0.608 at 16°C and 0.597 at 36°C. When those values are entered into the Farmer and Dawson (1982) equation for B_{H₂O} and then divided into 0.600 (B_{NH₃}), the resulting B_{NH₃}/B_{H₂O} values are 1.005 at 16°C and 0.998 at 36°C. Due to the minimal weight this range of values carry on the resulting ambient air NH₃ concentration, and the lack of applicable NH₃ diffusion coefficients in the literature, B_{NH₃}/B_{H₂O} was assigned the constant value of 1.

V_{TUBE} is the water vapor density at the surface of each ice-packed 25x250 mm glass test tube of the condensate collecting device. This value is dependent on the temperature at the tube surface and the saturation pressure of water vapor at that same temperature. A tube surface temperature measurement of 3°C was found with an infrared thermometer during the study and was assumed for all condensate conversions. The resulting value for V_{TUBE} (4.855x10⁻⁶ g/cm³) was calculated by the following equation, modified from Farmer and Dawson (1982):

$$V_{TUBE} = [(P_{H_2O} \times 0.0022) / T_{TUBE}]$$

Where P_{H₂O} is the saturation pressure of water at 3°C, T_{TUBE} is the measured temperature of the tube surface (3°C) and 0.0022 is a constant.

Conversely, the water vapor density of the ambient air (V_{AIR}) was not assigned a constant value. V_{AIR} is found by a similar equation as V_{TUBE} but will fluctuate due to variation in measured ambient air temperatures (Farmer and Dawson, 1982):

$$V_{\text{AIR}} = [(P_{\text{H}_2\text{O}} \times 0.0022) / T_{\text{AIR}}]$$

Here, T_{AIR} is the ambient air temperature and $P_{\text{H}_2\text{O}}$ is the saturation pressure of water at that same temperature. Because of the natural variation in T_{AIR} , a specific value for V_{AIR} was determined for every atmospheric NH_3 calculation.

2.6. Determining water-atmosphere NH_3 flux

The direction and magnitude of the water-atmosphere flux of NH_3 can be determined from the calculated atmospheric concentration of NH_3 , a calculated atmospheric equilibrium concentration of NH_3 and an exchange velocity (e.g. Asman et al., 1994; Quinn et al., 1988, 1996; Johnson et al. 2008; Wentworth et al., 2016). The difference between the atmospheric and equilibrium NH_3 concentrations reveals the direction of flux, with a positive value denoting water-atmosphere NH_3 emission and a negative value denoting NH_3 deposition. By multiplying that difference by an air-side exchange velocity, a rate of water-atmosphere NH_3 flux can be determined (Wentworth et al., 2016):

$$F_{\text{NH}_3} = k_g * [\text{NH}_{3(\text{eq})} - \text{NH}_{3(\text{g})}]$$

Here, F_{NH_3} is the water-atmosphere NH_3 flux ($\text{ng m}^{-2} \text{s}^{-1}$), k_g is the air-side exchange velocity (m/s), $\text{NH}_{3(\text{eq})}$ is the calculated atmospheric equilibrium NH_3 concentration ($\mu\text{g}/\text{m}^3$), and $\text{NH}_{3(\text{g})}$ is the measured atmospheric NH_3 concentration ($\mu\text{g}/\text{m}^3$). As presented by Wentworth et al. (2016) from McKee (2001), the exchange velocity k_g is determined as:

$$k_g = w / 770 + [45 * (17.0305^{1/3})],$$

where w is the measured wind speed (m/s). The atmospheric equilibrium concentration ($\text{NH}_{3(\text{eq})}$) is found by:

$$\text{NH}_{3(\text{eq})} = \text{NH}_{3(\text{aq})} * K_H$$

where $\text{NH}_{3(\text{aq})}$ is the concentration of aqueous NH_3 and K_H is the dimensionless Henry's Law constant (Wentworth et al., 2016). The following calculation is performed to estimate the proportion of NH_3 of total ammonia (NH_X) in the water:

$$\text{NH}_{3(\text{aq})} = \text{NH}_X * P_{\text{NH}_3}$$

where P_{NH_3} is the NH_3 proportion factor derived from:

$$P_{\text{NH}_3} = K_a / (K_a + \text{H}^+)$$

Here, K_a is the acid dissociation factor as determined from the acid dissociation coefficient ($\text{p}K_a$) of ammonium in marine water, and H^+ is the concentration of hydrogen ions as determined from the measured pH of the water (Bell et al., 2007; Wentworth et al., 2016):

$$\text{H}^+ = 10^{-\text{pH}}$$

$$K_a = 10^{-\text{p}K_a}$$

To calculate $\text{p}K_a$, the measured water temperature (t) in °C and salinity (S) in ppt are needed (Bell et al., 2007):

$$\text{p}K_a = 10.0423 - (0.0315536 * t) + (0.003071 * S)$$

Finally, the measured water temperature (T) in kelvin is utilized to determine the Henry's Law constant (Wentworth et al., 2016):

$$K_H = 1 / [17.93 * (T / 273.15) * e^{(4092/T)-9.70}]$$

By the mathematical model outlined above, measurements of wind speed, water temperature, pH and salinity, and calculations of the atmospheric and water concentrations of NH₃ are applied to produce an estimate of the water-atmosphere flux of NH₃.

2.7. Statistical analyses

The statistical significance of differences between reported mean values were determined by one-way ANOVA when all assumptions for that test were met. If the data proved to be non-normal, a Kruskal-Wallis non-parametric test was used instead (Kruskal and Wallis, 1952). When testing required unplanned comparisons to be made between multiple (>2) factor levels, post hoc procedures were also performed. Following significant ANOVA tests, post hoc comparisons were evaluated by Tukey's Honestly Significant Difference test (Tukey, 1949). Post hoc comparisons following a Kruskal-Wallis test were evaluated for significance by the Holm-Bonferroni stepwise method (Holm, 1979). All statistical procedures were performed in R (version 3.5.1) with the mgcv (version 1.8-26), multcomp (version 1.4-8), and nlme (version 3.1-137) packages (R Core Team, 2018; Wood, 2011; Hothorn et al., 2008; Pinheiro et al., 2020).

3. Results

3.1. NH₃ flux parameters of all Coastal Bend sites

The regionwide observation of all ten sites took place September 2018 - April 2019. Any use of "analysis period" and/or "study period" associated with regionwide investigations herein is in reference only to that defined time range. Observations of all sites, with the exception of

BB and LB, were also made in August 2018. As those data can be of benefit when identifying and assessing important influences on water-atmosphere NH_3 flux, they are not being excluded entirely from this study. Instead, those observations will be referenced and identified when needed, but will not contribute to any regionwide comparisons.

3.1.1. Surface water NH_4^+ concentrations

Concentrations of surface water NH_4^+ ($n = 438$) varied greatly across all Coastal Bend sites between September 2018 and April 2019. Thirty eight sample concentrations were below detection ($0.1 \mu\text{M NH}_4^+$) and therefore reported at half ($0.05 \mu\text{M NH}_4^+$) the detection limit, while 19 sample concentrations measured greater than $10.0 \mu\text{M NH}_4^+$. Monthly mean NH_4^+ water concentrations ranged from $1.59 \pm 1.09 \mu\text{M NH}_4^+$ in December to $5.70 \pm 2.83 \mu\text{M}$ in September across all sites, with a grand mean for the eight-month period of $2.80 \mu\text{M NH}_4^+$ (Table 5). Following the maximum mean concentration in September, surface water NH_4^+ values declined throughout fall, reached a minimum in December, and then increased over the remaining winter months. The difference in the mean NH_4^+ concentrations of September and December is statistically significant ($\chi^2(2) = 18.65, p = 0.007$) by a Kruskal-Wallis (KW) test and Holm-Bonferroni (HB) post hoc procedure. Monthly NH_4^+ values reached a winter maximum in February at $2.99 \pm 3.67 \mu\text{M}$ and following a moderate decline in March ($2.42 \pm 1.84 \mu\text{M}$), increased to a spring monthly maximum ($3.45 \pm 2.46 \mu\text{M}$) in April.

Table 5. Monthly mean water NH₄⁺ concentrations and standard deviations (in parentheses) in μM for all Coastal Bend sites, September 2018 - April 2019.

	September 2018	October 2018	November 2018	December 2018	January 2019	February 2019	March 2019	April 2019	8 mo. mean
LB	2.76 (0.85)	0.68 (0.45)	0.05 (<0.01)	1.80 (0.52)	0.82 (1.34)	0.64 (0.04)	1.10 (0.19)	4.09 (1.18)	1.49 (1.34)
MB	4.33 (2.80)	1.29 (0.11)	0.05 (<0.01)	2.57 (3.06)	1.19 (0.54)	0.45 (0.06)	0.86 (0.84)	2.18 (0.74)	1.61 (1.37)
SAB	5.05 (2.34)	4.79 (2.34)	0.24 (0.33)	3.80 (0.89)	3.15 (0.18)	1.27 (0.28)	1.17 (0.24)	1.96 (0.53)	2.68 (1.78)
AB	5.37 (2.73)	1.09 (0.85)	0.06 (0.01)	0.34 (0.31)	1.76 (0.17)	0.35 (0.14)	0.52 (0.81)	2.70 (2.98)	1.52 (1.79)
CB	2.72 (1.61)	1.25 (1.14)	0.05 (<0.01)	0.15 (0.08)	1.74 (0.17)	0.05 (<0.01)	1.42 (0.67)	4.65 (3.38)	1.50 (1.58)
<i>No. mean</i>	4.04 (1.25)	1.82 (1.68)	0.09 (0.08)	1.73 (1.53)	1.73 (0.88)	0.55 (0.46)	1.01 (0.34)	3.12 (1.19)	1.76
CCB	7.88 (4.11)	4.08 (2.11)	5.23 (4.46)	2.18 (2.75)	3.62 (0.97)	2.29 (2.32)	2.80 (2.22)	3.45 (1.95)	3.94 (1.88)
UL	5.06 (3.17)	5.47 (3.69)	3.48 (2.50)	1.05 (1.07)	3.81 (1.88)	2.94 (1.19)	3.94 (3.54)	2.09 (1.67)	3.48 (1.46)
GM	4.26 (3.55)	2.98 (2.61)	1.32 (0.65)	0.91 (1.01)	1.87 (0.80)	6.54 (4.76)	6.19 (3.33)	2.34 (1.49)	3.30 (2.15)
BB	7.42 (6.27)	2.64 (2.29)	5.24 (7.22)	1.32 (0.45)	0.39 (0.52)	11.77 (1.33)	4.21 (0.67)	9.80 (1.77)	5.35 (4.05)
LL	12.18 (2.04)	0.58 (0.26)	2.33 (0.96)	1.73 (0.62)	1.49 (0.54)	3.64 (0.93)	2.04 (0.60)	1.22 (0.84)	3.15 (3.76)
<i>So. mean</i>	7.36 (3.10)	3.15 (1.81)	3.52 (1.74)	1.44 (0.52)	2.23 (1.46)	5.44 (3.90)	3.84 (1.58)	3.78 (3.46)	3.84
All mean	5.70 (2.83)	2.48 (1.79)	1.80 (2.15)	1.59 (1.09)	1.98 (1.17)	2.99 (3.67)	2.42 (1.84)	3.45 (2.46)	2.80

Mean Surface water concentrations for each site during the analysis period ranged from $1.49 \pm 1.34 \mu\text{M NH}_4^+$ at LB to $5.35 \pm 4.05 \mu\text{M NH}_4^+$ at BB (Table 5). These extremes were found at the northern and southern regions of the study area, respectively, and reflect the wider observation that northern sites had a combined mean NH₄⁺ concentration ($1.76 \pm 0.52 \mu\text{M}$) significantly lower than that of the southern sites ($3.84 \pm 0.89 \mu\text{M}$), by a KW test and HB post hoc procedure ($\chi^2(2) = 17.12, p < 0.001$). In the northern subregion, the mean NH₄⁺ concentration of SAB ($2.68 \pm 1.78 \mu\text{M}$) was significantly greater than the combined mean of the other northern sites ($1.53 \pm 0.05 \mu\text{M NH}_4^+$) by one-way ANOVA ($F(1,38) = 4.315, p = 0.045$). Conversely, while the mean NH₄⁺ concentration of BB ($5.35 \pm 4.05 \mu\text{M}$) was greater the

combined mean ($3.47 \pm 0.34 \mu\text{M}$) of the remaining southern sites, the difference between those two values did not prove to be statistically significant by a KW test ($\chi^2(2) = 1.245, p = 0.265$).

3.1.2. Atmospheric NH_3 concentrations

The Coastal Bend displayed varying atmospheric NH_3 concentrations across the eight-month analysis period, with generally lower values October through February and relatively high values in September, March and April (Table 6). Mean atmospheric NH_3 concentrations peaked in September ($4.03 \pm 1.55 \mu\text{g}/\text{m}^3$) which was significantly greater than the minimum in January ($1.55 \pm 0.59 \mu\text{g}/\text{m}^3$) by a KW test and HB post hoc procedure ($\chi^2(2) = 24.89, p = 0.001$). A seasonal pattern is discernible in the monthly atmospheric NH_3 means, however an abrupt increase in December ($2.29 \pm 0.92 \mu\text{g}/\text{m}^3$) disrupted that trend. Spatial analysis of mean atmospheric NH_3 concentrations reveals less variation, as site values range between $1.79 \pm 1.51 \mu\text{g}/\text{m}^3$ (LB) and $2.98 \pm 2.38 \mu\text{g}/\text{m}^3$ (BB) and display no significant differences by a KW test ($\chi^2(2) = 9.536, p = 0.389$). The northern subregion mean of atmospheric NH_3 concentrations ($2.17 \pm 0.37 \mu\text{g}/\text{m}^3$) was diminished relative to southern sites ($2.59 \pm 0.45 \mu\text{g}/\text{m}^3$), but not significantly, also by a KW test ($\chi^2(2) = 1.815, p = 0.178$).

Table 6. Monthly atmospheric NH₃ concentrations in µg/m³ with standard deviations (in parentheses, for mean values) from September 2018 - April 2019.

	September 2018	October 2018	November 2018	December 2018	January 2019	February 2019	March 2019	April 2019	8 mo. mean
LB	5.07	1.00	1.54	1.71	0.57	0.54	2.79	1.07	1.79 (1.51)
MB	2.77	1.74	2.13	2.47	1.69	1.09	2.41	1.51	1.98 (0.56)
SAB	5.96	2.79	1.07	2.35	1.84	1.06	0.82	0.88	2.10 (1.72)
AB	3.41	2.51	2.28	1.00	1.55	1.61	3.58	1.92	2.23 (0.91)
CB	4.81	3.81	1.83	0.68	2.45	2.48	3.96	2.18	2.78 (1.33)
<i>No. mean</i>	4.40 (1.30)	2.37 (1.07)	1.77 (0.49)	1.64 (0.79)	1.62 (0.68)	1.36 (0.73)	2.71 (1.22)	1.51 (0.55)	2.17
CCB	6.16 (1.48)	1.49 (0.82)	1.17 (0.26)	3.18 (0.77)	1.40 (0.23)	2.32 (1.46)	2.88 (0.87)	3.98 (2.03)	2.82 (1.67)
UL	4.91 (2.27)	1.78 (1.61)	1.64 (0.68)	2.34 (0.90)	1.17 (0.58)	1.83 (0.03)	2.22 (0.02)	2.65 (0.14)	2.32 (1.14)
GM	2.35 (0.53)	2.33 (0.90)	1.66 (0.88)	2.58 (1.27)	0.91 (0.22)	1.46 (0.27)	1.74 (0.10)	2.36 (1.21)	1.92 (0.57)
BB	1.80	2.50	1.95	3.49	1.49	2.07	1.84	8.69	2.98 (2.38)
LL	3.00	2.20	1.28	3.14	2.40	2.70	6.14	2.24	2.89 (1.44)
<i>So. mean</i>	3.65 (1.83)	2.06 (0.42)	1.54 (0.32)	2.95 (0.47)	1.47 (0.56)	2.07 (0.47)	2.96 (1.83)	3.98 (2.72)	2.59
All mean	4.03 (1.55)	2.22 (0.78)	1.66 (0.41)	2.29 (0.92)	1.55 (0.59)	1.71 (0.69)	2.84 (1.47)	2.75 (2.26)	2.38

3.1.3. Additional measurements for determining water-atmosphere NH₃ flux

Additional observations used for the calculation of water-atmosphere NH₃ flux are included in the tables below and are reported both by monthly mean (Table 7) and by site mean (Table 8). Surface water temperature, used to calculate the NH₃ fraction of NH_x, did not vary significantly between sites, as determined by a KW test ($\chi^2(2) = 1.356, p = 0.998$). That parameter does however reflect the cooling and warming of the observed seasons when assessed by monthly mean. Air temperature follows suit with seasonal fluctuation apparent, yet no significant variation between the sites, as tested by one-way ANOVA ($F(9,70) = 0.105, p = 0.999$). The other meteorological parameter, wind speed, is the lone observation which

influences the NH₃ exchange velocity (k_g). Monthly mean values for wind speed range from 3.15 ± 1.71 m/s in December to 5.86 ± 1.77 m/s in April, which displays a significant difference by one-way ANOVA and a Tukey’s Honestly Significant Difference (HSD) test (F(7,72) = 2.832, *p* = 0.012). Site-specific means ranged from 3.36 ± 1.39 m/s at CB to 5.80 ± 1.37 m/s at UL, however this difference was not significant by one-way ANOVA (F(9,70) = 1.305, *p* = 0.250). Observed surface water salinity showed no significant variance by month by a KW test ($\chi^2(2) = 2.743$, *p* = 0.908), yet differs significantly between minimum (CB, 9.9 ± 1.7 ppt) and maximum (LL, 32.8 ± 3.1 ppt) site means by one-way ANOVA and HSD testing (F(9,70) = 50.26, *p* < 0.001). pH is a critical factor to the partitioning of NH_x between NH₃ and NH₄⁺ in water, as an increased H⁺ concentration shifts the equilibrium to a greater fraction of NH₄⁺, and a decreased H⁺ concentration shifts the equilibrium towards greater NH₃. Monthly mean pH values ranged from 8.17 ± 0.13 in September to 8.38 ± 0.17 in March, with the difference between those extremes being statistically significant (F(7,72) = 3.805, *p* = 0.028) by one-way ANOVA and HSD testing. No significant differences in mean pH values were found between any of the sites, also determined by one-way ANOVA (F(9,70) = 1.771, *p* = 0.089).

Table 7. Additional measurements for calculating water-atmosphere NH₃ flux reported by monthly mean with standard deviations (in parentheses) for all Coastal Bend sites, September 2018 - April 2019.

	September 2018	October 2018	November 2018	December 2018	January 2019	February 2019	March 2019	April 2019	8 mo. mean
Water temp. (°C)	29.1 (1.2)	26.4 (1.5)	23.2 (4.2)	17.3 (1.8)	17 (0.8)	17.8 (1.1)	19.6 (2.8)	29.1 (0.6)	26.4 (4.5)
Salinity (ppt)	25.2 (9.3)	23.6 (9.4)	22.2 (10.2)	20.8 (12.4)	22.7 (9.4)	22.2 (7.5)	20.8 (7.0)	25.2 (6.4)	23.6 (1.5)
pH	8.17 (0.13)	8.26 (0.09)	8.33 (0.11)	8.35 (0.11)	8.18 (0.12)	8.20 (0.15)	8.38 (0.17)	8.36 (0.22)	8.26 (0.09)
Air temp. (°C)	28.2 (1.7)	26.0 (2.5)	26.8 (2.8)	20.1 (2.8)	20.2 (2.7)	20.0 (1.3)	19.4 (3.1)	28.2 (2.3)	26.0 (3.6)
Wind speed (m/s)	4.13 (1.68)	4.88 (0.92)	4.25 (1.10)	3.15 (1.71)	5.35 (2.49)	3.59 (1.04)	4.49 (2.06)	5.86 (1.77)	4.46 (0.72)

Table 8. Additional measurements for calculating water-atmosphere NH₃ flux reported by site mean with standard deviations (in parentheses) for all Coastal Bend sites, September 2018 - April 2019.

	Water temperature (°C)	Salinity (ppt)	pH	Air temperature (°C)	Wind speed (m/s)
LB	22.0 (4.9)	14.6 (5.3)	8.33 (0.09)	22.7 (4.7)	4.48 (1.11)
MB	22.1 (5.1)	24.5 (3.8)	8.26 (0.16)	22.8 (4.9)	4.32 (2.14)
SAB	23.0 (5.0)	11.7 (3.9)	8.39 (0.16)	23.4 (5.0)	3.66 (1.02)
AB	22.1 (5.8)	15.3 (1.8)	8.30 (0.15)	22.9 (5.3)	4.15 (1.17)
CB	21.8 (5.6)	9.9 (1.7)	8.27 (0.09)	23.5 (3.9)	3.36 (1.39)
<i>No. mean</i>	22.2 (0.5)	15.2 (5.6)	8.30 (0.05)	23.0 (0.4)	3.99 (0.47)
CCB	21.1 (4.6)	29.5 (4.1)	8.29 (0.07)	22.9 (4.0)	4.56 (1.55)
UL	21.6 (4.5)	29.0 (3.7)	8.21 (0.14)	23.1 (4.0)	5.80 (1.37)
GM	21.2 (5.1)	28.2 (3.2)	8.15 (0.12)	22.4 (4.3)	5.36 (1.57)
BB	20.8 (4.4)	29.0 (2.0)	8.21 (0.25)	24.2 (3.9)	4.30 (2.28)
LL	21.1 (4.2)	32.8 (3.1)	8.36 (0.20)	22.8 (3.0)	4.63 (2.41)
<i>So. mean</i>	21.2 (0.3)	29.7 (1.8)	8.20 (0.08)	23.1 (0.7)	4.93 (0.63)
All mean	21.7 (0.7)	22.5 (8.6)	8.28 (0.07)	23.1 (0.5)	4.46 (0.83)

3.1.4. NH_{3(eq)} values

NH_{3(eq)} is largely influenced by the water concentration of NH_x, and to varying degrees by water temperature, pH and salinity. During this study, NH_{3(eq)} monthly means assumed a U pattern; beginning with a maximum in September ($8.85 \pm 4.03 \mu\text{g}/\text{m}^3$), descending to a minimum in January ($0.95 \pm 0.61 \mu\text{g}/\text{m}^3$), and then rebounding to $3.76 \pm 1.13 \mu\text{g}/\text{m}^3$ in April (Table 9, Figure 2). Significant differences between the NH_{3(eq)} minimum in January and both the maximum in September ($\chi^2(2) = 43.23, p < 0.001$), and the value calculated for April ($\chi^2(2) = 43.23, p = 0.011$), were both found by KW and HB testing. A grand mean of $2.85 \mu\text{g}/\text{m}^3$ was determined for the study, with monthly mean values below $2.00 \mu\text{g}/\text{m}^3$ NH₃ from November to March, and above $3.40 \mu\text{g}/\text{m}^3$ NH₃ for the remaining months. Considering NH_{3(eq)} spatially, site mean values ranged from $1.75 \pm 2.14 \mu\text{g}/\text{m}^3$ for CB to $4.48 \pm 4.49 \mu\text{g}/\text{m}^3$ for CCB, however no significant differences existed between those or any of the sites by a KW test ($\chi^2(2) = 11.55, p = 0.240$). Using the same northern-southern spatial delineation made earlier, the mean of northern

site $\text{NH}_{3(\text{eq})}$ values ($2.31 \pm 0.96 \mu\text{g}/\text{m}^3$) was significantly less than the southern sites ($3.39 \pm 1.02 \mu\text{g}/\text{m}^3 \text{NH}_3$) by a KW test ($\chi^2(2) = 5.267, p = 0.022$). Among northern locations, SAB displayed a mean $\text{NH}_{3(\text{eq})}$ ($4.02 \pm 3.62 \mu\text{g}/\text{m}^3$) more than twice that of another site, but that difference was not significant as determined by a KW test of the northern site $\text{NH}_{3(\text{eq})}$ means ($\chi^2(2) = 4.500, p = 0.343$). In the south, BB joined CCB with a relatively high mean $\text{NH}_{3(\text{eq})}$ ($4.39 \pm 4.23 \mu\text{g}/\text{m}^3$), while GM had the lowest mean $\text{NH}_{3(\text{eq})}$ of $2.13 \pm 1.42 \mu\text{g}/\text{m}^3$. That difference in $\text{NH}_{3(\text{eq})}$ extremes was not significant however, as determined by a KW test of southern site $\text{NH}_{3(\text{eq})}$ means ($\chi^2(2) = 2.574, p = 0.632$).

Table 9. Monthly mean $\text{NH}_{3(\text{eq})}$ values and standard deviations (in parentheses) in $\mu\text{g}/\text{m}^3$ for all Coastal Bend sites, September 2018 - April 2019.

	September 2018	October 2018	November 2018	December 2018	January 2019	February 2019	March 2019	April 2019	8 mo. mean
LB	4.76 (1.48)	1.18 (0.78)	0.09 (<0.01)	1.11 (0.32)	0.31 (0.51)	0.62 (0.04)	1.02 (0.18)	6.13 (1.77)	1.90 (2.25)
MB	6.49 (4.20)	2.25 (0.28)	0.05 (<0.01)	1.58 (1.88)	0.28 (0.13)	0.25 (0.03)	0.87 (0.86)	3.53 (1.20)	1.91 (2.20)
SAB	10.33 (4.79)	8.02 (5.54)	0.62 (0.87)	5.92 (1.39)	1.73 (0.10)	0.86 (0.19)	2.23 (0.45)	2.47 (0.67)	4.02 (3.62)
AB	8.96 (4.55)	1.29 (1.01)	0.13 (0.02)	0.16 (0.14)	1.18 (0.12)	0.24 (0.10)	0.56 (0.88)	3.30 (3.64)	1.98 (3.01)
CB	5.73 (3.39)	1.90 (1.74)	0.12 (<0.01)	0.10 (0.05)	0.83 (0.08)	0.02 (<0.01)	1.00 (0.47)	4.26 (3.10)	1.75 (2.14)
<i>No. mean</i>	7.25 (2.32)	2.93 (2.88)	0.20 (0.24)	1.77 (2.40)	0.86 (0.61)	0.40 (0.33)	1.14 (0.64)	3.94 (1.38)	2.31
CCB	16.01 (8.29)	5.35 (2.08)	4.02 (2.91)	1.62 (2.23)	1.78 (0.49)	1.00 (1.00)	1.39 (1.05)	4.68 (2.16)	4.48 (4.94)
UL	6.02 (4.12)	6.28 (3.48)	1.84 (1.20)	1.00 (1.14)	1.67 (1.02)	1.20 (0.50)	1.70 (1.55)	2.94 (2.08)	2.83 (2.13)
GM	4.51 (3.70)	3.11 (1.76)	0.75 (0.29)	0.45 (0.51)	0.68 (0.33)	2.17 (1.50)	2.82 (1.60)	2.55 (1.42)	2.13 (1.42)
BB	13.84 (11.70)	4.05 (3.51)	5.50 (7.56)	0.73 (0.25)	0.20 (0.16)	2.49 (0.28)	3.88 (0.62)	4.46 (0.81)	4.39 (4.23)
LL	11.81 (1.98)	0.71 (0.31)	1.43 (0.59)	0.92 (0.33)	0.82 (0.30)	1.53 (0.39)	4.35 (1.28)	3.26 (2.24)	3.10 (3.75)
<i>So. mean</i>	10.44 (4.98)	3.90 (2.16)	2.71 (1.98)	0.94 (0.43)	1.03 (0.68)	1.68 (0.63)	2.83 (1.30)	3.58 (0.94)	3.39
All mean	8.85 (4.03)	3.41 (2.45)	1.45 (1.87)	1.36 (1.69)	0.95 (0.61)	1.04 (0.83)	1.98 (1.31)	3.76 (1.13)	2.85

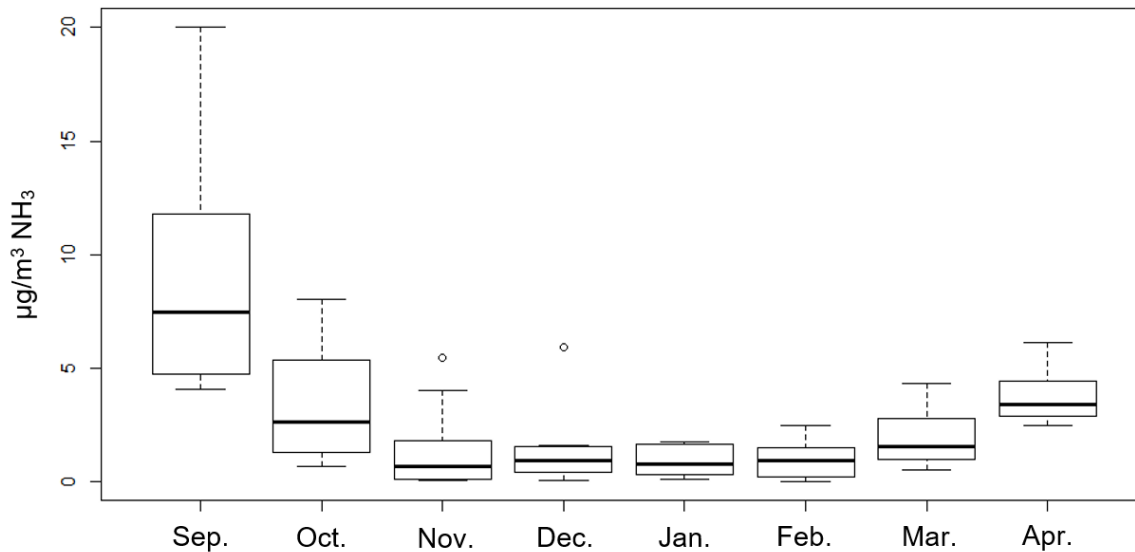


Figure 2. Boxplot of monthly $\text{NH}_{3(\text{eq})}$ values for all Coastal Bend sites, September 2018 - April 2019. Bold horizontal lines represent the mean, rectangles the interquartile range and outermost horizontal lines the range. Circles represent individual outliers.

3.2. Water-atmosphere NH_3 fluxes of all Coastal Bend sites

Monthly mean water-atmosphere NH_3 fluxes for the three sites local to the Corpus Christi metropolitan area (CCB, UL, GM) were compiled from observations obtained from multiple site visits each month. Monthly NH_3 fluxes for the remaining seven Coastal Bend sites were determined as the mean of three flux rates, each of which was calculated from observations made during a single day. As a result, the monthly mean NH_3 fluxes reported herein are composites of either, 1. multiple calculated NH_3 fluxes from a range of days sampled within a particular month (Corpus Christi sites) or, 2. multiple calculated NH_3 fluxes from a single day sampled within a particular month (all other sites).

Table 10. Monthly mean water-atmosphere NH₃ flux values and standard deviations (in parentheses) in ng m⁻² s⁻¹ for all Coastal Bend sites, September 2018 - April 2019.

	September 2018	October 2018	November 2018	December 2018	January 2019	February 2019	March 2019	April 2019	8 mo. mean
LB	-1.94 (9.24)	1.09 (4.70)	-7.70 (<0.01)	-1.55 (0.83)	-1.01 (2.03)	0.38 (0.20)	-8.23 (0.82)	33.68 (11.77)	1.84 (13.32)
MB	24.61 (27.78)	3.22 (1.77)	-6.51 (<0.01)	-2.60 (5.50)	-2.92 (0.26)	-3.88 (0.16)	-5.36 (2.99)	19.84 (11.85)	3.30 (12.09)
SAB	14.32 (15.73)	33.01 (34.95)	-1.62 (3.17)	10.09 (3.93)	-0.35 (0.31)	-0.83 (0.78)	5.93 (1.90)	8.88 (3.77)	8.68 (11.41)
AB	21.01 (17.24)	-6.46 (5.35)	-8.81 (0.10)	-3.62 (0.61)	-2.53 (0.78)	-4.01 (0.29)	-11.12 (3.23)	9.15 (24.09)	-0.80 (10.68)
CB	4.72 (17.47)	-7.81 (7.10)	-5.89 (<0.01)	-0.74 (0.06)	-6.40 (0.32)	-12.51 (<0.01)	-4.47 (0.72)	12.20 (18.13)	-2.61 (7.84)
<i>No. mean</i>	<i>12.54 (11.09)</i>	<i>4.61 (16.56)</i>	<i>-6.11 (2.75)</i>	<i>0.32 (5.57)</i>	<i>-2.64 (2.35)</i>	<i>-4.17 (5.04)</i>	<i>-4.65 (6.46)</i>	<i>16.75 (10.44)</i>	<i>2.08</i>
CCB	25.64 (32.22)	19.42 (7.48)	12.03 (10.02)	-9.90 (8.65)	1.47 (3.55)	-3.90 (5.47)	-9.89 (9.93)	2.26 (14.32)	4.64 (13.23)
UL	4.95 (12.26)	27.26 (21.18)	1.15 (6.94)	-9.77 (5.44)	3.31 (24.28)	-4.27 (3.88)	-3.02 (13.82)	0.08 (11.70)	2.46 (11.05)
GM	12.13 (24.30)	2.46 (9.83)	-3.91 (2.09)	-11.40 (4.43)	-1.99 (3.04)	4.89 (6.27)	8.50 (12.43)	-1.05 (12.61)	1.20 (7.44)
BB	54.05 (52.54)	5.14 (13.46)	24.68 (52.67)	-8.63 (0.78)	-14.74 (1.56)	0.87 (0.58)	9.26 (2.80)	-13.22 (2.53)	7.18 (22.99)
LL	24.45 (5.50)	-10.25 (2.16)	0.73 (2.75)	-2.14 (0.33)	-14.79 (2.79)	-5.10 (1.68)	-7.32 (5.24)	8.93 (19.66)	-0.69 (12.43)
<i>So. mean</i>	<i>24.24 (18.77)</i>	<i>8.81 (14.75)</i>	<i>6.94 (10.47)</i>	<i>-8.37 (6.37)</i>	<i>-5.35 (6.24)</i>	<i>-1.50 (4.62)</i>	<i>-0.49 (7.66)</i>	<i>-0.60 (12.68)</i>	<i>2.96</i>
All mean	18.39 (15.79)	6.71 (14.95)	0.42 (10.47)	-4.03 (6.37)	-4.00 (6.24)	-2.84 (4.62)	-2.57 (7.66)	8.08 (12.68)	2.52

A grand mean NH₃ water-atmosphere flux of 2.52 ± 3.57 ng m⁻² s⁻¹ was found across all sites during the analysis period (Table 10). This value denotes net emission of NH₃ from surface waters between September 2018 and April 2019 across the Texas Coastal Bend. The monthly mean NH₃ flux values comprising the grand mean vary widely, from a minimum of -4.03 ± 6.37 ng m⁻² s⁻¹ in December to a maximum of 18.39 ± 15.79 ng m⁻² s⁻¹ in September. That maximum value in September proves to be significantly greater than the mean NH₃ flux of each winter month (December, January, February) and March, by KW and HB testing (all, $\chi^2(2) = 26.31$, $p < 0.020$).

From the September maximum, the monthly flux values decreased throughout fall and into winter, transitioning from NH₃ emission to deposition in December (Table 10). From that minimum, the NH₃ flux values increased in January, February and March yet remained negative, and then increased again in April to reach their second highest monthly mean value of $8.08 \pm 12.68 \text{ ng m}^{-2} \text{ s}^{-1} \text{ NH}_3$. All considered, four of the observed months featured mean NH₃ emission, while four months' mean fluxes displayed deposition. From a seasonal perspective, the fall months (September, October, November) and spring months (March, April) featured upward mean water-atmosphere fluxes of 8.58 ± 9.24 and $2.75 \pm 7.53 \text{ ng m}^{-2} \text{ s}^{-1} \text{ NH}_3$ respectively, while the mean NH₃ flux of the winter months was depositional at $-3.62 \pm 0.68 \text{ ng m}^{-2} \text{ s}^{-1}$. That negative NH₃ flux value of winter proved to be significantly less than the mean NH₃ flux values of both fall ($\chi^2(2) = 12.67, p < 0.001$) and spring ($\chi^2(2) = 12.67, p = 0.045$) by KW and HB testing.

Site mean water-atmosphere NH₃ fluxes during the analysis period ranged from $-2.61 \pm 7.84 \text{ ng m}^{-2} \text{ s}^{-1}$ for CB to $8.68 \pm 11.41 \text{ ng m}^{-2} \text{ s}^{-1}$ for SAB, displaying an extent of variation that was considerably less than the temporal variation just reviewed (Table 10, Figure 3). As a result, the difference between those NH₃ flux value extremes was not significant ($\chi^2(2) = 7.501, p = 0.585$) by KW and HB testing. Of all site mean NH₃ fluxes, three were depositional, with two of those values no less than $-1.00 \text{ ng m}^{-2} \text{ s}^{-1}$. On the contrary, all of the seven positive site mean NH₃ flux values were greater than $1.00 \text{ ng m}^{-2} \text{ s}^{-1}$, with four of those $3.30 \text{ ng m}^{-2} \text{ s}^{-1}$ or higher. The NH₃ fluxes of SAB in the north and BB ($7.18 \pm 22.99 \text{ ng m}^{-2} \text{ s}^{-1}$) in the south represent the highest values found in their respective ends of the Coastal Bend. Among the northern sites, the mean NH₃ flux of SAB was nearly three times the magnitude of the next highest mean value at MB ($3.30 \pm 12.09 \text{ ng m}^{-2} \text{ s}^{-1}$). In the south, the mean NH₃ flux of BB was over 50% greater than

the next highest at CCB ($4.64 \pm 13.23 \text{ ng m}^{-2} \text{ s}^{-1}$). Despite those relatively great NH_3 flux means, there were no significant differences between any of the sites of the northern subregion ($\chi^2(2) = 7.399, p = 0.116$), or between those in the south ($\chi^2(2) = 1.396, p = 0.845$), as determined by KW and HB testing.

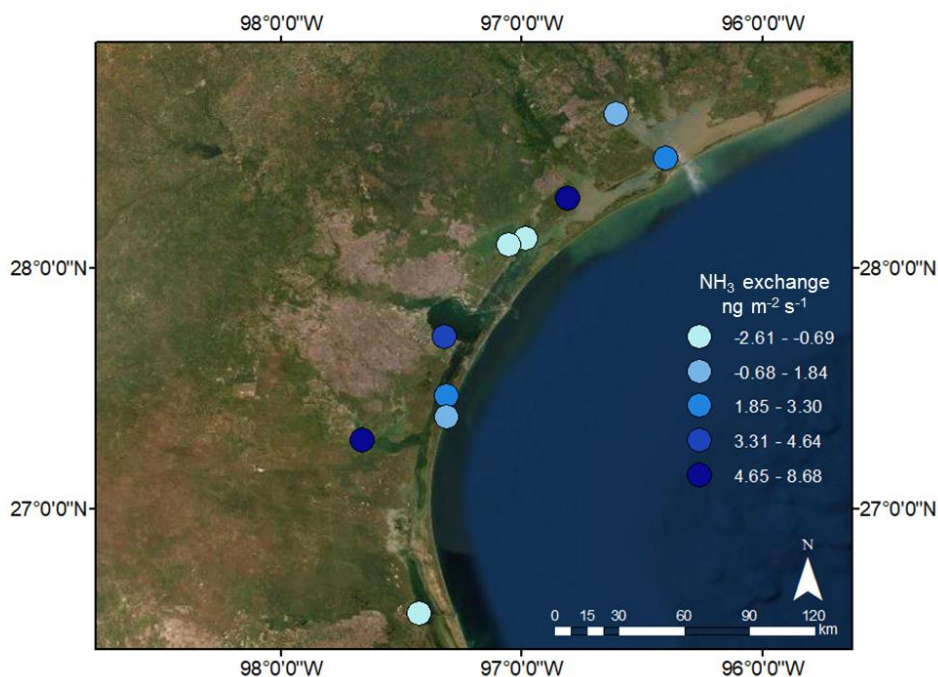


Figure 3. Map displaying site water-atmosphere NH_3 fluxes by specified ranges of mean values in $\text{ng m}^{-2} \text{ s}^{-1}$, September 2018 - April 2019.

3.3. NH_3 flux parameters of Corpus Christi area sites

The proximity of CCB, UL and GM to the study’s headquarters at Texas A&M University - Corpus Christi (TAMUCC) allowed those sites to be observed more regularly (weekly to biweekly) than the others of the greater Coastal Bend region. The objective of that yearlong campaign was to gain additional insight into water-atmosphere NH_3 flux through its higher temporal resolution sampling. In addition, the complete year of observation allows for comparisons to be made between all four seasons and all twelve months of the year. Being that

these conditions were particular to the three Corpus Christi area sites in this study, their results are being examined in a separate context.

Monthly mean surface water NH_4^+ concentrations for the local sites ranged from a minimum of $1.03 \pm 0.48 \mu\text{M}$ in May, to a maximum of $5.73 \pm 1.90 \mu\text{M}$ in September, which displayed a significant difference by one-way ANOVA and HSD testing ($F(11,24) = 2.578, p = 0.016$) (Table 11). Seasonal trends are evident, as mean NH_4^+ concentrations increased from the May minimum over the summer months before reaching a maximum in September. A steady decline over the fall followed, with a low reached in December ($1.38 \pm 0.70 \mu\text{M NH}_4^+$). NH_4^+ concentrations rebounded in January ($3.10 \pm 1.07 \mu\text{M NH}_4^+$) and continued to increase until March ($4.31 \pm 1.73 \mu\text{M}$). The study period concluded with NH_4^+ concentrations falling in April to $2.62 \pm 0.72 \mu\text{M}$. Site mean NH_4^+ concentrations displayed a relatively narrow range, with CCB ($3.48 \pm 1.90 \mu\text{M}$) exceeding the other two sites, yet not to a significant degree as determined by one-way ANOVA ($F(2,33) = 0.578, p = 0.567$).

Table 11. Monthly mean water NH_4^+ concentrations and standard deviations (in parentheses) in μM for Corpus Christi area sites, May 2018 - April 2019.

	May 2018	June 2018	July 2018	August 2018	September 2018	October 2018
CCB	0.75 (0.30)	2.46 (3.07)	1.99 (1.42)	5.07 (3.66)	7.88 (4.11)	4.08 (2.11)
UL	1.58 (0.91)	0.50 (0.45)	0.74 (1.11)	3.13 (2.29)	5.06 (3.17)	5.47 (3.69)
GM	0.75 (0.55)	2.61 (2.58)	3.85 (4.38)	2.55 (2.83)	4.26 (3.55)	2.98 (2.61)
<i>All mean</i>	<i>1.03 (0.48)</i>	<i>1.86 (1.18)</i>	<i>2.20 (1.56)</i>	<i>3.58 (1.32)</i>	<i>5.73 (1.90)</i>	<i>4.18 (1.25)</i>
November 2018	December 2018	January 2019	February 2019	March 2019	April 2019	12 mo. mean
5.23 (4.46)	2.18 (2.75)	3.62 (0.97)	2.29 (2.32)	2.80 (2.22)	3.45 (1.95)	3.48 (1.90)
3.48 (2.50)	1.05 (1.07)	3.81 (1.88)	2.94 (1.19)	3.94 (3.54)	2.09 (1.67)	2.82 (1.64)
1.32 (0.65)	0.91 (1.01)	1.87 (0.80)	6.54 (4.76)	6.19 (3.33)	2.34 (1.49)	3.01 (1.89)
<i>3.35 (1.96)</i>	<i>1.38 (0.70)</i>	<i>3.10 (1.07)</i>	<i>3.92 (2.29)</i>	<i>4.31 (1.73)</i>	<i>2.62 (0.72)</i>	<i>3.10 (0.34)</i>

Monthly mean atmospheric NH_3 concentrations varied considerably throughout the year, comprising a wide range of values and displaying little evidence of a discernable seasonal pattern

(Table 12). Sizable spikes in atmospheric NH₃ concentrations occurred in June (5.42 ± 3.02 $\mu\text{g}/\text{m}^3$ NH₃), September (4.47 ± 1.94 $\mu\text{g}/\text{m}^3$ NH₃) and December (2.70 ± 0.44 $\mu\text{g}/\text{m}^3$ NH₃), effectively disrupting any temporal trends at those times. Spatially, site mean NH₃ concentrations did not vary significantly from one another ($\chi^2(2) = 3.464$, $p = 0.177$), as determined by a KW test. The values ranged from a low at GM (2.02 ± 0.67 $\mu\text{g}/\text{m}^3$ NH₃) to a high at CCB (3.49 ± 2.22 $\mu\text{g}/\text{m}^3$ NH₃).

Table 12. Monthly mean atmospheric NH₃ concentrations and standard deviations (in parentheses) in $\mu\text{g}/\text{m}^3$ for Corpus Christi area sites, May 2018 - April 2019.

	May 2018	June 2018	July 2018	August 2018	September 2018	October 2018	
CCB	3.51 (4.35)	8.88 (2.87)	4.42 (0.81)	2.43 (1.31)	6.16 (1.48)	1.49 (0.82)	
UL	2.13 (0.55)	4.12 (0.89)	3.66 (1.52)	2.03 (1.09)	4.91 (2.27)	1.78 (1.61)	
GM	2.59 (2.98)	3.27 (1.48)	1.69 (0.64)	1.31 (0.93)	2.35 (0.53)	2.33 (0.90)	
<i>All mean</i>	<i>2.74 (0.70)</i>	<i>5.42 (3.02)</i>	<i>3.25 (1.41)</i>	<i>1.92 (0.57)</i>	<i>4.47 (1.94)</i>	<i>1.87 (0.43)</i>	
	November 2018	December 2018	January 2019	February 2019	March 2019	April 2019	12 mo. mean
	1.17 (0.26)	3.18 (0.77)	1.40 (0.23)	2.32 (1.46)	2.88 (0.87)	3.98 (2.03)	3.49 (2.22)
	1.64 (0.68)	2.34 (0.90)	1.17 (0.58)	1.83 (0.03)	2.22 (0.02)	2.65 (0.14)	2.54 (1.12)
	1.66 (0.88)	2.58 (1.27)	0.91 (0.22)	1.46 (0.27)	1.74 (0.10)	2.36 (1.21)	2.02 (0.67)
	<i>1.49 (0.28)</i>	<i>2.70 (0.44)</i>	<i>1.16 (0.24)</i>	<i>1.87 (0.43)</i>	<i>2.28 (0.57)</i>	<i>3.00 (0.87)</i>	<i>2.68 (0.74)</i>

Values of additional parameters necessary for calculating water-atmosphere NH₃ flux are displayed by site mean in Table 13. Of the water quality measurements, mean surface water temperatures and salinities did not vary significantly between sites, as determined by KW tests ($\chi^2(2) = 0.399$, $p = 0.819$, $\chi^2(2) = 0.164$, $p = 0.921$, respectively). GM did display a significantly lower mean surface water pH (8.12 ± 0.12) than both of the other sites ($F(2,33) = 6.591$, both $p < 0.008$) by one-way ANOVA and HSD testing, while CCB had a relatively lower mean wind speed (4.70 ± 1.62 m/s) that was not statistically significant ($F(2,33) = 2.138$, $p = 0.134$), also by one-way ANOVA. Notable temporal trends of the water measurements include mean monthly salinities diminishing nearly continuously from August (36.4 ± 0.88 ppt) until reaching a

minimum in March (24.6 ± 1.73 ppt), and variable monthly mean pH values, that ranged from 8.09 ± 0.21 in September to 8.42 ± 0.04 in April. The monthly extremes of salinity differed significantly ($F(11,24) = 13.46$, $p < 0.001$), while those of pH did not ($F(11,24) = 1.404$, $p = 0.234$), both by one-way ANOVA. Of the meteorological observations, the minimum and maximum monthly wind speeds differed significantly, from 3.47 ± 1.38 m/s in February to 7.56 ± 1.69 m/s in April, as determined by one-way ANOVA and HSD testing ($F(11,24) = 2.841$, $p = 0.042$).

Table 13. Additional parameters for calculating water-atmosphere NH₃ flux reported by site mean with standard deviations (in parentheses) for Corpus Christi area sites, May 2018 - April 2019.

	Water temperature (°C)	Salinity (ppt)	pH	Air temperature (°C)	Wind speed (m/s)
CCB	24.2 (5.9)	31.7 (4.7)	8.30 (0.07)	25.6 (5.1)	4.70 (1.62)
UL	24.9 (6.2)	32.3 (6.0)	8.27 (0.17)	25.5 (4.9)	5.98 (1.33)
GM	24.0 (5.8)	30.7 (4.6)	8.12 (0.12)	24.8 (4.9)	5.38 (1.42)
<i>All mean</i>	<i>24.4 (0.5)</i>	<i>31.6 (0.8)</i>	<i>8.23 (0.10)</i>	<i>25.3 (0.5)</i>	<i>5.35 (0.64)</i>

Resulting from surface water NH₄⁺ concentrations and the water quality parameters reviewed above, NH_{3(eq)} values for the Corpus Christi sites are shown in Table 14. There was considerable variation in mean monthly NH_{3(eq)} values, which ranged from a minimum of 1.02 ± 0.59 µg/m³ NH₃ in December to a maximum of 8.85 ± 6.25 µg/m³ NH₃ in September. That difference in extremes proved to be statistically significant ($\chi^2(2) = 23.93$, $p = 0.028$), as determined by KW and HB testing. A seasonal trend was evident as values increased over the summer, and then diminished from the September maximum to the December minimum. From that low, NH_{3(eq)} values increased gradually over the winter months before quickly increasing to 3.39 ± 1.13 µg/m³ NH₃ in April. There was notable variation between the site mean NH_{3(eq)} values as well, as CCB (5.00 ± 4.68 µg/m³) exceeded the other sites, more than doubling the

NH_{3(eq)} of GM ($2.43 \pm 1.53 \mu\text{g}/\text{m}^3$). That difference did not prove significant however, as determined by KW and HB testing ($\chi^2(2) = 2.281, p = 0.320$).

Table 14. Monthly mean NH_{3(eq)} values and standard deviations (in parentheses) in $\mu\text{g}/\text{m}^3$ for Corpus Christi area sites, May 2018 - April 2019.

	May 2018	June 2018	July 2018	August 2018	September 2018	October 2018	
CCB	1.15 (0.52)	5.30 (6.03)	5.41 (4.76)	12.29 (6.45)	16.01 (8.29)	5.35 (2.08)	
UL	4.02 (3.95)	2.19 (1.96)	2.49 (3.39)	6.11 (3.93)	6.02 (4.12)	6.28 (3.48)	
GM	0.89 (0.69)	3.88 (3.87)	4.94 (5.39)	2.39 (2.49)	4.51 (3.70)	3.11 (1.76)	
<i>All mean</i>	<i>2.02 (1.74)</i>	<i>3.79 (1.55)</i>	<i>4.28 (1.57)</i>	<i>6.93 (5.00)</i>	<i>8.85 (6.25)</i>	<i>4.91 (1.63)</i>	
	November 2018	December 2018	January 2019	February 2019	March 2019	April 2019	12 mo. mean
	4.02 (2.91)	1.62 (2.23)	1.78 (0.49)	1.00 (1.00)	1.39 (1.05)	4.68 (2.16)	5.00 (4.68)
	1.84 (1.20)	1.00 (1.14)	1.67 (1.02)	1.20 (0.50)	1.70 (1.55)	2.94 (2.08)	3.12 (1.99)
	0.75 (0.29)	0.45 (0.51)	0.68 (0.33)	2.17 (1.50)	2.82 (1.60)	2.55 (1.42)	2.43 (1.53)
	<i>2.20 (1.66)</i>	<i>1.02 (0.59)</i>	<i>1.38 (0.61)</i>	<i>1.46 (0.63)</i>	<i>1.97 (0.75)</i>	<i>3.39 (1.13)</i>	<i>3.52 (1.33)</i>

3.4. Water-atmosphere NH₃ fluxes of Corpus Christi area sites

The grand mean water-atmosphere flux value for the local sites was $2.54 \pm 1.23 \text{ ng m}^{-2} \text{ s}^{-1}$ NH₃, denoting net emission over the course of the twelve-month study (Table 15). A monthly mean NH₃ flux minimum of $-11.57 \pm 14.77 \text{ ng m}^{-2} \text{ s}^{-1}$ was reached in June, following diminishing flux values in the late spring (Figure 4). Values increased dramatically to the late summer, until a maximum mean NH₃ flux was reached in August ($24.85 \pm 17.08 \text{ ng m}^{-2} \text{ s}^{-1}$). That difference between the NH₃ flux means of June and August was significant, as were the differences between August's maximum and the NH₃ fluxes of May and July (all: $F(11,24) = 3.209, p < 0.008$), as determined by one-way ANOVA and HSD testing. Monthly NH₃ fluxes remained upward and relatively elevated throughout the fall months, before decreasing in November and becoming depositional again in December ($-10.36 \pm 0.91 \text{ ng m}^{-2} \text{ s}^{-1}$ NH₃). That December value was significantly lower than the NH₃ flux means of both September and

October (both: $F(11,24) = 3.209$, $p < 0.010$), by one-way ANOVA and HSD testing. The areawide mean NH_3 flux increased in January to $0.93 \pm 2.69 \text{ ng m}^{-2} \text{ s}^{-1}$, before it fell back to negative values in February and March. A return to a positive mean NH_3 flux occurred in April ($0.43 \pm 1.68 \text{ ng m}^{-2} \text{ s}^{-1} \text{ NH}_3$), although of very slight magnitude.

Table 15. Monthly mean water-atmosphere NH_3 flux values and standard deviations (in parentheses) in $\text{ng m}^{-2} \text{ s}^{-1}$ for Corpus Christi area sites, May 2018 - April 2019.

	May 2018	June 2018	July 2018	August 2018	September 2018	October 2018	
CCB	-12.02 (16.27)	-24.85 (29.63)	3.18 (21.04)	39.45 (33.32)	25.64 (32.22)	19.42 (7.48)	
UL	11.49 (27.57)	-14.20 (16.69)	-11.57 (11.96)	29.04 (26.43)	4.95 (12.26)	27.26 (21.18)	
GM	-12.18 (20.51)	4.33 (29.44)	6.39 (11.54)	6.06 (18.17)	12.13 (24.30)	2.46 (9.83)	
<i>All mean</i>	<i>-4.24 (13.62)</i>	<i>-11.57 (14.77)</i>	<i>-0.66 (9.58)</i>	<i>24.85 (17.08)</i>	<i>14.24 (10.50)</i>	<i>16.38 (12.68)</i>	
	November 2018	December 2018	January 2019	February 2019	March 2019	April 2019	12 mo. mean
	12.03 (10.02)	-9.90 (8.65)	1.47 (3.55)	-3.90 (5.47)	-9.89 (9.93)	2.26 (14.32)	3.57 (18.02)
	1.15 (6.94)	-9.77 (5.44)	3.31 (24.28)	-4.27 (3.88)	-3.02 (13.82)	0.08 (11.70)	2.87 (13.86)
	-3.91 (2.09)	-11.40 (4.43)	-1.99 (3.04)	4.89 (6.27)	8.50 (12.43)	-1.05 (12.61)	1.19 (7.55)
	<i>3.09 (8.15)</i>	<i>-10.36 (0.91)</i>	<i>0.93 (2.69)</i>	<i>-1.10 (5.18)</i>	<i>-1.47 (9.29)</i>	<i>0.43 (1.68)</i>	<i>2.54 (1.23)</i>

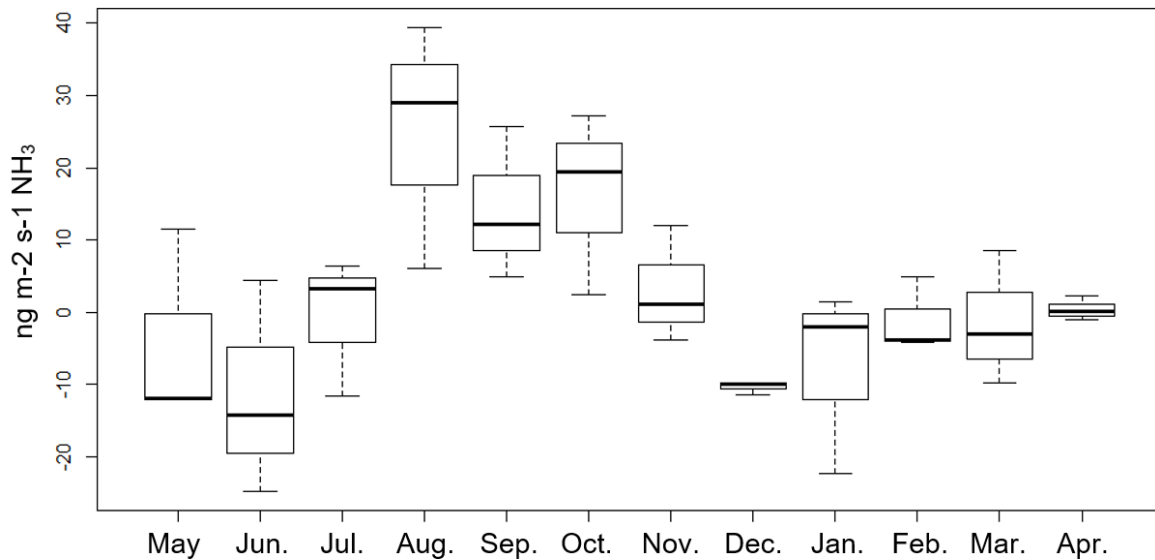


Figure 4. Boxplot of monthly water-atmosphere NH_3 fluxes of Corpus Christi area sites, May 2018 - April 2019. Bold horizontal lines represent the mean, rectangles the interquartile range and outermost horizontal lines the range. Circles represent individual outliers.

There are no statistically significant differences between the three local sites' mean NH_3 water-atmosphere flux values as determined by one-way ANOVA ($F(2,33) = 0.134, p = 0.875$) (Table 15). All site mean NH_3 flux values were positive, with the highest of those calculated at CCB ($3.57 \pm 18.02 \text{ ng m}^{-2} \text{ s}^{-1}$) being threefold greater than the minimum site mean NH_3 flux determined for GM ($1.19 \pm 7.55 \text{ ng m}^{-2} \text{ s}^{-1}$). Across North Padre Island, the mean NH_3 flux of UL ($2.87 \pm 13.86 \text{ ng m}^{-2} \text{ s}^{-1}$) was nearer in magnitude to CCB than nearby GM.

4. Discussion

4.1. Temporal analysis of Coastal Bend water-atmosphere NH_3 fluxes

Throughout the Coastal Bend, seasonal variation in water-atmosphere NH_3 flux was evident with the difference between the mean values of fall ($8.51 \pm 9.12 \text{ ng m}^{-2} \text{ s}^{-1}$) and winter ($-3.62 \pm 0.68 \text{ ng m}^{-2} \text{ s}^{-1}$) being statistically significant ($\chi^2(2) = 12.67, p < 0.001$), by KW and HB testing (Table 16, Figure 5). Within each individual season, noteworthy NH_3 flux trends were observed as well. Due to this, the temporal discussion which follows examines the three seasons (fall, winter, spring) separately and by month, following the September - April chronology of the study period.

Table 16. Monthly and seasonal mean water-atmosphere NH₃ flux values, atmospheric NH₃ concentrations, NH_{3(eq)} values and surface water NH₄⁺ concentrations of all Coastal Bend sites, September 2018 - April 2019. Standard deviations are displayed (in parentheses).

	NH₃ flux (ng m ⁻² s ⁻¹)	Atmospheric NH₃ (μg/m ³)	NH_{3(eq)} value (μg/m ³)	Water NH₄⁺ conc. (μM)
September 2018	18.39 (15.79)	4.03 (1.55)	8.85 (4.03)	5.70 (2.83)
October 2018	6.71 (14.95)	2.22 (0.78)	3.41 (2.45)	2.48 (1.79)
November 2018	0.42 (10.47)	1.66 (0.41)	1.45 (1.87)	1.80 (2.15)
<i>Fall mean</i>	<i>8.51 (9.12)</i>	<i>2.64 (1.24)</i>	<i>4.57 (3.83)</i>	<i>3.33 (2.08)</i>
December 2018	-4.03 (6.37)	2.29 (0.92)	1.36 (1.69)	1.59 (1.09)
January 2019	-4.00 (6.24)	1.55 (0.59)	0.95 (0.61)	1.98 (1.17)
February 2019	-2.84 (4.62)	1.71 (0.69)	1.04 (0.83)	2.99 (3.67)
<i>Winter mean</i>	<i>-3.62 (0.68)</i>	<i>1.85 (0.39)</i>	<i>1.12 (0.22)</i>	<i>2.19 (0.72)</i>
March 2019	-2.57 (7.66)	2.84 (1.47)	1.98 (1.31)	2.42 (1.84)
April 2019	8.08 (12.68)	2.75 (2.26)	3.76 (1.13)	3.45 (2.46)
<i>Spring mean</i>	<i>2.75 (7.53)</i>	<i>2.80 (0.06)</i>	<i>2.87 (1.26)</i>	<i>2.94 (0.73)</i>
8 mo. mean	2.52 (7.97)	2.38 (0.82)	2.85 (2.64)	2.80 (1.32)

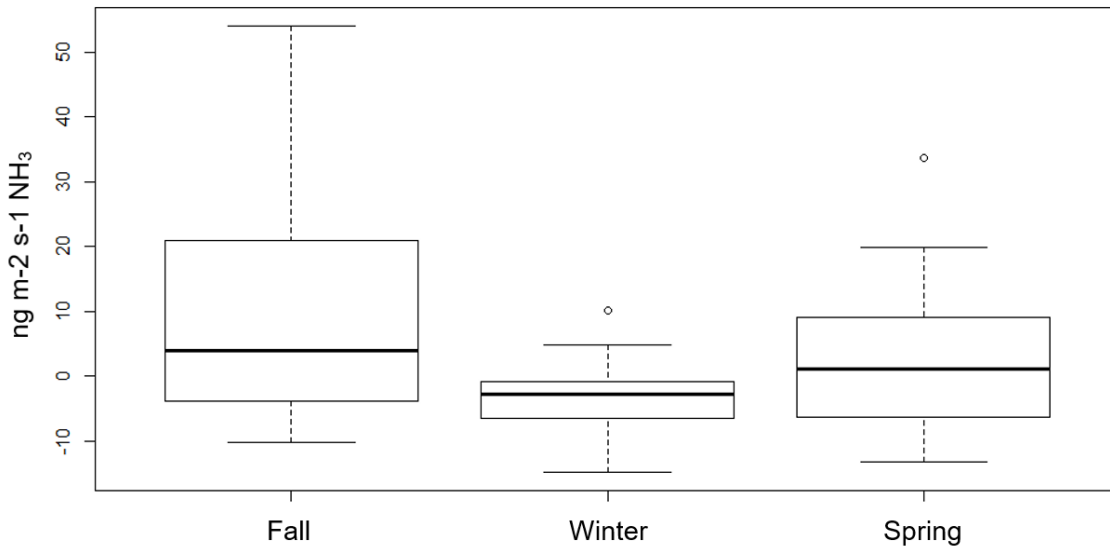


Figure 5. Boxplot of seasonal water-atmosphere NH₃ flux values for all Coastal Bend sites, September 2018 - April 2019. Bold horizontal lines represent the mean, rectangles the interquartile range and outermost horizontal lines the range. Circles represent individual outliers.

4.1.1. Fall months (September 2018 - November 2018)

The significantly greater seasonal NH_3 flux of fall was driven primarily by the maximum monthly flux ($18.62 \pm 15.79 \text{ ng m}^{-2} \text{ s}^{-1} \text{ NH}_3$) observed in September (Figure 6). During that month, the mean NH_4^+ surface water concentration ($5.70 \pm 2.83 \mu\text{M}$) and warm water temperatures produced a $\text{NH}_{3(\text{eq})}$ value ($8.85 \pm 4.03 \mu\text{g/m}^3$) great enough to overcome a relatively high mean atmospheric NH_3 concentration ($4.03 \pm 1.55 \mu\text{g/m}^3$), to produce the study's highest monthly NH_3 emission.

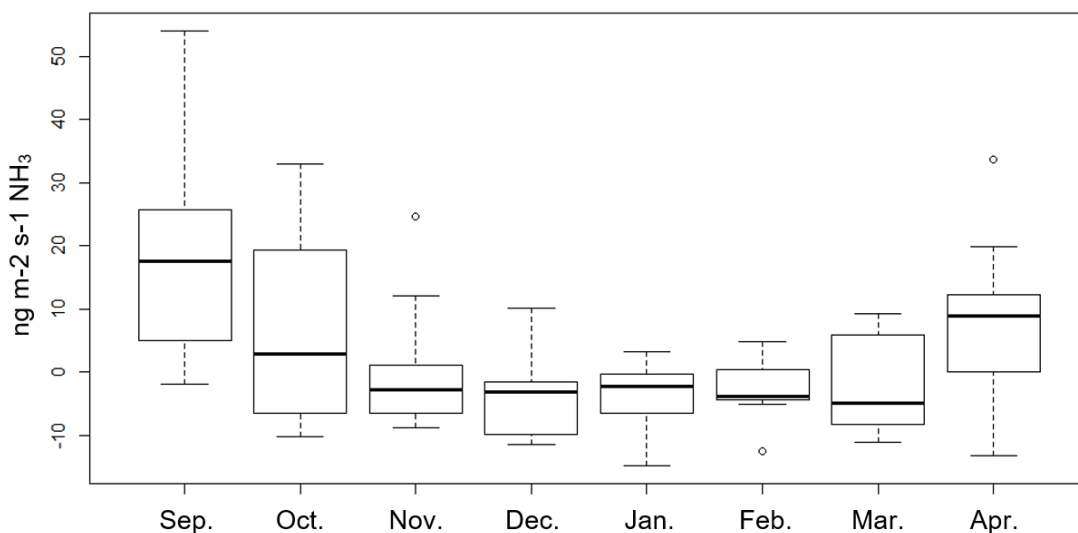


Figure 6. Boxplot of monthly water-atmosphere NH_3 flux values for all Coastal Bend sites, September 2018 - April 2019. Bold horizontal lines represent the mean, rectangles the interquartile range and outermost horizontal lines the range. Circles represent individual outliers.

All sites of the Coastal Bend displayed elevated surface water NH_4^+ concentrations in September, with the highest values observed in the south. The mean surface water NH_4^+ concentration of the southern subregion ($7.36 \pm 3.10 \mu\text{M}$) far exceeded that of the north ($4.04 \pm 1.25 \mu\text{M}$), and was driven by remarkably high concentrations at CCB ($7.88 \pm 4.11 \mu\text{M NH}_4^+$) and BB ($7.42 \pm 6.27 \mu\text{M NH}_4^+$), as well as the highest individual monthly mean NH_4^+

concentration of the entire study at LL ($12.18 \pm 2.04 \mu\text{M}$). Measured DO at LL on September 30 was only 69.8% of saturation (4.83 mg/l) at 10 cm depth, which suggests a great amount of water column respiration was occurring at that time. A similarly low DO percentage (82.8% of sat.) was observed the same day at BB, and during the two September sampling dates at CCB (September 6: 77.0% sat., September 19: 82.8% of sat.). From the simultaneously high NH_4^+ and low DO measurements, it can be reasoned that high rates of microbial OM processing were producing the elevated NH_4^+ concentrations at that time. Strong water-atmosphere NH_3 emission resulted, and ultimately contributed to the monthly maximum NH_3 flux for the entire region.

Northern sites displayed a similar pattern for NH_4^+ and DO in September, but not to nearly the same extremes. Water NH_4^+ concentrations at those sites were elevated relative to other months, with MB ($4.33 \pm 2.80 \mu\text{M}$), SAB ($5.05 \pm 2.34 \mu\text{M}$) and AB ($5.37 \pm 2.73 \mu\text{M}$) all displaying their respective monthly NH_4^+ maximums for the study. DO was relatively diminished across the northern sites in September, with DO saturation values being below each site's respective eight-month average. Just as with the southern sites, it appears that high rates of microbial activity contributed to the elevated water NH_4^+ concentrations observed in the north and likewise produced strong NH_3 emission.

September also featured the highest monthly rainfall total of the eight-month study. Estimated average precipitation across the Coastal Bend totaled 44 cm in September, with only LL having received less than 40 cm that month (NOAA, 2019). Notably, the September sampling dates of the northern sites (September 12 and 19), coincided with and shortly followed seven consecutive days of rainfall between September 9 and 16. That rain event alone deposited an estimated total of 30 cm or more across much of the Coastal Bend (NOAA, 2019). It appears

that the substantial rainfall of September may have also played a role in the elevated NH_4^+ concentrations and water-atmosphere NH_3 emissions observed that month.

Rain-driven surface inflow events have been shown to deliver pulses of riverine nutrients and organic matter to the estuary systems of the Coastal Bend (Whitledge, 1989; Longley, 1994; Mooney and McClelland, 2012). Depending on the seasonality of such an event and the land use characteristics of its supplying watershed, the dissolved organic matter (DOM) transported to bay waters can vary greatly in its carbon to nitrogen ratio (C:N), level of degradation, lability and subsequent bioavailability (Lebreton et al., 2016; Wu et al., 2019). While the bioavailability proportion of DOM has been shown to be lower in the summer than winter throughout the region, DOM originating from phytoplankton biomass has been noted as having low C:N and therefore is more bioavailable in estuarine systems (Wu et al., 2019).

Due to the temperate climate of the Coastal Bend, water temperatures rarely approach freezing and thus provide year-round opportunity for the emergence and growth of phytoplankton communities in the estuaries and river systems of the region (Pennock et al., 1999 and references therein). Seasonally, the greatest levels of primary production have been observed in the summer months, although elevated chlorophyll-*a* (chl-*a*) concentrations have been observed locally, in each of the other seasons (Pennock et al., 1999; Lebreton et al., 2016; Wetz et al., 2017). While chl-*a* concentrations were not measured in this study, it seems likely that such seasonal phytoplankton succession occurred in 2018, featuring growth in the spring and early summer and breakdown and remineralization in the later summer/early fall. If this assumption is valid, the phytoplankton biomass decaying at the end of the season would be of great nutritional quality, and therefore highly bioavailable to the microbial communities resident of the observed waters. The elevated NH_4^+ concentrations measured regionwide in September

then appear to be an effect of both the breakdown of the summer phytoplankton communities and the abundant rainfall which allowed for the transport and distribution of such bioavailable organic matter across estuarine surface waters. The water-atmosphere NH_3 emission observed that same month is then a consequence of the combined effects of these seasonal cycles.

Wet weather continued into October, with substantial (>2.5 cm) localized rainfall occurring from the 8th to the 9th from CB northward, and on the 15th in the southern end of the region at BB and LL (NOAA, 2019). The Corpus Christi area sites were observed three times in October, with only the first of those dates (October 3) having occurred recent to substantial rainfall (>2.5 cm, September 26 - October 1) (NOAA, 2019). In contrast to the surface water NH_4^+ response observed the month before however, the regionwide mean NH_4^+ concentration dropped to $2.48 \pm 1.79 \mu\text{M NH}_4^+$ in October. Despite this decline, sustained warm water temperatures helped force the $\text{NH}_{3(\text{eq})}$ value ($3.41 \pm 2.45 \mu\text{g/m}^3$) well above the mean atmospheric concentration ($2.22 \pm 0.78 \text{ ng m}^3$) to produce NH_3 emission for the month ($6.71 \pm 14.95 \text{ ng m}^{-2} \text{ s}^{-1} \text{ NH}_3$). The magnitude of that NH_3 flux value was further supported by increased wind speeds from the month before. While not nearly to the same extreme as September, the net NH_3 emission of October still helped to influence a positive regionwide NH_3 flux mean for the fall season.

The considerable decline in surface water NH_4^+ across the region despite the rain events may indicate stronger influence from a biological cycle nearing its end in October. It is possible that the breakdown and remineralization of the summer phytoplankton community was diminishing by October's sampling, resulting in lesser abundance of bioavailable DOM. The loss of this high-quality source of DOM paired with rainfall and increased surface inflow would have resulted in the delivery of freshwater with a comparatively lower proportion of

phytoplankton biomass than the freshwater received earlier in the fall (Wu et al., 2019). Furthermore, such elevated surface inflows would have caused a diluting and/or flushing effect on existing water column NH_4^+ , which would also have been subject to nitrification, uptake and other sources of removal (Dorado et al., 2015). Essentially, without new, high-quality DOM sources being received by estuary waters, the rate of NH_4^+ production would fall below that of NH_4^+ assimilation and transformation, resulting in declining water concentrations over time. Consequently, water-atmosphere NH_3 emission would then diminish in magnitude, just as what was observed across much of the Coastal Bend in October.

Net regional NH_3 emission was observed again in November, although the magnitude of that flux had diminished to near zero ($0.42 \pm 10.47 \text{ ng m}^{-2} \text{ s}^{-1}$) (Table 17). Notably, the mean $\text{NH}_{3(\text{eq})}$ ($1.45 \pm 1.87 \text{ } \mu\text{g/m}^3$) value for the month did not exceed the mean atmospheric NH_3 value ($1.66 \pm 0.41 \text{ } \mu\text{g/m}^3$), yet the resulting mean NH_3 flux value was not negative. This anomaly is explained by the extremely low surface water NH_4^+ concentrations and subsequently low $\text{NH}_{3(\text{eq})}$ values observed throughout the northern subregion in November. At three of the five northern sites (LB, MB and CB), all measured NH_4^+ water concentrations were below detection ($0.10 \text{ } \mu\text{M NH}_4^+$) and thus reported at half that value from zero ($0.05 \text{ } \mu\text{M NH}_4^+$). The two remaining sites, AB and SAB, produced individual samples above the detection limit but their overall mean NH_4^+ values remained very low ($0.06 \pm 0.01 \text{ } \mu\text{M}$ and $0.24 \pm 0.33 \text{ } \mu\text{M}$, respectively). Combined, these concentrations produced some of the lowest $\text{NH}_{3(\text{eq})}$ values calculated during the study, effectively driving the regionwide $\text{NH}_{3(\text{eq})}$ mean lower than the atmospheric NH_3 mean.

Table 17. Site mean water-atmosphere NH₃ flux values, atmospheric NH₃ concentrations, NH_{3(eq)} values and surface water NH₄⁺ concentrations of all Coastal Bend sites, November 2018. Standard deviations are displayed (in parentheses).

	NH₃ flux (ng m ⁻² s ⁻¹)	Atmospheric NH₃ (μg/m ³)	NH_{3(eq)} value (μg/m ³)	Water NH₄⁺ conc. (μM)
LB	-7.70 (<0.01)	1.54	0.09 (<0.01)	0.05 (<0.01)
MB	-6.51 (<0.01)	2.13	0.05 (<0.01)	0.05 (<0.01)
SAB	-1.62 (3.17)	1.07	0.62 (0.87)	0.24 (0.33)
AB	-8.81 (0.10)	2.28	0.13 (0.02)	0.06 (0.01)
CB	-5.89 (<0.01)	1.83	0.12 (<0.01)	0.05 (<0.01)
<i>No. mean</i>	<i>-6.11 (2.75)</i>	<i>1.77 (0.49)</i>	<i>0.20 (0.24)</i>	<i>0.09 (0.08)</i>
CCB	12.03 (10.02)	1.17 (0.26)	4.02 (2.91)	5.23 (4.46)
UL	1.15 (6.94)	1.64 (0.68)	1.84 (1.20)	3.48 (2.50)
GM	-3.91 (2.09)	1.66 (0.88)	0.75 (0.29)	1.32 (0.65)
BB	24.68 (52.67)	1.95	5.49 (7.56)	5.24 (7.22)
LL	0.73 (2.75)	1.28	1.43 (0.59)	2.33 (0.96)
<i>So. mean</i>	<i>6.94 (11.52)</i>	<i>1.54 (0.32)</i>	<i>2.71 (1.98)</i>	<i>3.52 (1.75)</i>
All mean	0.42 (10.47)	1.66 (0.41)	1.45 (1.87)	1.80 (2.15)

In contrast to the greatly diminished NH₄⁺ concentrations of the northern subregion (mean: 0.09 ± 0.08 μM), the mean concentration of the southern sites (3.52 ± 1.74 μM) remained near its eight-month average in November. While it is suspected that comparably less high-quality DOM existed in the northern waters at that time, the great disparity in NH₄⁺ between the subregions may also be a simple result of timing. Each of the northern sites were observed on November 7; 18 days past the last substantial (>1.5 cm) rainfall and just two days before a regionwide rain event on November 9 (NOAA, 2019). In contrast, the Corpus Christi area sites were sampled twice in November (Nov. 3 and 17), with the latter of those dates producing elevated water NH₄⁺ concentrations, particularly at CCB (8.77 ± 3.36 μM) and UL (4.97 ± 2.19 μM). Another southern site, BB, was sampled even later in the month and produced a NH₄⁺ concentration of 5.24 ± 7.22 μM. Such elevated NH₄⁺ concentrations ultimately produced strong NH₃ emission at CCB (12.03 ± 10.02 ng m⁻² s⁻¹) and BB (24.68 ± 52.67 ng m⁻² s⁻¹), which in turn boosted November's regionwide NH₃ flux value past zero.

In addition to rainfall, the influence of wastewater may help to explain the elevated surface water NH_4^+ concentrations observed at CCB and to an extent, UL, while both wastewater and nonpoint septic inflows may do the same for BB. Corpus Christi Bay receives freshwater from the Nueces River via Nueces Bay. Longley (1994) estimated that 38% of total N loading to the Nueces estuary system was a result of wastewater releases within the watershed. Treated wastewater contributes highly bioavailable DOM to receiving waters which, following a substantial rain event, could result in an enriched freshwater plume that would quickly be processed in receiving bodies (Wu et al., 2019 and references therein). Explained in greater detail later in this discussion, surface circulation within Corpus Christi Bay is predominantly seaward, with a general north-to-south movement of waters nearer to the barrier islands (Brock, 2001). This often results in the transport of bay waters southward to the Upper Laguna Madre (Whitledge, 1989).

Following a weather event on November 9 which deposited approximately 3 cm of rain at the CCB site, sampling on the 17th revealed a water NH_4^+ concentration of $8.77 \pm 3.36 \mu\text{M}$ there, and a $4.97 \pm 2.19 \mu\text{M}$ concentration at UL (NOAA, 2019). With no direct surface inflows to the Upper Laguna Madre, and considering the general south moving surface currents in the area, it can be argued that the surge in NH_4^+ at UL resulted from the transport of wastewater-contributed DOM to the site. Considering the seasonality of the observations, the in-situ production of NH_4^+ from autochthonous DOM seems less likely. It is possible that a similar, readily bioavailable DOM source is responsible for the elevated NH_4^+ concentrations observed at BB as well. The work of Felix and Campbell (2019) supports this theory, as they produced isotopic evidence of a predominant septic/sewage source of DON in Baffin Bay during the period of November 2017 - February 2018.

Ultimately, the fall season across the Coastal Bend was defined by net water-atmosphere NH_3 emission, which was of remarkable magnitude in September, but diminished over the remaining months. High rainfall totals early in the season and the breakdown of summer phytoplankton communities produced elevated surface water NH_4^+ concentrations which drove strong NH_3 emission. Regular rain events continued into October, however NH_4^+ concentrations dropped and thus, the magnitude of NH_3 emission declined relative to the month before. November produced near zero surface water NH_4^+ concentrations among northern sites which led to NH_3 deposition over those waters. Greatly elevated NH_4^+ concentrations - particularly at CCB and BB - produced strong NH_3 emission at those sites, which in turn prohibited the regionwide water-atmosphere NH_3 flux value to drop below zero.

4.1.2. Winter months (December 2018 - February 2019)

Considered together, the winter months produced net NH_3 deposition across the Coastal Bend ($-3.62 \pm 0.68 \text{ ng m}^{-2} \text{ s}^{-1}$). Within the season, December produced the study's monthly water-atmosphere NH_3 flux minimum ($-4.03 \pm 6.37 \text{ ng m}^{-2} \text{ s}^{-1}$), with January and February displaying net NH_3 deposition as well. Of the winter months, December had the highest mean atmospheric NH_3 concentration ($2.29 \pm 0.92 \text{ } \mu\text{g/m}^3$) and the lowest NH_4^+ water concentration ($1.59 \pm 1.09 \text{ } \mu\text{M}$), which combined to produce the minimum NH_3 flux.

Corpus Christi area sites were sampled three times in December (Dec 1, 13, 22) and each displayed diminishing surface water NH_4^+ concentrations throughout the month. The other southern sites - BB and LL - were sampled just once in December and displayed lower water NH_4^+ concentrations compared to a month earlier (Table 18). Across that subregion, a monthly mean NH_4^+ concentration of $1.59 \pm 0.52 \text{ } \mu\text{M}$ resulted, which was lower than the northern sites ($1.73 \pm 1.53 \text{ } \mu\text{M}$). Within the northern subregion, the three most northern sites - SAB, MB and

LB - all displayed sharp increases in NH_4^+ from the month before, which effectively drove the subregion NH_4^+ mean past that of the south. Notably, a weather event produced an estimated 3.5 cm or more of rainfall across the northern end of the Coastal Bend from December 7 - 8 (NOAA, 2019). While rain was received throughout the region on those dates, the more substantial totals received in the far north would have caused elevated surface inflow to SAB, MB and LB. Riverine DOM would have been delivered to the bays following the rain event, and its eventual processing may have caused the increased NH_4^+ concentrations observed at those sites on December 19.

Table 18. Site mean water-atmosphere NH_3 flux values, atmospheric NH_3 concentrations, $\text{NH}_{3(\text{eq})}$ values and surface water NH_4^+ concentrations of all Coastal Bend sites, December 2018. Standard deviations are displayed (in parentheses).

	NH_3 flux ($\text{ng m}^{-2} \text{s}^{-1}$)	Atmospheric NH_3 ($\mu\text{g}/\text{m}^3$)	$\text{NH}_{3(\text{eq})}$ value ($\mu\text{g}/\text{m}^3$)	Water NH_4^+ conc. (μM)
LB	-1.55 (0.83)	1.71	1.11 (0.32)	1.80 (0.52)
MB	-2.60 (5.50)	2.47	1.58 (1.88)	2.57 (3.06)
SAB	10.09 (3.93)	2.35	5.92 (1.39)	3.80 (0.89)
AB	-3.62 (0.61)	1.00	0.16 (0.14)	0.34 (0.31)
CB	-0.74 (0.06)	0.68	0.10 (0.05)	0.15 (0.08)
<i>No. mean</i>	<i>0.32 (5.57)</i>	<i>1.64 (0.79)</i>	<i>1.77 (2.40)</i>	<i>1.73 (1.53)</i>
CCB	-9.90 (8.65)	3.18 (0.77)	1.62 (2.23)	2.18 (2.75)
UL	-9.77 (5.44)	2.34 (0.90)	1.00 (1.14)	1.05 (1.07)
GM	-11.40 (4.43)	2.58 (1.27)	0.45 (0.51)	0.91 (1.01)
BB	-8.63 (0.78)	3.49	0.73 (0.25)	1.32 (0.45)
LL	-2.14 (0.33)	3.14	0.92 (0.33)	1.73 (0.62)
<i>So. mean</i>	<i>-8.37 (3.62)</i>	<i>2.95 (0.47)</i>	<i>0.94 (0.43)</i>	<i>1.44 (0.52)</i>
All mean	-4.03 (6.37)	2.29 (0.92)	1.36 (1.69)	1.59 (1.09)

The elevated NH_4^+ concentrations of the most northern sites helped drive that subregion's mean NH_3 flux value just above zero ($0.32 \pm 5.57 \text{ ng m}^{-2} \text{ s}^{-1}$) for December (Table 18). This contrasts with the negative NH_3 flux value of the southern subregion ($-8.37 \pm 3.62 \text{ ng m}^{-2} \text{ s}^{-1}$), which was of great enough magnitude to drive December's regionwide NH_3 flux to the eight-

month minimum. Aside from diminished surface water NH_4^+ , the strong NH_3 deposition in the south was driven by increased atmospheric NH_3 concentrations. CCB and the most southern sites - BB and LL - displayed the highest atmospheric NH_3 concentrations in December, all of which measured $>3.0 \mu\text{g}/\text{m}^3$. Wind direction may have influenced these concentrations as northern winds were present on December 18 during sampling at BB and LL, and on December 1 at CCB, UL and GM. Berner and Felix (2020) produced isotopic evidence of a predominant agricultural component of atmospheric NH_3 collected in the Corpus Christi area in December 2016. The early winter application of fertilizer to area cotton and sorghum plantations was identified as a probable source, which under the right meteorological conditions, would volatilize and be available for atmospheric transport (Zeng et al., 2018). Considering that sampling of BB and LL took place on December 22, with moderately warm air temperatures (19-22°C) and a north wind present, it may be possible that recently fertilized cropland to the north of those sites may have contributed to elevated atmospheric NH_3 concentrations at those sites.

Just a month later, the mean atmospheric NH_3 concentration ($1.55 \pm 0.59 \mu\text{g}/\text{m}^3$) of the Coastal Bend dropped to its eight-month minimum. This was driven largely by a substantial decrease in atmospheric NH_3 across the southern subregion from December to January. During all January sampling dates (CCB, UL, GM: Jan. 7 and 21, BB and LL: Jan. 22) the wind direction was from the south or south-southeast, contrasting with the northern winds present during December's sampling. With less opportunity for arriving air masses to receive terrestrial inputs of NH_3 , the resulting atmospheric concentrations in January were much lower than the month before. LL was an exception, having received possible urban sources of NH_3 from the town of Port Mansfield immediately to the south. Conversely, CCB, which also has urbanized land south of the site, featured its eight-month minimum NH_3 concentration in January ($1.40 \pm$

0.23 $\mu\text{g}/\text{m}^3$), from two sampling dates both featuring southern winds. A study wide minimum atmospheric mean was also determined for the other two Corpus Christi area sites (GM, $0.91 \pm 0.22 \mu\text{g}/\text{m}^3 \text{NH}_3$), UL $1.17 \pm 0.58 \mu\text{g}/\text{m}^3 \text{NH}_3$). Despite the overall low values, that result neatly displays a gradual enrichment of atmospheric NH_3 as air masses moved northward from the Gulf of Mexico, across North Padre Island and into the city of Corpus Christi (Figure 7).

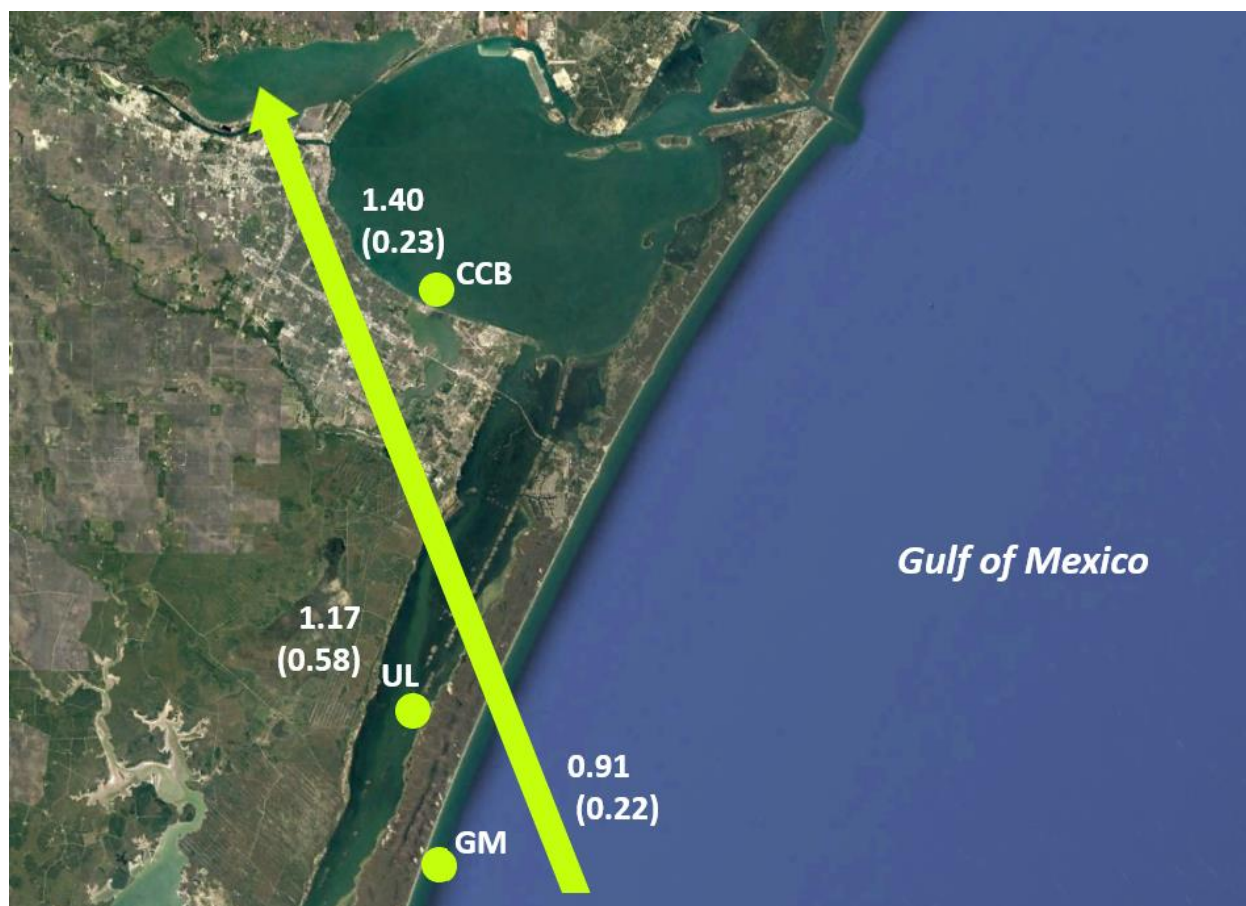


Figure 7. Map of Corpus Christi area sites with mean atmospheric NH_3 concentrations in $\mu\text{g}/\text{m}^3$ and standard deviations (in parentheses). Arrow represents the path of SSE wind through the region.

Along with the atmospheric NH_3 minimum, the lowest mean $\text{NH}_{3(\text{eq})}$ value of the study ($0.95 \pm 1.69 \mu\text{g}/\text{m}^3$) was determined for the Coastal Bend in January. As that value remained less than the mean atmospheric NH_3 concentration, NH_3 deposition continued. Elevated wind

speeds in January helped to increase the magnitude of that NH_3 deposition ($-4.00 \pm 6.24 \text{ ng m}^{-2} \text{ s}^{-1}$) near to that observed in December and served to support the depositional NH_3 flux for the greater winter season. Such overall conditions were sustained through February as similarly low mean $\text{NH}_{3(\text{eq})}$ ($1.04 \pm 0.83 \text{ } \mu\text{g/m}^3$) and mean atmospheric NH_3 ($1.04 \pm 0.83 \text{ } \mu\text{g/m}^3$) values produced a third consecutive negative NH_3 flux value ($-2.84 \pm 4.62 \text{ ng m}^{-2} \text{ s}^{-1}$) to close the winter months.

Of note during February, BB had the second highest monthly surface water NH_4^+ concentration observed during the study ($11.77 \pm 1.33 \text{ } \mu\text{M}$), yet a NH_3 flux value ($0.87 \pm 0.58 \text{ ng m}^{-2} \text{ s}^{-1}$) that barely exceeded zero. This is explained by the well below-average pH measured at BB on February 22 (7.90), along with a seasonally cool water temperature (16.7°C), which helped to produce a $\text{NH}_{3(\text{eq})}$ value of $2.49 \pm 0.28 \text{ } \mu\text{g/m}^3$. The elevated NH_4^+ concentration was observed with a DO level at 70% of saturation, which suggests high rates of microbial OM processing were occurring at that time. Excessive respiration from that activity likely caused the surface water pH to drop, which in turn helped to lower the $\text{NH}_{3(\text{eq})}$ value near to the measured atmospheric NH_3 concentration.

While it has already been mentioned how supporting parameters can temper the effect of exceedingly large or small NH_4^+ concentrations on resulting $\text{NH}_{3(\text{eq})}$ values, this particular case will be used to detail the direct influence of pH. Simply, had the pH value at BB been measured at the site average (8.21) on February 22 with all other measurements remaining the same, a NH_3 flux value of $6.03 \text{ ng m}^{-2} \text{ s}^{-1}$ would have resulted. By this example, the magnitude of NH_3 emission increased substantially by increasing the observed pH value to the site's eight-month average value. This displays not only the influence surface water pH has on water-atmosphere NH_3 exchange, but also the need to directly measure all supporting parameters when quantifying

point-in-time NH₃ fluxes. Had the site average pH value of BB been applied across each monthly calculation, the NH₃ emission in February would have been grossly overestimated.

When comparing the winter season against fall, it is apparent that another important parameter exerted considerable influence on water-atmosphere NH₃ flux. Water temperatures cooled greatly between November and December and remained low throughout the remaining winter months. That, combined with relatively diminished NH₄⁺ concentrations, drove resulting NH_{3(eq)} values to the lowest of the study period. The three lowest monthly mean NH_{3(eq)} values were calculated for the three winter months, with over half of the contributing site mean NH_{3(eq)} values falling below 1.0 µg/m³. Atmospheric NH₃ concentrations were diminished to a similar magnitude as water NH₄⁺ concentrations during the winter, however due to the greatly reduced NH_{3(eq)} values, were still great enough to maintain NH₃ deposition. Even as water NH₄⁺ values increased gradually through the season, the net effect on water-atmosphere NH₃ fluxes was not pronounced. As a result, NH₃ deposition persisted throughout the season and drove the mean NH₃ flux of winter significantly lower than fall.

4.1.3. Spring months (March 2019 - April 2019)

The mean water-atmosphere NH₃ flux of the Coastal Bend changed little from February, remaining depositional in March at a remarkably similar magnitude ($-2.57 \pm 7.66 \text{ ng m}^{-2} \text{ s}^{-1}$) (Table 19). The region's mean surface water NH₄⁺ concentration diminished slightly in March, while the mean atmospheric NH₃ concentration increased. That trend of increasing atmospheric NH₃ existed nearly regionwide, with only the concentrations observed at SAB and BB having decreased from the previous month. The northern sites displayed the greatest magnitude of change, as atmospheric NH₃ increased 60% at CB, more than doubled at both MB and AB, and improved better than fivefold at LB. While southern winds were observed consistently during

February sampling of the northern sites, wind direction was more variable the next Month. On March 21 all northern sites were sampled, with wind directions from the N at CB, E at AB and SAB, and ESE at MB and LB being recorded. While a northern wind brings terrestrial NH_3 sources to the coast, an eastern wind moves air from the Gulf of Mexico inland. With consistently elevated water NH_4^+ concentrations and net NH_3 emission occurring at GM February through March, it should be considered that much of the nearshore Gulf was producing water-atmosphere NH_3 emission during that time. If that was indeed the case, the elevated atmospheric NH_3 concentrations observed in the northern end of the Coastal Bend may have resulted from marine emissions.

Surface water NH_4^+ concentrations across the Coastal Bend decreased as a whole in March but displayed moderate local increases at CCB and UL in the south, and at AB, MB and LB in the north (Table 19). Notably, CB displayed a great increase ($1.42 \pm 0.67 \mu\text{M NH}_4^+$) from the sub-detection concentrations found a month earlier. When considering that the site had not received rainfall of any considerable volume ($>0.5 \text{ cm}$) since February 2, the elevated NH_4^+ concentration observed there on March 21 appears to be a result of regeneration within the water column (NOAA, 2019).

Phytoplankton biomass may have been available for processing at that time, which would have contributed highly bioavailable material to the OM pool (Wu et al., 2019). Lebreton et al. (2016) observed elevated chl-*a* concentrations in the Aransas River during February and March 2011, following a “minor” rain event which occurred in January. In 2018-2019, rain events in December and January may have similarly fueled phytoplankton growth in the Aransas River, leading to the eventual transport of that biomass to CB. During growth stages, a resident algal community utilizes available NH_4^+ and effectively depletes surface water concentrations (Wetz

et al., 2016). The relatively low NH_4^+ concentrations observed at CB on February 15 may indicate such activity was occurring at that time. By late March, the microbial breakdown of that algal community may have contributed to the elevated NH_4^+ concentrations observed then. Being that a relatively low surface water NH_4^+ concentration ($0.52 \pm 0.81 \mu\text{M}$) was found at AB that same day (March 21), it appears the location of CB - much nearer to the mouth of the Aransas River - allowed it to receive river-transported OM sooner, and possibly in greater volume. It also should be considered that riverine NH_4^+ may have been transported to CB by that very same mechanism. Regardless of origin, the elevated NH_4^+ concentration at CCB resulted in a greatly diminished magnitude of NH_3 deposition ($-4.47 \pm 0.72 \text{ ng m}^{-2} \text{ s}^{-1}$) in March, which otherwise may have approached that found at nearby AB ($-11.12 \pm 3.23 \text{ ng m}^{-2} \text{ s}^{-1}$).

Table 19. Site mean water-atmosphere NH_3 flux values and surface water NH_4^+ concentrations of all Coastal Bend sites, March - April 2019. Standard deviations are displayed (in parentheses).

	NH_3 flux ($\text{ng m}^{-2} \text{ s}^{-1}$)	Water NH_4^+ conc. (μM)	NH_3 flux ($\text{ng m}^{-2} \text{ s}^{-1}$)	Water NH_4^+ conc. (μM)
<i>Month, yr.</i>	<i>March 2019</i>	<i>March 2019</i>	<i>April 2019</i>	<i>April 2019</i>
LB	-8.23 (0.82)	1.10 (0.19)	33.68 (11.77)	4.09 (1.18)
MB	-5.36 (2.99)	0.86 (0.84)	19.84 (11.85)	2.18 (0.74)
SAB	5.93 (1.90)	1.17 (0.24)	8.88 (3.77)	1.96 (0.53)
AB	-11.12 (3.23)	0.52 (0.81)	9.15 (24.09)	2.70 (2.98)
CB	-4.47 (0.72)	1.42 (0.67)	12.20 (18.13)	4.65 (3.38)
<i>No. mean</i>	<i>-4.65 (6.46)</i>	<i>1.01 (0.34)</i>	<i>16.75 (10.44)</i>	<i>3.12 (1.19)</i>
CCB	-9.89 (9.93)	2.80 (2.22)	2.26 (14.32)	3.45 (1.95)
UL	-3.02 (13.82)	3.94 (3.54)	0.08 (11.70)	2.09 (1.67)
GM	8.50 (12.43)	6.19 (3.33)	-1.05 (12.61)	2.34 (1.49)
BB	9.26 (2.80)	4.21 (0.67)	-13.22 (2.53)	9.80 (1.77)
LL	-7.32 (5.24)	2.04 (0.60)	8.93 (19.66)	1.22 (0.84)
<i>So. mean</i>	<i>-0.49 (8.90)</i>	<i>3.84 (1.58)</i>	<i>-0.60 (8.04)</i>	<i>3.78 (3.46)</i>
All mean	-2.57 (7.66)	2.42 (1.84)	8.08 (12.68)	3.45 (2.46)

By April, the surface water NH_4^+ concentrations of all the northern sites had increased, with the mean NH_4^+ concentration of the subregion exceeding that of March threefold (Table 19). The April subregion NH_4^+ value was influenced by the high concentrations observed at CB

($4.65 \pm 3.38 \mu\text{M NH}_4^+$) and LB ($4.09 \pm 1.18 \mu\text{M NH}_4^+$), both eight-month maximums for the respective sites. Rainfall may have also contributed to those effects, as the northern sites received two substantial (>1.5 cm) rainfalls (March 30-31 and April 7) prior to their sampling on April 12 (NOAA, 2019). A very different situation occurred in the south, where the mean NH_4^+ concentration of April ($3.78 \pm 3.46 \mu\text{M}$) fell slightly from the month before. The mean NH_4^+ concentrations of UL, GM and LL all declined in April, while those at CCB and BB increased. The NH_4^+ concentration observed at BB ($9.80 \pm 1.77 \mu\text{M}$) was by far the greatest of all Coastal Bend sites for the month and effectively drove the monthly mean NH_4^+ of the southern sites above that of the north.

Timing appears to have played a role in the elevated NH_4^+ concentration found at BB, as an estimated 2.5 cm of rain fell the night before water samples were taken on April 25. That rainfall followed the event of March 30-31 which deposited approximately 3.8 cm at the site. Prior to these rains, a substantial (>1 cm) event had not occurred at BB since January 26 (NOAA, 2019). It appears that the rain events recent to April's sampling may have forced highly NH_4^+ enriched wastewater and septic effluents into Baffin Bay. Such sources would also have contributed bioavailable DOM, which would eventually be processed and drive further increases in surface water NH_4^+ concentrations (Wu et al., 2019). DOM contributions from the breakdown of a late winter phytoplankton community may have influenced the elevated April NH_4^+ concentration at BB as well, possibly having originated in the upstream reaches of the bay's tributaries (Wetz et. al, 2017).

While the entire Coastal Bend region may exhibit a year-round succession of phytoplankton communities in its waters, early spring blooms of diatom-dominated communities have been associated with the more favorable conditions provided by river inflows (Pennock et

al., 1999; Dorado et al., 2015). Considering that three of the five sites of the southern subregion do not have direct river input, the waters of those sites could feature low phytoplankton production at times when more river-influenced sites have greater production. That is how it appears in April, when the mean NH_4^+ concentration of the southern sites dropped slightly from that of March, driven by individual NH_4^+ declines at UL, GM and LL - the three southern sites without direct river inflows. On the contrary, the April mean NH_4^+ concentration of Nueces River-supplied CCB ($3.45 \pm 1.95 \mu\text{M}$) increased from March. While wastewater inputs to the Nueces watershed are well documented, inflows from that source in April may also have included phytoplankton biomass (Longley, 1994).

April was the first month to feature net NH_3 emission since November, and its magnitude was only eclipsed by that of September. April's flux value ($8.08 \pm 12.68 \text{ ng m}^{-2} \text{ s}^{-1}$) was driven by strong NH_3 emission in the northern end of the Coastal Bend which featured monthly NH_3 flux maximums at LB ($33.68 \pm 11.77 \text{ ng m}^{-2} \text{ s}^{-1}$) and CB ($12.20 \pm 18.13 \text{ ng m}^{-2} \text{ s}^{-1}$), and the second highest values of the study calculated for MB ($19.84 \pm 11.85 \text{ ng m}^{-2} \text{ s}^{-1}$) and AB ($9.15 \pm 24.09 \text{ ng m}^{-2} \text{ s}^{-1}$). The southern subregion displayed net NH_3 deposition in April ($-0.60 \pm 8.04 \text{ ng m}^{-2} \text{ s}^{-1}$) although three of the five sites there produced NH_3 emission. At BB, an unusually high atmospheric NH_3 concentration bested the high surface water NH_4^+ concentration to produce a strongly depositional NH_3 flux for the month ($-13.22 \pm 2.53 \text{ ng m}^{-2} \text{ s}^{-1}$). The elevated atmospheric NH_3 concentration at BB could have been a product of NH_3 emission from the Cayo del Grullo extension of Baffin Bay to the north, which receives inflow from the heavily wastewater-laden San Fernando Creek (Wetz et al., 2017). Alternatively, the very warm air temperature (30.3°C) and northern winds present during and prior to sampling may have allowed for the production and transport of NH_3 from nearby volatilizing agricultural sources (Felix and

Berner, 2020). Ultimately, the magnitude of the resulting NH_3 deposition at BB was great enough to drive the southern NH_3 flux mean to a negative value.

The spring season saw the recovery of surface water NH_4^+ concentrations from wintertime lows, and gradually increasing atmospheric NH_3 concentrations across much of the Coastal Bend. The suspected breakdown of winter phytoplankton communities paired with rain-driven contributions of NH_4^+ and DOM appear to have elevated NH_4^+ concentrations, while warming temperatures and northern winds helped to contribute to the observed increase in atmospheric NH_3 . As was observed at other times, these seasonal changes affected water-atmosphere NH_3 fluxes gradually in spring, as the regional mean remained depositional in March, before returning to emission in April. Additionally, increasing wind speeds, which reached a monthly maximum in April, helped to improve the magnitude of those NH_3 fluxes. When considering the spring season in an annual context, it appears much like fall to be a transitional period where an interplay of seasonal biotic and meteorological cycles produces widespread effects on the conditions which influence the direction and magnitude of NH_3 flux. As a result, a reversal in the direction of water-atmosphere NH_3 exchange was observed within each of those seasons.

4.2. Spatial analysis of Coastal Bend water-atmosphere NH_3 fluxes

The surface water NH_4^+ concentration of the southern sites ($3.84 \pm 1.85 \mu\text{M}$) was more than twice that of the northern sites ($1.76 \pm 1.30 \mu\text{M}$) across the eight-month study period, yet the difference in mean $\text{NH}_{3(\text{eq})}$ values between south ($3.39 \pm 3.05 \mu\text{M}$) and north ($2.31 \pm 2.37 \mu\text{M}$) was not nearly as pronounced (Table 20). As was identified in the temporal analysis, the influence of other water-side parameters can serve to diminish the influence of surface water NH_4^+ once mean $\text{NH}_{3(\text{eq})}$ values are calculated. Of the southern sites, the lower mean pH and

higher salinities effectively suppressed its mean $\text{NH}_{3(\text{eq})}$ value. The mean atmospheric NH_3 concentrations of the two subregions were closer still, and by the time NH_3 flux was figured, the southern sites ($2.96 \pm 3.05 \text{ ng m}^{-2} \text{ s}^{-1}$) and the northern sites ($2.08 \pm 4.34 \text{ ng m}^{-2} \text{ s}^{-1}$) both displayed net NH_3 emission of a very similar magnitude. While these resulting values may appear to suggest homogeneity in water-atmosphere NH_3 flux across the Coastal Bend, the conditions driving those results are quite different between the latitudinal ends of the region.

Table 20. Monthly mean water NH_4^+ concentrations, $\text{NH}_{3(\text{eq})}$ values, atmospheric NH_3 concentrations and NH_3 water-atmosphere flux values of the northern and southern subregions of the Coastal Bend, September 2018 - April 2019. Standard deviations are displayed (in parentheses).

	Sep 2018	Oct 2018	Nov 2018	Dec 2018	Jan 2019	Feb 2019	Mar 2019	Apr 2019	8 mo. mean
NH_3 flux ($\text{ng m}^{-2} \text{ s}^{-1}$)									
Northern sites mean	12.54 (11.09)	4.61 (16.56)	-6.11 (2.75)	0.32 (5.57)	-2.64 (2.35)	-4.17 (5.04)	-4.65 (6.46)	16.75 (10.44)	2.08 (8.52)
Southern sites mean	24.24 (18.77)	8.81 (14.75)	6.94 (10.47)	-8.37 (6.37)	-5.35 (6.24)	-1.50 (4.62)	-0.49 (7.66)	-0.60 (12.68)	2.96 (10.32)
Atmos. NH_3 ($\mu\text{g}/\text{m}^3$)									
Northern sites mean	4.40 (1.30)	2.37 (1.07)	1.77 (0.49)	1.64 (0.79)	1.62 (0.68)	1.36 (0.73)	2.71 (1.22)	1.51 (0.55)	2.17 (1.01)
Southern sites mean	3.65 (1.83)	2.06 (0.42)	1.54 (0.32)	2.95 (0.47)	1.47 (0.56)	2.07 (0.47)	2.96 (1.83)	3.98 (2.72)	2.59 (0.94)
$\text{NH}_{3(\text{eq})}$ value ($\mu\text{g}/\text{m}^3$)									
Northern sites mean	7.25 (2.32)	2.93 (2.88)	0.20 (0.24)	1.77 (2.40)	0.86 (0.61)	0.40 (0.33)	1.14 (0.64)	3.94 (1.38)	2.31 (2.37)
Southern sites mean	10.44 (4.98)	3.90 (2.16)	2.71 (1.98)	0.94 (0.43)	1.03 (0.68)	1.68 (0.63)	2.83 (1.30)	3.58 (0.94)	3.39 (3.05)
NH_4^+ conc. (μM)									
Northern sites mean	4.04 (1.25)	1.82 (1.68)	0.09 (0.08)	1.73 (1.53)	1.73 (0.88)	0.55 (0.46)	1.01 (0.34)	3.12 (1.19)	1.76 (1.30)
Southern sites mean	7.36 (3.10)	3.15 (1.81)	3.52 (1.74)	1.44 (0.52)	2.23 (1.46)	5.44 (3.90)	3.84 (1.58)	3.78 (3.46)	3.84 (1.85)

Beyond the simple latitudinal delineation, it appears that specific estuary systems and individual waters within the Coastal Bend possess distinctive water-atmosphere NH_3 flux characteristics. As such, a higher resolution spatial analysis is needed. In order to meet that demand, the investigation which follows includes analyses of the water-atmosphere NH_3 flux

characteristics of San Antonio Bay and the Lavaca-Colorado and Mission-Aransas estuary systems. The surface waters local to the Corpus Christi area will then be covered within their own geographical context later in this discussion. The spatial analysis is being presented in such a manner to avoid redundancy and to provide a greater level of detail on specific outstanding processes that drive the water-atmosphere NH_3 flux process in the Coastal Bend.

4.2.1 Water-atmosphere NH_3 flux characteristics of San Antonio Bay

Across eight months of observation, the mean water-atmosphere NH_3 flux of SAB ($8.68 \pm 11.41 \text{ ng m}^{-2} \text{ s}^{-1}$) was the highest of all Coastal Bend sites (Figure 8). Among only the northern sites, the mean NH_3 flux of SAB was significantly greater than the mean of the others ($\chi^2(2) = 5.927, p < 0.015$) by KW and HB testing. This should not be surprising considering the magnitude of the net NH_3 emission at SAB, and that the northern subregion also featured the Coastal Bend's NH_3 flux minimum at CB ($-2.61 \pm 7.84 \text{ ng m}^{-2} \text{ s}^{-1}$). The significant greater NH_3 flux of SAB appears to be driven by the high surface water NH_4^+ concentrations observed at the site, along with a comparatively high mean pH, which also was a maximum across all sites (Table 21). Both the mean water NH_4^+ concentration and $\text{NH}_{3(\text{eq})}$ value of SAB exceed those of every other northern site by twofold, while its mean atmospheric NH_3 concentration was below the northern subregion average.

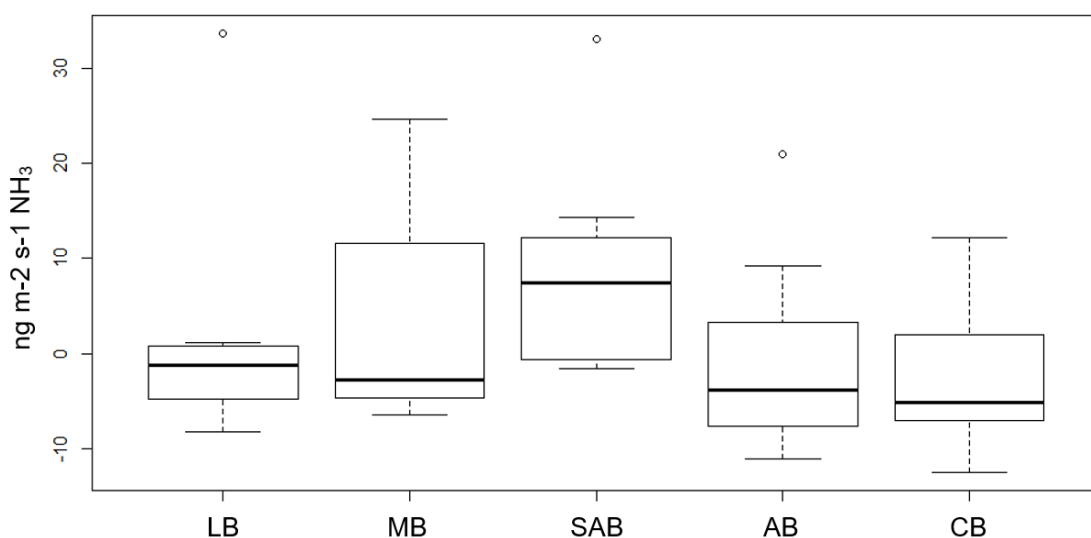


Figure 8. Boxplot of water-atmosphere NH_3 flux values for all northern subregion sites, September 2018 - April 2019. Bold horizontal lines represent the mean, rectangles the interquartile range and outermost horizontal lines the range. Circles represent individual outliers.

Table 21. Mean water NH_4^+ concentrations, $\text{NH}_{3(\text{eq})}$ values, atmospheric NH_3 concentrations and NH_3 water-atmosphere flux values of the northern subregion sites, September 2018 - April 2019. Standard deviations are displayed (in parentheses).

	NH_3 flux ($\text{ng m}^{-2} \text{s}^{-1}$)	Atmospheric NH_3 ($\mu\text{g}/\text{m}^3$)	$\text{NH}_{3(\text{eq})}$ value ($\mu\text{g}/\text{m}^3$)	Water NH_4^+ conc. (μM)	pH
LB	1.84 (13.32)	1.79 (1.51)	1.90 (2.25)	1.49 (1.34)	8.33 (0.09)
MB	3.30 (12.09)	1.98 (0.56)	1.91 (2.20)	1.61 (1.37)	8.26 (0.16)
SAB	8.68 (11.41)	2.10 (1.72)	4.02 (3.62)	2.68 (1.78)	8.39 (0.16)
AB	-0.80 (10.68)	2.23 (0.91)	1.98 (3.01)	1.52 (1.79)	8.30 (0.15)
CB	-2.61 (7.84)	2.78 (1.33)	1.75 (2.14)	1.50 (1.58)	8.27 (0.09)
<i>No. mean</i>	<i>2.08 (4.34)</i>	<i>2.17 (0.37)</i>	<i>2.31 (0.96)</i>	<i>1.76 (0.52)</i>	<i>8.31 (0.05)</i>

San Antonio Bay is the primary bay of the Guadalupe estuary system. The bay receives surface inflow from the Guadalupe River which is met by the San Antonio River ~9 km upstream of the estuary. Because of this, the total land area draining to the Guadalupe estuary includes the watersheds of both the San Antonio and Guadalupe rivers. Once combined, this watershed features the greatest percentages of both urbanized and agricultural land of all the

Coastal Bend estuary system watersheds (Bricker et al., 2007) (Appendix B). Additionally, San Antonio Bay is relatively small and receives a relatively great volume of freshwater inflow; a combination that produces the shortest residence time of all the Coastal Bend estuarine waters (Longley, 1994) (Appendix C). The high inflow to water volume of San Antonio Bay results in approximately 80% of total estimated N loading to the bay being delivered from river input, which is more than twice that estimated of the other two northern estuary systems (Longley, 1994). Being that the inorganic N transported by river inflow is dominated by NO_3^- rather than NH_4^+ , this mechanism cannot be directly related to resulting bay water NH_4^+ concentrations (Whitledge, 1989). Instead, it should be considered that the OM deposited by such substantial river inflow provides an abundance of raw material for estuarine microbial communities to break down and produce NH_4^+ .

Whitledge (1989) performed water quality assessments of San Antonio Bay for the Texas Water Development Board following a major flood event that occurred in the watershed of the San Antonio and Guadalupe rivers in July 1987. According to Whitledge (1989) in the months following the storm, a distinct freshwater plume was evident which deposited river-transported materials as it moved through the bay. The plume proceeded in a counterclockwise direction, leaving the mouth of the Guadalupe River and coursing along the western shore of the bay (Figure 9). Diminished DO levels along the path of the plume were observed, resulting from high rates of decomposition, and NH_4^+ concentrations increased considerably from May to August that year (Whitledge, 1989). Later, the same counterclockwise freshwater circulation pattern in San Antonio Bay was identified by MacIntyre and Cullen (1996) from an assessment of salinity gradients within the bay. These prior observations suggest that the location of our

study site (Aransas National Wildlife Refuge fishing pier) on the western shore of the bay was well positioned to receive riverine deposits of OM.

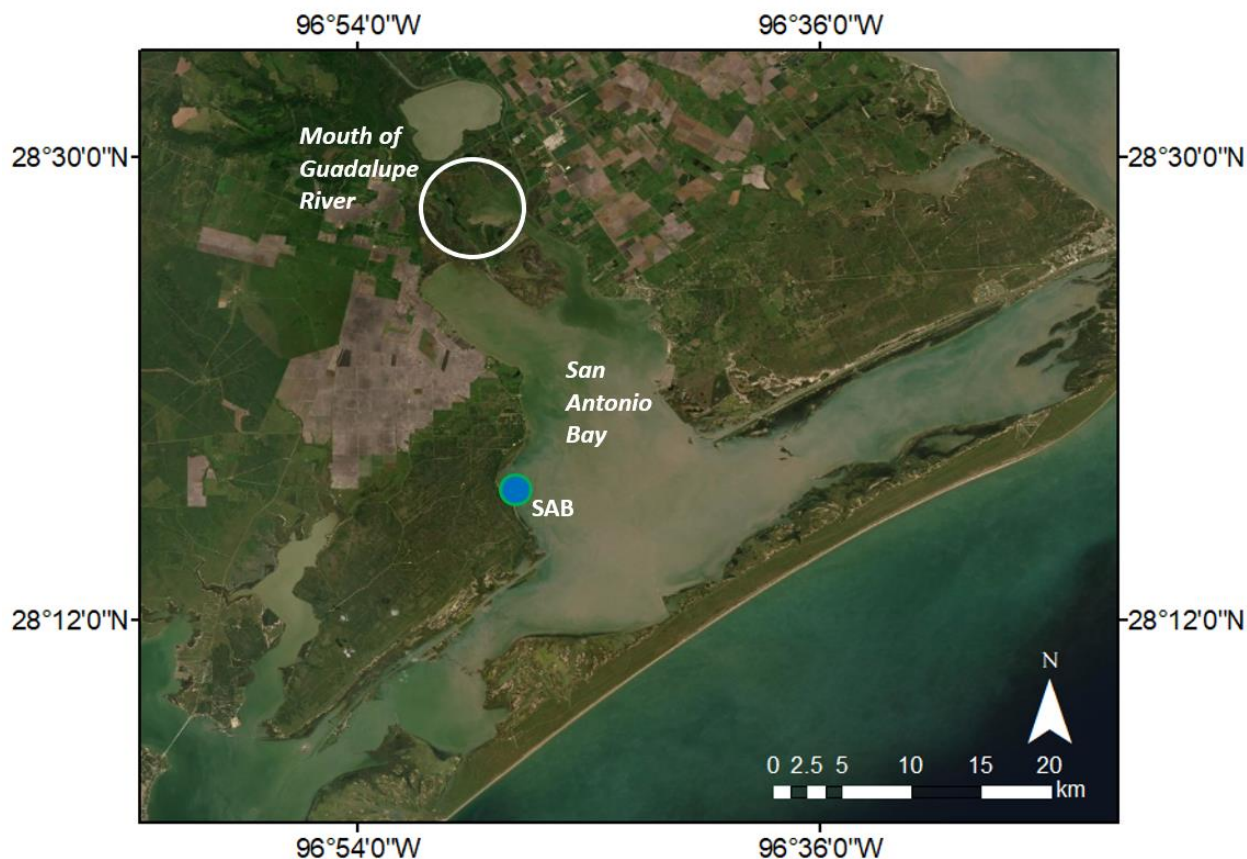


Figure 9. Map of San Antonio Bay displaying the mouth of the Guadalupe River and the SAB study site.

Before sampling for this study first took place at SAB in August 2018, a major rain event occurred over much of the Coastal Bend region between June 18 and 21. Approximately 23 cm of rain fell at SAB during that time, and was followed by additional rain events from July 5 to 9, and on August 1 (NOAA, 2019). The first water samples were obtained from SAB on August 19 and produced the mean NH_4^+ concentration of $4.03 \pm 0.86 \mu\text{M}$ for that month, which was followed by concentrations of $5.05 \pm 2.34 \mu\text{M}$ and 4.79 ± 2.34 in September and October, respectively (Table 22). Comparatively, the average NH_4^+ concentration of the remaining northern sites (MB, CB and AB) that were sampled beginning in August 2018, was 1.39 ± 0.29

μM in August, $4.14 \pm 1.33 \mu\text{M}$ in September, and $1.21 \pm 0.11 \mu\text{M}$ in October. While these mean concentrations reflect the seasonal NH_4^+ peak observed in September across the greater Coastal Bend, the August and October mean values contrast with the consistently elevated NH_4^+ concentrations observed at SAB during those same months.

Table 22. Mean water NH_4^+ concentrations of the northern subregion sites, August 2018 - October 2018. Values in bottom row represent the mean monthly NH_4^+ concentrations of MB, AB and CB only. Standard deviations are displayed (in parentheses).

NH_4^+ conc. (μM)	August 2018	September 2018	October 2018
SAB	4.03 (0.86)	5.05 (2.34)	4.79 (2.34)
MB	1.65 (0.70)	4.33 (2.80)	1.29 (0.11)
AB	1.08 (1.64)	5.37 (2.73)	1.09 (0.85)
CB	1.43 (1.66)	2.72 (1.61)	1.25 (1.14)
<i>MB, AB, CB mean</i>	<i>1.39 (0.29)</i>	<i>4.14 (1.33)</i>	<i>1.21 (0.11)</i>

Measured surface water DO levels were well below saturation at SAB during September and October sampling (71.9% and 73.7% of saturation, respectively) while remaining much nearer to saturation at the other northern sites (Table 23). This suggests that a considerably greater amount of microbial respiration was occurring in the water column of SAB during that time. It can be theorized that an influx of OM was received by the bay after the major rain event in June, followed by additional material from the rainfalls of July and early August. The OM was gradually deposited, processed into NH_4^+ and then resuspended by wind-driven mixing. Due both to the considerable volume of inflow from the Guadalupe River and the freshwater circulation patterns of San Antonio Bay, the amount of OM delivered to the SAB site likely exceeded that received by other northern bays following the same rain events. Because of this abundant supply of OM, the cycle of decomposition and resuspension may have continued for months beyond the summer rain events and supported the consistently elevated water NH_4^+ concentrations observed at SAB from August through October.

Table 23. Measured surface water DO % of saturation of the northern subregion sites, September 2018 - October 2018.

	September 2018	October 2018
DO (%) saturation		
LB	97.0	94.6
MB	90.5	129.0
SAB	71.9	73.7
AB	92.4	95.6
CB	85.7	85.4
<i>No. mean</i>	<i>87.5</i>	<i>95.6</i>

Wastewater contributions to the river inflow are worth considering here as well. The San Antonio River receives multiple state-permitted municipal outfalls before reaching the estuary, including those from the cities of Floresville, Falls City, Goliad and Kenedy (via Escondido Creek) (TCEQ, 2019). Likewise, the Guadalupe River receives wastewater from two outfall sites permitted to the city of Victoria. Furthermore, two municipalities discharge wastewater into an adjacent bayou (Tivoli) and directly into San Antonio Bay (Austwell) (TCEQ, 2019). Likely resulting from these outfalls, Wu et al. (2019) found a significantly greater concentration of bioavailable N in the San Antonio River than both the Aransas and Mission rivers. It appears that such high-quality material enriched the river inflow to San Antonio Bay and further contributed to the relatively high NH_4^+ concentrations and water-atmosphere NH_3 emissions that were commonly observed at SAB.

The site at San Antonio Bay displayed net water-atmosphere NH_3 emission that was of a greater magnitude than any site observed in this study. Furthermore, SAB consistently exhibited surface water NH_4^+ concentrations far greater than those of any nearby sites. Being situated on the western shore of San Antonio Bay, SAB was positioned to receive OM-enriched freshwater plumes as they entered the bay and then circulated in a counterclockwise direction. By this mechanism, the substantial rain events and subsequent inflows of the summer months would

have deposited considerable amounts of OM near SAB. Diminished DO concentrations which accompanied elevated NH_4^+ levels suggest that the microbial processing of that OM was occurring at those times. Additionally, wastewater inflow to the San Antonio and Guadalupe rivers was likely received at the site, providing highly bioavailable DOM and further contributing to elevated NH_4^+ concentrations. As a result, SAB produced anomalous water-atmosphere NH_3 fluxes, many times of exceptional magnitude. These conditions appear to be unique to SAB and the Guadalupe Estuary as the NH_3 fluxes of nearby sites were less often upward and typically much closer to zero.

4.2.2. Water-atmosphere NH_3 flux characteristics of two Coastal Bend primary-secondary bay estuary systems

The estuary systems of the Coastal Bend share similar geomorphic characteristics and typically are comprised of both a primary, more seaward bay and secondary, more inland bays (Montagna et al., 2018). In the northern subregion of this study two distinct estuary systems were sampled at both primary and secondary bay: Lavaca-Colorado estuary (MB and LB), Mission-Aransas estuary (AB and CB) (Figure 10). In contrast, the third northern system - the Guadalupe estuary - was sampled from only its primary bay (SAB). Being that multiple sites within the Lavaca-Colorado and Mission-Aransas estuary systems were observed, comparisons of the water-atmosphere NH_3 fluxes and supporting parameters between primary and secondary bays are possible. Such spatial comparisons present a valuable opportunity for further detailed analysis of NH_3 flux characteristics and will be investigated here.

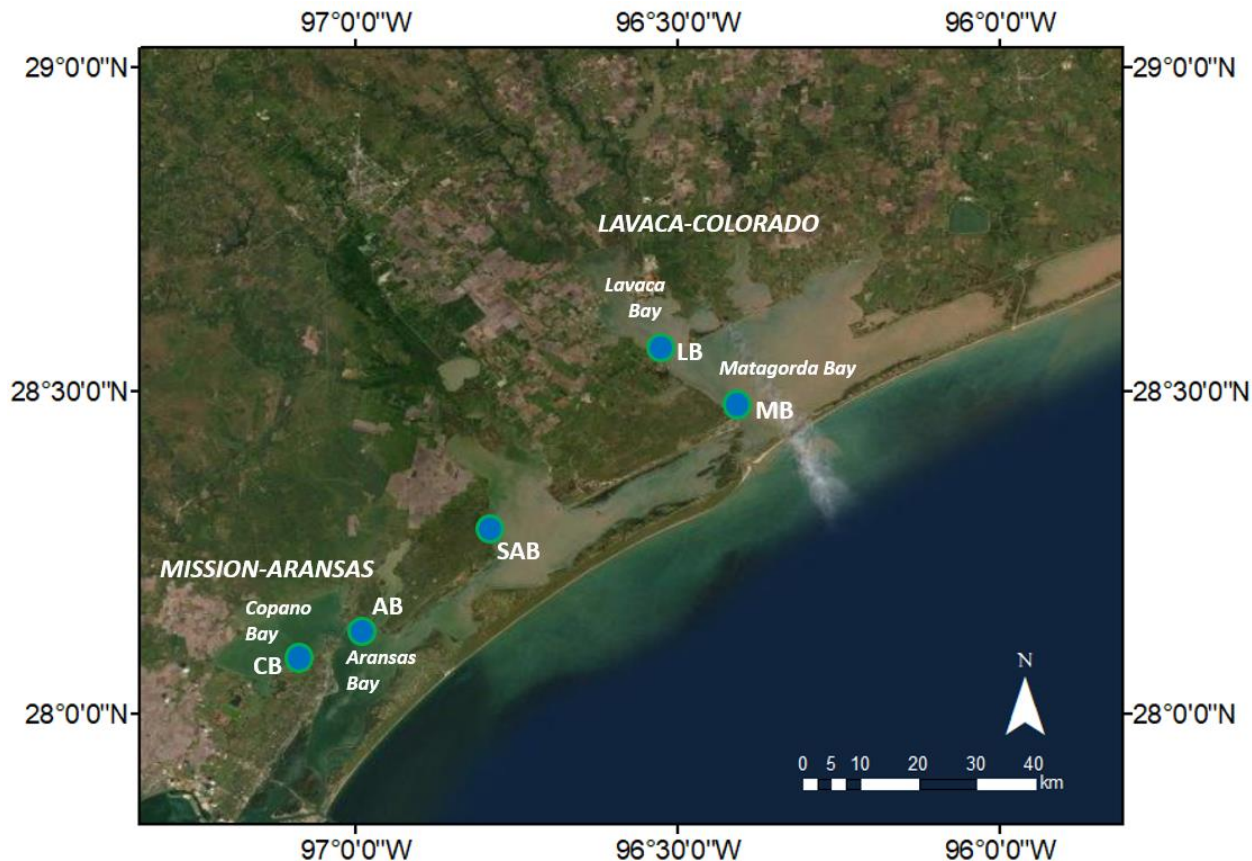


Figure 10. Map displaying the Lavaca-Colorado and Mission-Aransas estuaries, their respective bays and the study sites of the northern subregion.

Within the Lavaca-Colorado system, the mean NH_3 fluxes of LB ($1.84 \pm 13.32 \text{ ng m}^{-2} \text{ s}^{-1}$) and MB ($3.30 \pm 12.09 \text{ ng m}^{-2} \text{ s}^{-1}$) both denote net NH_3 emission of a comparable magnitude. The mean NH_3 fluxes of AB ($-0.80 \pm 10.68 \text{ ng m}^{-2} \text{ s}^{-1}$) and CB ($-2.61 \pm 7.84 \text{ ng m}^{-2} \text{ s}^{-1}$) denote net NH_3 deposition of a similar magnitude for the Mission-Aransas sites. As a result, the differences between the site mean NH_3 fluxes within those estuary systems are not significant (Lavaca-Colorado: $\chi^2(2) = 0.011$, $p = 0.916$, Mission-Aransas: $\chi^2(2) = 0.044$, $p = 0.834$) both by KW and HB testing. As NH_3 fluxes are influenced by surface water NH_4^+ concentrations, the above result has support in the analysis of Montagna et al. (2018) which found no significant differences in NH_4^+ concentrations between bays within the same estuary system. In the Lavaca-Colorado system, the lower salinity and higher pH observed of secondary (Lavaca) versus

primary (Matagorda) bays, mitigate the effect of slightly differing water NH_4^+ concentrations to produce $\text{NH}_3(\text{eq})$ values for the two bays which are nearly identical (MB: $1.91 \pm 2.20 \mu\text{g}/\text{m}^3 \text{NH}_3$, LB: $1.90 \pm 2.25 \mu\text{g}/\text{m}^3 \text{NH}_3$) (Table 23). The influence of pH and salinity had the opposite effect at the Mission-Aransas estuary. There, the $\text{NH}_3(\text{eq})$ values of the bays (AB: $1.98 \pm 3.01 \mu\text{g}/\text{m}^3$, CB: $1.75 \pm 2.14 \mu\text{g}/\text{m}^3$) diverged further than their mean water NH_4^+ concentrations, once factored with the additional water-side parameters.

Table 24. Monthly mean NH_3 water-atmosphere flux values, water NH_4^+ concentrations, pH values, salinity values, $\text{NH}_3(\text{eq})$ values and atmospheric NH_3 concentrations of individual sites within the Lavaca-Colorado and Mission-Aransas estuary systems. Standard deviations are displayed (in parentheses).

	NH_3 flux ($\text{ng m}^{-2} \text{s}^{-1}$)	Atmospheric NH_3 ($\mu\text{g}/\text{m}^3$)	$\text{NH}_3(\text{eq})$ value ($\mu\text{g}/\text{m}^3$)	Water NH_4^+ conc. (μM)	pH	Salinity (ppt)
8 mo. mean, LB	1.84 (13.32)	1.79 (1.51)	1.90 (2.25)	1.49 (1.34)	8.33 (0.09)	14.6 (5.29)
8 mo. mean, MB	3.30 (12.09)	1.98 (0.56)	1.91 (2.20)	1.61 (1.37)	8.26 (0.16)	24.5 (3.76)
<i>Lavaca-Col. mean</i>	<i>2.57 (1.03)</i>	<i>1.89 (0.13)</i>	<i>1.91 (0.01)</i>	<i>1.55 (0.08)</i>	<i>8.30 (0.05)</i>	<i>19.6 (7.00)</i>
8 mo. mean, AB	-0.80 (10.68)	2.23 (0.91)	1.98 (3.01)	1.52 (1.79)	8.30 (0.15)	15.3 (1.83)
8 mo. mean, CB	-2.61 (7.84)	2.78 (1.33)	1.75 (2.14)	1.50 (1.58)	8.27 (0.09)	9.9 (1.74)
<i>Mission-Ar. mean</i>	<i>-1.71 (1.28)</i>	<i>2.51 (0.39)</i>	<i>1.87 (0.16)</i>	<i>1.51 (0.01)</i>	<i>8.29 (0.02)</i>	<i>12.6 (3.82)</i>

Within the Lavaca-Colorado estuary, the mean atmospheric NH_3 concentrations of MB ($1.98 \pm 0.56 \mu\text{g}/\text{m}^3 \text{NH}_3$) and LB ($1.79 \pm 1.51 \mu\text{g}/\text{m}^3 \text{NH}_3$) were similar and helped produce mean NH_3 fluxes of the same direction and of a comparable magnitude (Table 24). Interestingly here, the mean atmospheric NH_3 concentration for the more inland, secondary bay (LB) was lower than that for the more seaward primary bay (MB). Consistently from October to February, measured atmospheric NH_3 at LB was less than that found at MB, despite the sites being measured within 90 minutes of one another and wind direction remaining the same at each location. As wind direction was from the south to southeast on four of five of the sampling dates, the greater atmospheric NH_3 concentrations observed at MB suggest the contribution of an urban NH_3 source local to the sampling site in the community of Port O'Connor, and/or a marine

NH₃ source; particularly during the late winter/early spring when NH₃ emission was often observed at the Gulf of Mexico site.

The water-atmosphere NH₃ fluxes of the Mission-Aransas sites were the only negative mean values calculated for the northern Coastal Bend sites during the eight-month study (Table 24). While of a similar magnitude, the lower mean NH_{3(eq)} value for CB coupled with a higher mean atmospheric NH₃ concentration resulted in a NH₃ flux value ($-2.61 \pm 7.84 \text{ ng m}^{-2} \text{ s}^{-1}$) lower than that of AB ($-0.80 \pm 10.68 \text{ ng m}^{-2} \text{ s}^{-1}$). Despite the sites only being 7.7 km apart, the mean atmospheric NH₃ concentration of CB was nearly 25% greater than that of AB. The positioning of the sites could offer an explanation, as CB was situated downwind of the towns of Fulton and Rockport while AB - positioned northeast of those populated areas - was not. As urban centers can be a localized source of atmospheric NH₃, due to vehicle and industrial emissions, CB may have received such contributions during six of the eight months observed when south or southeast winds were occurring at the time of sampling (Behera et al., 2013; Gong et al., 2011).

Four of the five sites of the northern subregion are included among the Lavaca-Colorado and Mission-Aransas estuaries. That point alone may help to explain why the water-atmosphere NH₃ flux characteristics observed of SAB appear to be contradictory of the subregion. When excluding SAB, inter-estuary consistency is apparent in the NH₃ fluxes of the remaining systems. Both estuaries produced a majority of depositional water-atmosphere NH₃ fluxes, owing to relatively low surface water NH₄⁺ concentrations during much of the sampling period. The Mission-Aransas sites produced greater mean atmospheric NH₃ concentrations relative to the Lavaca-Colorado sites, most likely the result of their proximity to the more densely populated areas of Rockport and Fulton. Intra-estuary variation in supporting NH₃ flux parameters was evident, once again for atmospheric NH₃, as the more inland secondary bay site of LB had an

anomalously lower concentration than that of MB, while the more inland CB site had a comparably greater concentration than AB. Such findings underscore the importance of observing multiple sites within estuary systems, as conditions within and conditions among may display unexpected variation and thus call for further investigation.

4.3. Temporal analysis of Corpus Christi area water-atmosphere NH₃ fluxes

Twelve total months of observation has allowed for a yearlong analysis of the water-atmosphere NH₃ fluxes of three sites local to the Corpus Christi metropolitan area. While the Corpus Christi area field campaign contributed to the regionwide study of the Coastal Bend, CCB UL and GM will be considered here together, within their more limited geographical context and separate from the rest of the Coastal Bend. Such an exclusion allows for analysis of all four seasons and twelve months, thus expanding the temporal range of water-atmosphere NH₃ flux investigation introduced earlier.

Beginning in May, low surface water NH₄⁺ concentrations paired with relatively moderate atmospheric NH₃ concentrations - all close to each site's respective twelve-month mean - led to net NH₃ deposition in the Corpus Christi area that month ($-4.24 \pm 13.62 \text{ ng m}^{-2} \text{ s}^{-1}$) (Table 24). UL was a notable exception, as a comparatively greater surface NH₄⁺ concentration ($1.58 \pm 0.91 \text{ } \mu\text{M}$) paired with a relatively lower atmospheric NH₃ concentration ($2.13 \pm 0.55 \text{ } \mu\text{g/m}^3$) led to net NH₃ emission ($11.49 \pm 27.57 \text{ ng m}^{-2} \text{ s}^{-1}$). A single substantial (>2.5 cm) rain even occurred in the area May 20-21 which resulted in a greatly elevated surface water NH₄⁺ concentration at UL on May 25 (NOAA, 2019). That measurement, paired with a relatively diminished atmospheric NH₃ concentration, produced an unusually high rate of NH₃ emission ($53.40 \pm 18.57 \text{ ng m}^{-2} \text{ s}^{-1}$). The magnitude of the May 25 exchange was great enough to ultimately drive the NH₃ flux at UL to a positive mean value in May.

Surface water NH_4^+ concentrations had increased considerably by June, however the mean atmospheric NH_3 concentration increased nearly threefold, resulting in net deposition across the area sites at the greatest magnitude calculated over the twelve-month period ($-11.57 \pm 14.77 \text{ ng m}^{-2} \text{ s}^{-1} \text{ NH}_3$) (Table 24). The atmospheric NH_3 concentrations observed at CCB were especially high during this time, resulting in a greatly depositional mean NH_3 flux ($-24.85 \pm 29.63 \text{ ng m}^{-2} \text{ s}^{-1}$) and ultimately influencing the areawide monthly minimum NH_3 flux mean in June. Upwind NH_3 emissions from Oso Bay are suspected of causing the exceptionally high atmospheric concentrations observed at CCB during this period. The elevated mean surface water NH_4^+ concentrations of the month - particularly at CCB and GM - were driven by considerable rainfall received in the area June 18-21. Further analysis of both the atmospheric NH_3 concentrations of CCB and the surface water NH_4^+ responses to the June rain event is offered later in this discussion.

Table 25. Monthly and seasonal mean water-atmosphere NH_3 flux values, atmospheric NH_3 concentrations, $\text{NH}_{3(\text{eq})}$ values and surface water NH_4^+ concentrations of Corpus Christi area sites, May 2018 - April 2019. Standard deviations are displayed (in parentheses).

	NH_3 flux ($\text{ng m}^{-2} \text{ s}^{-1}$)	Atmospheric NH_3 ($\mu\text{g}/\text{m}^3$)	$\text{NH}_{3(\text{eq})}$ value ($\mu\text{g}/\text{m}^3$)	Water NH_4^+ conc. (μM)
June 2018	-11.57 (14.77)	5.42 (3.02)	3.79 (1.55)	1.86 (1.18)
July 2018	-0.66 (9.58)	3.25 (1.41)	4.28 (1.57)	2.20 (1.56)
August 2018	24.85 (17.08)	1.92 (0.57)	6.93 (5.00)	3.58 (1.32)
<i>Summer mean</i>	<i>4.21 (18.69)</i>	<i>3.53 (1.77)</i>	<i>5.00 (1.69)</i>	<i>2.55 (0.91)</i>
September 2018	14.24 (10.50)	4.47 (1.94)	8.85 (6.25)	5.73 (1.90)
October 2018	16.38 (12.68)	1.87 (0.43)	4.91 (1.63)	4.18 (1.25)
November 2018	3.09 (8.15)	1.49 (0.28)	2.20 (1.66)	3.35 (1.96)
<i>Fall mean</i>	<i>11.24 (7.14)</i>	<i>2.61 (1.62)</i>	<i>5.32 (3.34)</i>	<i>4.42 (1.21)</i>
December 2018	-10.36 (0.91)	2.70 (0.44)	1.02 (0.59)	1.38 (0.70)
January 2019	0.93 (2.69)	1.16 (0.24)	1.38 (0.61)	3.10 (1.07)
February 2019	-1.10 (5.18)	1.87 (0.43)	1.46 (0.63)	3.92 (2.29)
<i>Winter mean</i>	<i>-3.51 (6.02)</i>	<i>1.91 (0.77)</i>	<i>1.29 (0.23)</i>	<i>2.80 (1.30)</i>
March 2019	-1.47 (9.29)	2.28 (0.57)	1.97 (0.75)	4.30 (1.73)
April 2019	0.43 (1.68)	3.00 (0.87)	3.39 (1.13)	2.62 (0.72)
May 2018*	-4.24 (13.62)	2.74 (0.70)	2.02 (1.74)	1.03 (0.48)
<i>Spring mean</i>	<i>-1.76 (2.35)</i>	<i>2.67 (0.36)</i>	<i>2.46 (0.81)</i>	<i>2.65 (1.64)</i>
12 mo. mean	2.54 (10.81)	2.68 (1.24)	3.52 (2.41)	3.10 (1.36)

Following the minimum in June, the areawide water-atmosphere NH_3 flux value increased to near zero in July before reaching a twelve-month maximum in August ($24.85 \pm 17.08 \text{ ng m}^{-2} \text{ s}^{-1}$) (Table 25). The dramatic shift in extremes over the summer was a result of steadily increasing water NH_4^+ concentrations and $\text{NH}_{3(\text{eq})}$ values, along with atmospheric NH_3 concentrations in July and August which were diminished relative to the exceptionally high values of June. The major rain event of June appears to have influenced surface water NH_4^+ concentrations into July, when additional rainfall was received. A dry period followed, yet NH_4^+ concentrations increased considerably in August. With no rainfall to force freshwater inflows to CCB and UL or potential sediment porewater discharge at GM, the increase in surface water NH_4^+ appears to be a result of in-situ OM remineralization. Further supporting this explanation were the below-average pH values observed across the area sites along with gradually diminishing DO measurements at CCB throughout August. Due to the seasonality of these observations, it may be considered that the breakdown of summer phytoplankton communities was occurring in Corpus Christi Bay at this time (Turner et al., 2015).

August, September and October produced the three greatest monthly mean NH_3 fluxes of the Corpus Christi area sites during the study (Table 26). These were driven by individual NH_3 flux maximums at CCB ($39.45 \pm 33.32 \text{ ng m}^{-2} \text{ s}^{-1}$) and UL ($29.04 \pm 26.43 \text{ ng m}^{-2} \text{ s}^{-1}$) in August, and GM ($12.13 \pm 24.30 \text{ ng m}^{-2} \text{ s}^{-1}$) in September. Monthly mean water NH_4^+ concentrations during this three-month span were well above the area's twelve-month average, while atmospheric NH_3 concentrations in August and October were well below their twelve-month mean. In September, atmospheric NH_3 increased to the year's second highest mean value ($4.47 \pm 1.94 \text{ } \mu\text{g/m}^3$) but was outpaced by a mean $\text{NH}_{3(\text{eq})}$ value which reached its twelve-month maximum ($8.85 \pm 6.25 \text{ } \mu\text{g/m}^3$) that same month. As was discussed earlier, decaying summer

phytoplankton communities are suspected of providing a high-quality source of DOM available for biological processing in the area waters (Wu et al., 2019). The remineralization of this supply of bioavailable material would have sustained elevated surface water NH_4^+ concentrations, which in turn would influence NH_3 emission.

Table 26. Individual monthly mean water-atmosphere NH_3 flux values, atmospheric NH_3 concentrations, $\text{NH}_{3(\text{eq})}$ values and surface water NH_4^+ concentrations of Corpus Christi area sites, August 2018 - October 2018. Standard deviations are displayed (in parentheses).

	NH_3 flux ($\text{ng m}^{-2} \text{s}^{-1}$)	Atmospheric NH_3 ($\mu\text{g}/\text{m}^3$)	$\text{NH}_{3(\text{eq})}$ value ($\mu\text{g}/\text{m}^3$)	Water NH_4^+ conc. (μM)	Water temp. ($^{\circ}\text{C}$)
Aug 2018, CCB	39.45 (33.32)	2.43 (1.31)	12.29 (6.45)	5.07 (3.66)	31.9 (1.9)
Aug 2018, UL	29.04 (26.43)	2.03 (1.09)	6.11 (3.93)	3.13 (2.29)	32.0 (1.8)
Aug 2018, GM	6.06 (18.17)	1.31 (0.93)	2.39 (2.49)	2.55 (2.83)	30.2 (0.9)
<i>August mean</i>	<i>24.85 (17.08)</i>	<i>1.92 (0.57)</i>	<i>6.93 (5.00)</i>	<i>3.58 (1.32)</i>	<i>31.4 (1.0)</i>
Sep 2018, CCB	25.64 (32.22)	6.16 (1.48)	16.01 (8.29)	7.88 (4.11)	29.1 (0.3)
Sep 2018, UL	4.95 (12.26)	4.91 (2.27)	6.02 (4.12)	5.06 (3.17)	29.8 (0.4)
Sep 2018, GM	12.13 (24.30)	2.35 (0.53)	4.51 (3.70)	4.26 (3.55)	30.2 (1.0)
<i>September mean</i>	<i>14.24 (10.51)</i>	<i>4.47 (1.94)</i>	<i>8.85 (6.25)</i>	<i>5.73 (1.90)</i>	<i>29.7 (0.6)</i>
Oct 2018, CCB	19.42 (7.48)	1.49 (0.82)	5.35 (2.08)	4.08 (2.11)	26.0 (4.3)
Oct 2018, UL	27.26 (21.18)	1.78 (1.61)	6.28 (3.48)	5.47 (3.69)	26.6 (4.6)
Oct 2018, GM	2.46 (9.83)	2.33 (0.90)	3.11 (1.76)	2.98 (2.61)	27.4 (3.7)
<i>October mean</i>	<i>16.38 (12.68)</i>	<i>1.87 (0.43)</i>	<i>4.91 (1.63)</i>	<i>4.18 (1.25)</i>	<i>26.7 (0.7)</i>

Following a steady decline in mean water-atmosphere flux values from October, a winter minimum NH_3 flux for the Corpus Christi sites was reached in December ($-10.36 \pm 0.91 \text{ ng m}^{-2} \text{ s}^{-1}$). While nearly of the same magnitude as the twelve-month NH_3 flux minimum experienced in June, the conditions which allowed for December's low value were quite different. The mean monthly atmospheric NH_3 concentration measured that month barely exceeded the twelve-month average, compared to the mean NH_3 maximum which occurred in June (Table 27). Water NH_4^+ concentrations were similarly low between the two months, however December's $\text{NH}_{3(\text{eq})}$ values were among the smallest determined during the study; values for UL ($1.00 \pm 1.14 \mu\text{g}/\text{m}^3$) and GM ($0.45 \pm 0.51 \mu\text{g}/\text{m}^3$) were minimums for those respective sites. The resulting areawide mean $\text{NH}_{3(\text{eq})}$ value ($1.02 \pm 0.59 \mu\text{g}/\text{m}^3$) for December was a twelve-month low as well, and despite the

near-average mean atmospheric NH₃ concentration observed that month, the resulting NH₃ flux was strongly depositional; approaching the same magnitude as that calculated for June.

Table 27. Individual monthly mean water-atmosphere NH₃ flux values, atmospheric NH₃ concentrations, NH_{3(eq)} values and surface water NH₄⁺ concentrations of Corpus Christi area sites for June and December 2018. Standard deviations are displayed (in parentheses).

	NH₃ flux (ng m ⁻² s ⁻¹)	Atmospheric NH₃ (µg/m ³)	NH_{3(eq)} value (µg/m ³)	Water NH₄⁺ conc. (µM)	Water temp. (°C)
Jun 2018, CCB	-24.85 (29.63)	8.88 (2.87)	5.30 (6.03)	2.46 (3.07)	30.5 (0.8)
Jun 2018, UL	-14.20 (16.69)	4.12 (0.89)	2.19 (1.96)	0.50 (0.45)	33.1 (0.6)
Jun 2018, GM	4.33 (29.44)	3.27 (1.48)	3.88 (3.87)	2.61 (2.58)	29.8 (0.7)
<i>June mean</i>	<i>-11.57 (14.77)</i>	<i>5.42 (3.02)</i>	<i>3.79 (1.55)</i>	<i>1.86 (1.18)</i>	<i>31.1 (1.7)</i>
Dec 2018, CCB	-9.90 (8.65)	3.18 (0.77)	1.62 (2.23)	2.18 (2.75)	18.5 (2.6)
Dec 2018, UL	-9.77 (5.44)	2.34 (0.90)	1.00 (1.14)	1.05 (1.07)	20.2 (1.0)
Dec 2018, GM	-11.40 (4.43)	2.58 (1.27)	0.45 (0.51)	0.91 (1.01)	18.5 (0.7)
<i>December mean</i>	<i>-10.36 (0.91)</i>	<i>2.70 (0.44)</i>	<i>1.02 (0.59)</i>	<i>1.38 (0.70)</i>	<i>19.1 (1.0)</i>

Two situations have just been identified which can produce NH₃ deposition of an outstanding magnitude; 1. warm temperatures with very high atmospheric NH₃ concentrations and moderately low water NH₄⁺ concentrations, and 2. cold temperatures with near-average atmospheric NH₃ concentrations and moderately low water NH₄⁺ concentrations. The influence of the additional water-side parameters - particularly temperature - is evident in this comparison, especially when considering the NH_{3(eq)} values of the two months. In the case of situation 1 - as observed in June - a mean water NH₄⁺ concentration of 1.86 ± 1.18 µM along with warm water temperatures, contributed to a NH_{3(eq)} value of 3.79 ± 1.55 µg/m³ NH₃ (Table 27) For situation 2 - as observed in December - a mean water concentration of 1.38 ± 0.70 µM combined with cold water temperatures, resulted in a NH_{3(eq)} value of 1.02 ± 0.59 µg/m³ NH₃. Despite the similar surface water NH₄⁺ concentrations, an atmospheric NH₃ concentration nearly four times greater than that of December is required to cause NH₃ deposition in June. This displays both the remarkable magnitude of the atmospheric NH₃ concentrations observed in June, as well as the

sensitivity to water temperature inherent to the mathematical model used here to determine water-atmosphere NH_3 fluxes.

Despite similarly low water temperatures as December, the areawide mean NH_3 flux increased considerably in January to a positive value ($0.93 \pm 2.69 \text{ ng m}^{-2} \text{ s}^{-1}$). That sudden reversal of NH_3 flux was driven by a twofold increase in mean water NH_4^+ concentration coupled with a mean atmospheric NH_3 concentration which plummeted to its twelve-month minimum ($1.16 \pm 0.24 \text{ } \mu\text{g/m}^3$). Low water temperatures limited the magnitude of NH_3 emission, which otherwise could have been much greater due to the great discrepancy between water and air concentrations. A substantial ($>1.5 \text{ cm}$) rain event on January 15 appears to have influenced the elevated water NH_4^+ concentrations observed across the area six days later (NOAA, 2019). Southern winds observed on both January sampling dates (7 and 21) contributed to the relatively low atmospheric NH_3 concentrations, as arriving air masses from the Gulf of Mexico would not have been exposed to terrestrial NH_3 sources.

February saw another increase in mean water NH_4^+ concentration, however this was offset by a greater increase in atmospheric NH_3 which allowed the month's mean NH_3 flux to return to deposition ($-1.10 \pm 5.18 \text{ ng m}^{-2} \text{ s}^{-1}$). Another areawide increase in both surface water NH_4^+ and atmospheric NH_3 resulted in a similar mean NH_3 flux March ($-1.47 \pm 9.29 \text{ ng m}^{-2} \text{ s}^{-1}$). The increasing surface water NH_4^+ concentrations were led by those of GM, which exhibited its two highest monthly mean values for that parameter in February ($6.54 \pm 4.76 \text{ } \mu\text{M}$) and March ($6.19 \pm 3.33 \text{ } \mu\text{M}$). Those exceptional monthly means were driven by individual surface water NH_4^+ observations on February 17 ($10.64 \pm 2.16 \text{ } \mu\text{M}$) and March 3 ($9.14 \pm 1.27 \text{ } \mu\text{M}$). As no substantial ($>1.0 \text{ cm}$) rainfalls were received in the area between January 27 and March 19, the severely elevated NH_4^+ concentrations may have resulted from local regenerative processes

within the Gulf, or from NH_4^+ -enriched benthic porewater mixing into the water column by the agitation of shallow water sediments (NOAA, 2019). Water-atmosphere NH_3 fluxes at GM were strongly upward on those dates but tempered somewhat by low water temperatures.

The elevated surface water NH_4^+ concentration observed at UL on March 3 is suspected to have been influenced by the recent Gulf NH_3 emissions, which may have invaded the surface water of the Upper Laguna Madre following transport across North Padre Island. A strong depositional NH_3 flux at UL on February 17 ($-7.70 \pm 0.76 \text{ ng m}^{-2} \text{ s}^{-1}$) supports this explanation, as it appears likely that NH_3 deposition was occurring there for days prior to the March 3 observations. For the remainder of the month, the mean NH_3 fluxes of UL and CCB remained depositional at a great enough magnitude to drive the areawide NH_3 flux to a negative value for March ($-1.47 \pm 9.29 \text{ ng m}^{-2} \text{ s}^{-1}$).

The mean NH_3 flux across the area returned to emission in April ($0.43 \pm 1.68 \text{ ng m}^{-2} \text{ s}^{-1}$), even as the mean atmospheric NH_3 concentration ($3.00 \pm 0.87 \text{ } \mu\text{g/m}^3$) rose beyond its twelve-month average and the mean water NH_4^+ concentration ($2.62 \pm 0.72 \text{ } \mu\text{M}$) dipped below its average. Warming water temperatures paired with elevated pH values pushed the mean $\text{NH}_{3(\text{eq})}$ value over the mean atmospheric NH_3 value and allowed for net NH_3 emission to occur. An emerging spring phytoplankton community is suspected of utilizing available NH_4^+ at this time and driving pH values up as enhanced levels of photosynthesis resulting from such growth would have depleted CO_2 in the water column. All area sites displayed decreasing surface water NH_4^+ concentrations between their April sampling dates on the 5th and 18th, as atmospheric NH_3 concentrations at all sites increased. The atmospheric change likely resulted from western winds on April 18 which may have delivered NH_3 from inland sources to the coast. In contrast, had sampling been performed on a day with southern winds, it is likely that atmospheric NH_3

concentrations would have been comparatively diminished and the resulting net NH_3 emission calculated for the month would have increased considerably in magnitude.

Upon analysis, a distinct seasonal pattern emerges from this yearlong analysis of Corpus Christi area water-atmosphere NH_3 fluxes. Late spring/early summer displayed generally depositional water-atmosphere NH_3 fluxes, driven by excessive atmospheric NH_3 concentrations, while the late summer/early fall period produced the greatest water-atmosphere NH_3 emission of the study. Seasonal rain events paired with the breakdown of summer phytoplankton communities appear to have caused the dramatically increased water NH_4^+ concentrations observed in August and September and thus, the resulting water-atmosphere NH_3 emissions. From late fall through early spring, water-atmosphere NH_3 fluxes were generally depositional with values close to zero, with the strong NH_3 deposition observed in December being a notable exception. A positive mean water-atmosphere NH_3 flux value was produced again in April, although this too remained near zero. The conditions necessary to produce NH_3 deposition of great magnitude were present twice during the study - early summer and early winter - while the conditions needed for great NH_3 emission were present only in the late summer/early fall. It is believed that such seasonality is driven by annual biological and meteorological cycles and is therefore subject to inter-annual variability. For the Corpus Christi area at least, it should be expected that water-atmosphere NH_3 fluxes will remain close to zero for much of the year, with periods of great NH_3 emission and deposition occurring episodically. Due to the characteristic variability of the region's climate however, the exact timing and duration of those great magnitude events could vary greatly from year to year.

4.4. Spatial analysis of Corpus Christi area water-atmosphere NH₃ fluxes

The following spatial analysis takes advantage of the weekly to biweekly sampling of the Corpus Christi area sites to offer a high-resolution analysis of various surface water and atmospheric processes which directly influenced water-atmosphere NH₃ fluxes. Corpus Christi Bay, the Upper Laguna Madre and the nearshore Gulf of Mexico displayed both individual characteristics and site-to-site interactions which are worthy of detailed investigations. Particular attention will be given to various atmospheric dynamics, surface water transport and responses to rain events of the Corpus Christi area sites. Specific sampling periods have been selected that best exemplify these processes, however all respective occurrences are not necessarily discussed. This has been done to fulfill the objective of providing additional, detailed insight on localized water-atmosphere NH₃ flux dynamics by examination of the study's most apparent demonstrations.

4.4.1. Atmospheric NH₃ dynamics of Corpus Christi area

Previously, Berner and Felix (2020) observed a minimum mean atmospheric NH₃ concentration at a Gulf-side site on North Padre Island, among eight sites in the Corpus Christi area sampled over twelve months. The same was found of three sites here, as the mean atmospheric NH₃ concentration of GM was lower than all others, and considerably lower than that of CCB. With winds from the south to southeast present on 74% of the sampling dates, much of the air which was sampled had passed over only open water before reaching the site. With limited opportunity to pick up NH₃ emissions from terrestrial sources, the air at GM was often diminished in NH₃ relative to the other Corpus Christi area sites, including UL which was also located on the federally protected Padre Island National Seashore. As expected, the site of most urban influence - CCB - had the highest mean atmospheric NH₃ concentration, which was

driven by multiple periods of exceptionally high concentrations. Most notably was a period from May 25 to July 6, 2018, where remarkably high atmospheric NH_3 concentrations at CCB resulted in strong NH_3 deposition despite periodic surges in surface water NH_4^+ concentrations. Such dynamics helped characterize the water-atmosphere NH_3 flux signature of CCB and so, warrant a more detailed investigation.

On May 25 the atmospheric NH_3 concentration at CCB skyrocketed to $10.02 \mu\text{g}/\text{m}^3$ from $1.06 \mu\text{g}/\text{m}^3$ just a week earlier, and after three consecutive weeks of measurements well below $2.00 \mu\text{g}/\text{m}^3$ NH_3 (Figure 11). Wind direction during that time was consistent, blowing from either the southeast or south-southeast, while both air and water temperatures increased modestly ($27\text{-}32^\circ\text{C}$ and $26\text{-}30^\circ\text{C}$, respectively). A local rain event occurred overnight May 21-22 depositing approximately 2.5 cm at the CCB site, just three days prior to the order of magnitude rise in atmospheric NH_3 (NOAA, 2019). Following that dramatic increase, atmospheric NH_3 dropped on June 1 to $3.96 \mu\text{g}/\text{m}^3$ and then shot back up to $10.67 \mu\text{g}/\text{m}^3$ NH_3 on June 8. Atmospheric concentrations then remained considerably elevated ($> 8.5 \mu\text{g}/\text{m}^3$) for three more weeks, through July 6. That period included the rain event of June 18-21, with samples obtained on the 22nd - hours after the rainfall ended - and then again one week later, on June 29. On all sample dates from June 1 to July 6, winds were consistently from south-southeast to east-southeast, and both air and water temperatures remained steady. On July 6, both water and air temperatures dropped to 28.5°C and 20.0°C , respectively, as the wind blew from the north-northwest. Observed atmospheric NH_3 dropped to $5.06 \mu\text{g}/\text{m}^3$ on that date and would only exceed $5.0 \mu\text{g}/\text{m}^3$ NH_3 on four of the remaining 25 sampling dates of the study.

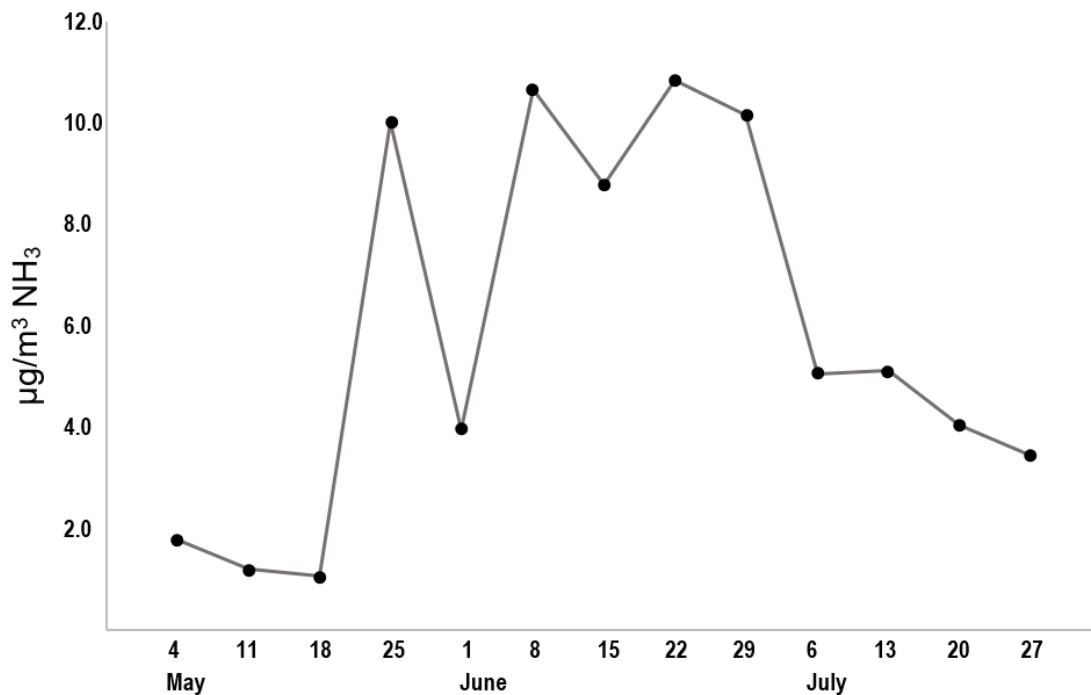


Figure 11. Graph of weekly atmospheric NH₃ concentrations in µg/m³ at CCB, May 4 - July 27, 2018.

Conversely, water NH₄⁺ concentrations at CCB were low (< 1.0 µM) to below detection between May 25 and June 8, before rising to 1.68 µM NH₄⁺ on June 15 and then rapidly increasing to 6.74 µM NH₄⁺ on June 22, following the rain event (Table 28). While high atmospheric NH₃ concentrations often coincided with high water NH₄⁺ concentrations during the study, the observation of diminished NH₄⁺ alongside extremely elevated atmospheric NH₃ at CCB the four weeks prior to the rain event is noteworthy, as is the great magnitude of NH₃ deposition resulting from those conditions. Low water NH₄⁺ concentrations were common across all Corpus Christi area sites in May and the first half of June, and while a brief rain event on May 20-21 temporarily elevated water NH₄⁺ concentrations on May 25, those values rapidly diminished by the next sampling one week later.

Table 28. Individual monthly mean water-atmosphere NH₃ flux values, atmospheric NH₃ concentrations and surface water NH₄⁺ concentrations of CCB, May 25 - July 6, 2018. Standard deviations are displayed (in parentheses).

CCB	NH₃ flux (ng m⁻² s⁻¹)	Atmospheric NH₃ (μg/m³)	Water NH₄⁺ conc. (μM)
<i>May 20-21 rain</i>			
May 25, 2018	-38.06 (0.16)	10.02	0.98 (0.02)
June 1, 2018	-30.66 (1.27)	3.96	0.22 (0.07)
June 8, 2018	-53.21 (<0.01)	10.67	0.05 (<0.01)
June 15, 2018	-37.39 (13.69)	8.77	1.27 (0.58)
<i>June 18-21 rain</i>			
June 22, 2018	26.73 (17.26)	10.85	7.80 (1.50)
June 29, 2018	-29.71 (7.50)	10.16	2.96 (0.41)
July 6, 2018	-9.90 (2.41)	5.06	1.37 (0.25)

While water column transformations and phytoplankton uptake may explain the low surface water NH₄⁺ observations, the continuously elevated atmospheric NH₃ concentrations at CCB appear to have resulted from sources away from the site. It is worth considering the time of atmospheric NH₃ sampling; during May and June local sites were visited beginning with CCB around 10:00 CST, followed by UL and GM just before and after noon. In Houston, TX, Gong et al. (2011) observed elevated morning atmospheric NH₃ concentrations which peaked around 11:00 CST during summer months and considered terrestrial sources such as dew evaporation and vegetation emissions as possible influences. With wind directions consistently from the S to SE during the May-June sampling of this study, such natural terrestrial sources should likewise be considered.

Another natural source local to CCB may have factored into the elevated atmospheric NH₃ concentrations observed during this time. Oso Bay, which surrounds the south side of Ward Island (location of TAMUCC) is a freshwater source which joins Corpus Christi Bay at an inlet ~1.3 km east of the CCB site (Figure 12). Oso Bay receives inflow from Oso Creek, a freshwater source draining a mixed agricultural and urban watershed from the southwest, as well

as processed cooling water from the Barney Davis Power Plant, a municipal wastewater outfall and multiple ephemeral urban discharges (Whitledge, 1989; Wetz et al., 2016). Excessive water NH_4^+ concentrations were observed at sites throughout Oso Bay by Wetz et al. (2016) with locations near the municipal outfall ($383 \mu\text{M} \pm 231 \text{NH}_4^+$) and near a drainage outlet of a local golf course ($96.0 \pm 128 \mu\text{M} \text{NH}_4^+$) - both on the western side of the bay - being particularly enriched. While water NH_4^+ observations varied greatly among locations and over time throughout the three-year study, the frequency and regularity of concentrations of such impressive magnitude offers enough evidence that substantial NH_4^+ loading has been occurring within Oso Bay (Wetz et al., 2016).

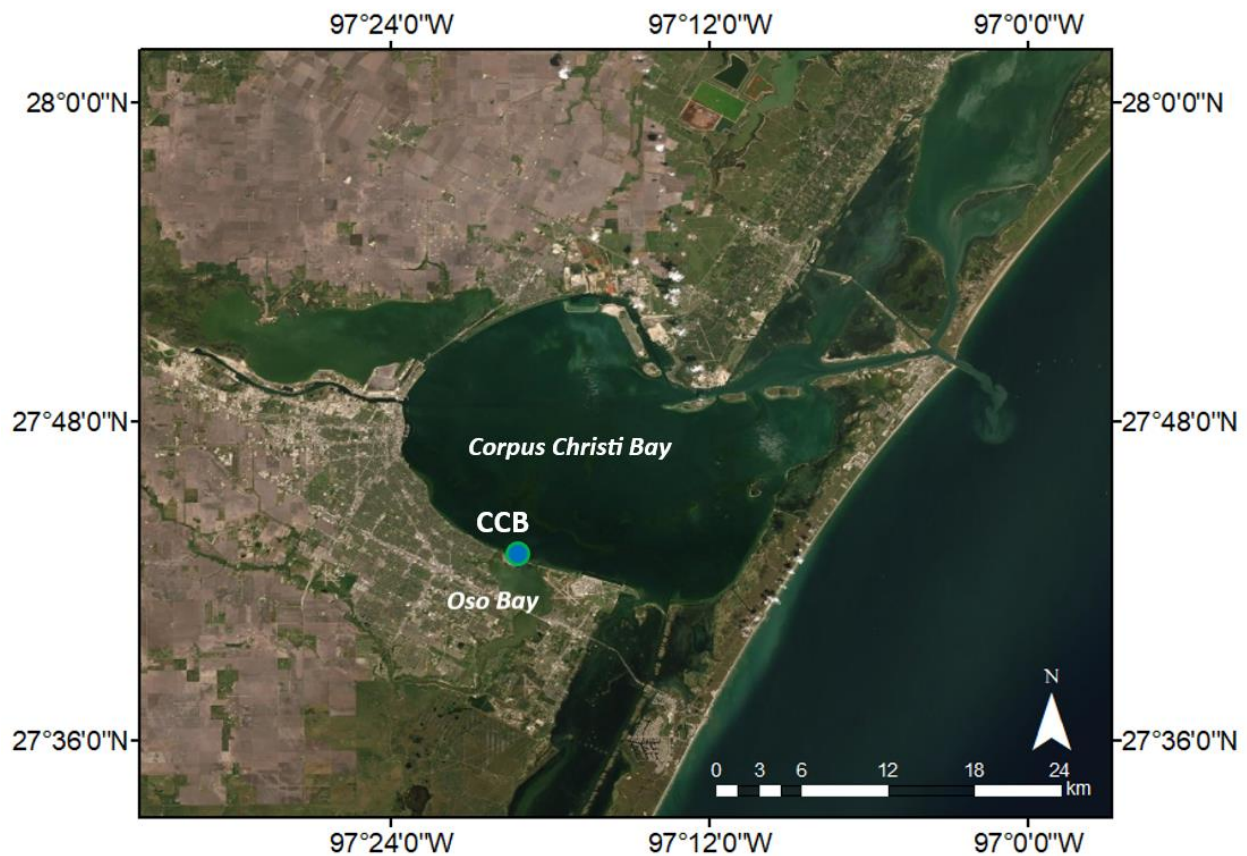


Figure 12. Map showing Oso Bay relative to Corpus Christi Bay and CCB site.

Sites on the western shore of Oso Bay received much of the DOM and NH_4^+ enriched inflow, however there was evidence that water from that end was being transported across the bay (Wetz et al., 2016). NH_4^+ processing within the water column was observed during that study as well, as a phytoplankton bloom was suspected of diminishing local water NH_4^+ concentrations in June 2012. Despite the lack of homogenous distribution and even with the potential for algal uptake, the substantial NH_4^+ inputs to Oso Bay combined with warm water temperatures and even moderate pH levels can facilitate NH_3 emission. When considering the remarkable NH_4^+ water concentrations observed by Wetz et al. (2016), the magnitude of such NH_3 emissions could be far greater than any observed in our study. With such a potentially tremendous atmospheric NH_3 source existing nearly immediately upwind of our Corpus Christi Bay sampling site, the suspicion of Oso Bay emissions causing locally elevated NH_3 concentrations is reasonable and warrants further investigation.

4.4.2. Surface water transport and NH_4^+ concentrations of Corpus Christi area

The mean October NH_4^+ concentration for the Corpus Christi area ($4.18 \pm 1.25 \mu\text{M}$) dropped from that of September ($5.73 \pm 1.90 \mu\text{M}$), within a greater seasonal trend of diminishing surface water NH_4^+ . Despite that decline in the areawide mean, the mean October NH_4^+ concentration of UL increased to $5.47 \pm 3.69 \mu\text{M}$, the twelve-month maximum at that site. That value was influenced by an exceptionally high NH_4^+ concentration found on October 20 ($9.24 \pm 1.68 \mu\text{M}$) (Table 29). Just to the north, NH_4^+ concentration of $6.09 \pm 2.04 \mu\text{M}$ was found at CCB on the same day. That measurement followed a localized rain event from October 18-19 which deposited > 3.0 cm at CCB, yet < 1.0 cm at UL (NOAA, 2019). Although elevated water NH_4^+ concentrations were found at each site just a day later, NH_4^+ at UL was more than 50% higher than that of CCB, despite receiving much less rainfall. This is noteworthy as the Upper Laguna

Madre features no direct freshwater inflows, while Corpus Christi Bay has multiple, including the Nueces River from the west and Oso Creek from the south. For a site served by such surface inflows, a sudden spike in nutrient concentrations is expected following a substantial rain event (Mooney and McClelland, 2012). To see such a pulse of NH_4^+ where there are no surface inflows and when little rain was received suggests a transport of that nutrient to the site by another mechanism.

Table 29. Surface water NH_4^+ concentrations of CCB and UL in μM , October 20, 2018. Standard deviations are displayed (in parentheses).

	CCB	UL
Water NH_4^+ conc. (μM)		
<i>October 18-19 rain</i>		
October 20, 2018	6.09 (2.04)	9.24 (1.68)

A northern wind was present during the sampling at both CCB and UL on October 20 and had been occurring consistently over the prior five days in the Corpus Christi area. With such a prolonged influence of consistent northern winds, it is likely that surface water was being transported from the bay southward towards the lagoon over that time. Wind is an important driver of surface currents in both Corpus Christi Bay and the Upper Laguna Madre, coupling with tidal action to determine surface circulation between the water bodies (Islam et al., 2011). This is a complex interaction however, and so conflicting reports on water movement between the bay and Upper Laguna Madre exist in the literature. Islam et al. (2011) suggested that the advection of saline waters from the Laguna Madre caused water column stratification in southeastern Corpus Christi Bay. Conversely, Hedgpeth (1947) identified an underwater sill along the southern rim of the Corpus Christi Bay basin that he suggested prevented the higher saline waters of the Laguna Madre from entering the bay, while allowing less dense freshwater plumes to migrate southward. Whitley (1989) observed bidirectional exchange between the

bay and lagoon, although six of eight observed months displayed predominant outflow from Corpus Christi Bay into the Laguna Madre.

Multiple observations from this study have agreed with the presence of a south moving, more fresh layer of water, including those of October 20. It is believed that the localized rainfall received at CCB from October 18-19 and subsequent inflow from the Nueces River may have migrated along the southern shore of Corpus Christi Bay, past CCB before turning southward at the junction of the bay and the Upper Laguna Madre, in a manner described by Whitley (1989). Surface inflow from Oso Bay may have joined the advancing plume just east of CCB, and considering the wastewater contributions to that bay, could have further enriched the plume in DOM and/or NH_4^+ (Wetz et al., 2016).

As with Oso Bay, wastewater inflows have been identified as contributing highly bioavailable DOM to the Nueces River (Longley, 1994; Wu et al., 2019). Following a rain event of great enough magnitude, such material would be transported into Nueces Bay and eventually, into Corpus Christi Bay. Whether from the Nueces River, Oso Bay or both, it is quite likely that the inflow received by Corpus Christi Bay following the October 18-19 rain event was enriched in high-quality DOM and/or NH_4^+ . It can be theorized then that a freshwater plume of such composition passed by the CCB site before being transported to UL along southward surface currents driven by the prevailing northern winds. Considering that the surface water of UL had a considerably higher NH_4^+ concentration than CCB on October 20, it is possible that due to timing, a more highly NH_4^+ concentrated area of the plume was measured at UL after having already passed by CCB when that site was observed.

4.4.3. Surface water NH_4^+ responses to rain events in Corpus Christi area

As been detailed numerous times in this discussion, rain events force changes in surface water NH_4^+ concentrations, which in turn influence the direction of resulting water-atmosphere NH_3 fluxes. A variety of mechanisms appear to govern this process including wet NH_4^+ deposition, inflows of DOM/ NH_4^+ enriched freshwater, surface transport of DOM/ NH_4^+ enriched water, submarine discharge of NH_4^+ enriched groundwater and the transfer of NH_4^+ enriched pore water from sediments into the water column. The frequent sampling of the Corpus Christi area sites during a relatively wet twelve-month period allowed for detailed observation of these surface waters' responses to periodic rain events. The following discussion offers an analysis of such observations, with the objective of providing further insight on the physical and biogeochemical processes which influence water-atmosphere NH_3 flux near the geographical center of the Coastal Bend.

A local weather event deposited 2.5 cm of rain between May 20-21, 2018 and appears to have affected the surface water NH_4^+ concentrations that were measured four days later at the Corpus Christi area sites (Table 30) (NOAA, 2019). According to unpublished data from the Felix Lab (TAMUCC), the NH_4^+ concentration of rainwater collected from that event was 41.17 μM ; the fourth greatest of 69 rainfalls measured for NH_4^+ between August 2016 and January 2019. Of the sites, UL featured the most dramatic increase in surface water NH_4^+ following the rain, reaching 2.74 μM on May 25, up from 0.62 μM a week earlier. This is noteworthy being that the Upper Laguna Madre has no direct river inflow, compared to the other two sites which receive inflows from tides (GM) and/or rivers (CCB). At UL, it's possible that the deposition of the high NH_4^+ concentration rainwater and/or perturbed sediments releasing NH_4^+ enriched porewater into the overlying water column may be responsible for the increase in surface water

NH₄⁺ observed there on May 25. By June 1, eleven days past the rainfall, surface NH₄⁺ concentrations at all sites had returned to their pre-rain event levels, being nearly identical to the concentrations observed on May 18. This result suggests rapid nitrification and/or uptake in the water column at each site, possibly coinciding with the growth of summer phytoplankton communities.

Table 30. Weekly mean surface water NH₄⁺ concentrations of Corpus Christi area sites in μM, May 4 - July 6, 2018. Standard deviations are displayed (in parentheses).

	CCB	UL	GM	<i>Corpus Christi sites mean</i>
Water NH₄⁺ conc.(μM)				
May 4, 2018	0.97 (0.21)	1.41 (0.49)	1.04 (0.30)	<i>1.14 (0.24)</i>
May 11, 2018	0.61 (0.09)	1.54 (0.37)	1.05 (0.54)	<i>1.07 (0.47)</i>
May 18, 2018	0.45 (0.40)	0.62 (0.39)	0.05 (<0.01)	<i>0.37 (0.29)</i>
<i>May 20-21 rain</i>				
May 25, 2018	0.98 (0.02)	2.74 (0.79)	0.86 (0.61)	<i>1.53 (1.05)</i>
June 1, 2018	0.22 (0.07)	0.60 (0.16)	0.08 (0.04)	<i>0.30 (0.27)</i>
June 8, 2018	0.05 (<0.01)	0.05 (<0.01)	0.05 (<0.01)	<i>0.05 (<0.01)</i>
June 15, 2018	1.27 (0.58)	1.04 (0.06)	1.99 (0.51)	<i>1.43 (0.50)</i>
<i>June 18-21 rain</i>				
June 22, 2018	7.80 (1.50)	0.31 (0.37)	5.80 (0.01)	<i>4.64 (3.88)</i>
June 29, 2018	2.96 (0.41)	0.50 (0.64)	5.14 (0.12)	<i>2.87 (2.32)</i>
July 6, 2018	1.37 (0.25)	2.44 (0.29)	10.67 (0.10)	<i>4.83 (5.09)</i>

Dry conditions existed throughout much of June, with surface NH₄⁺ concentrations remaining relatively diminished before sampling on June 15 (Table 30). Without precipitation or other inflows contributing, the increases in water NH₄⁺ concentrations observed on that date may have resulted from NH₄⁺ production in sediments and wind-driven mixing into the water columns. The major rain event of June 18 - 21 resulted in dramatic increases in water NH₄⁺ concentrations at CCB and GM on June 22, while UL displayed a notable decrease to 0.31 μM NH₄⁺. Felix Lab data for rainwater collected at TAMUCC during the rain event displayed a mean NH₄⁺ concentration (7.92 ± 2.81 μM) far lower than the rain collected from the May event.

Notably, the relatively NH_4^+ diminished rainwater and resulting surface runoff did not support a noticeable response in surface water NH_4^+ at UL, such as that observed in May.

The much greater volume and longer duration of precipitation of June's rain event appear to have afforded surface inflows a stronger influence on the resulting water NH_4^+ concentration at CCB than the May event did. GM responded to the rainfall with an elevated water NH_4^+ concentration similar to that of CCB, as well as diminished salinity from the week before (Table 31). These water column responses to the rain event at GM may be due to submarine groundwater discharge (SGD) occurring below the Gulf shoreline. Following the estimated 40+ cm of rain received at the GM site in the four days prior to sampling, standing water was witnessed across North Padre Island on June 22 and for weeks thereafter (NOAA, 2019). Such elevated groundwater levels create a land-side hydraulic gradient and will discharge into nearshore marine waters (Knee and Paytan, 2011). SGD has been identified as a transport mechanism for nutrients, either through the delivery of groundwater from the aquifer or by forcing enriched porewater from sediments into the overlying water column (Fear et al., 2007). As sediment porewater NH_4^+ concentrations up to two orders of magnitude greater than those of overlying water columns have been observed in the Coastal Bend, it is not unreasonable to suspect that GM possessed sediment NH_4^+ concentrations elevated beyond those of its surface water prior to the rainfall in June (Douglas et al., 2017). Such NH_4^+ enriched porewater may have then been forced into the water column by SGD following the rainfall, and/or released from sediments which were disturbed during the rain event.

Table 31. Weekly salinity measurements of Corpus Christi area sites, May 25 - July 6, 2018.

	CCB	UL	GM
Salinity (ppt)			
<i>May 20-21 rain</i>			
May 25, 2018	37.0	49.1	34.2
June 1, 2018	37.9	47.2	36.1
June 8, 2018	37.3	46.3	36.4
June 15, 2018	42.2	48.2	36.5
<i>June 18-21 rain</i>			
June 22, 2018	32.0	33.4	35.0
June 29, 2018	29.6	37.0	36.4
July 6, 2018	36.2	37.3	36.4

By June 29 the surface water NH_4^+ concentration of CCB had dropped substantially, suggesting that the initial pulse of water column NH_4^+ had been assimilated, nitrified or transported away from the site (Table 30). A week later, the water NH_4^+ concentration had decreased again to reach the lowest value recorded at the site in nearly a month. Conversely, in the weeks following the rain event water NH_4^+ concentrations at UL began to increase. Surface water NH_4^+ increased to $0.50 \pm 0.64 \mu\text{M NH}_4^+$ on June 29, and $2.44 \pm 0.29 \mu\text{M NH}_4^+$ on July 6, displaying a dramatically different response to the post-rainfall period than CCB. On July 6, the greatly increased water NH_4^+ concentrations were measured following 36 hours of variable winds over the site, with a northern wind occurring at the time of sampling. Such a break in the predominant south - southeasterly winds of the summer months may have permitted the transport of DOM-enriched water from Corpus Christi Bay to the Upper Laguna Madre at that time.

It appears that SGD may have sustained elevated water column NH_4^+ concentrations at GM in the weeks following the rain, which remained above $5 \mu\text{M NH}_4^+$ on June 29 and then exceeded $10 \mu\text{M NH}_4^+$ on July 6 (Table 30). The NH_4^+ value from July 6 far exceeded the water concentrations at the other sites and supports the argument that a different mechanism was influencing water NH_4^+ at GM at this time. Water-atmosphere NH_3 fluxes were strongly upward

at GM for four consecutive weeks, resulting in positive monthly mean values for both June and July. Comparatively, those same monthly mean NH₃ flux values at UL were negative. This suggests an interesting relationship between the water bodies which flank North Padre Island. On three of the four dates that NH₃ emission was calculated at the Gulf of Mexico site, NH₃ deposition was calculated for the site at the Upper Laguna Madre (Table 32). It appears that following a substantial rain event in the early summer, elevated groundwater levels result in SGD on the Gulf side of the island, which forces NH₄⁺ enriched porewater from the sediment into the water column. There, it increases in concentration until the equilibrium with the overlying air is breached and NH₃ emission begins. The airborne NH₃ is transported across the barrier island by southeastern winds where it increases its atmospheric concentration beyond equilibrium above the relatively NH₄⁺ depleted Upper Laguna Madre and begins to invade the surface water there. Essentially, what has been quantified here are nutrients from the coastal shelf volatilizing from the nearshore Gulf and depositing in nearby, inland waters. If this was not an isolated occurrence, the water-atmosphere flux of NH₃ may be an important link by which coastal marine waters supply nutrients to relatively oligotrophic coastal lagoons. Such NH₃ transport would then serve to support and sustain productivity within lagoon waters at times when nutrients are otherwise limited.

Table 32. Weekly mean water-atmosphere NH₃ fluxes of GM and UL, June 22 - July 13, 2018. Standard deviations are displayed (in parentheses).

	GM	UL
NH₃ flux (ng m ⁻² s ⁻¹)		
<i>June 18-21 rain</i>		
June 22, 2018	33.13 (0.09)	-11.59 (5.25)
June 29, 2018	42.60 (1.38)	-16.45 (26.58)
July 6, 2018	13.73 (0.16)	3.81 (1.61)
July 13, 2018	19.83 (5.12)	-17.00 (4.42)

4.5. Implications for Coastal Bend NH₃ budget

The water-atmosphere NH₃ fluxes reported in this study reflect a direction and a rate of NH₃ transfer that was theoretically occurring at a single location, at a particular point-in-time. It is believed however that water-atmosphere NH₃ exchange is a variable process, responding in real time as surface water and atmospheric conditions change. For this reason, any extrapolation of the calculated NH₃ fluxes is to be done with caution, as it is difficult to believe that homogenous conditions should exist across such vast surface waters and throughout thirty or more days of a month. With that understood, it can still be helpful to utilize the information provided by these NH₃ fluxes to estimate totals of NH₃ deposition and emission over estuary waters.

As water-atmosphere NH₃ fluxes are essentially rates, producing annual totals of emission or deposition resulting from the process is straightforward but requires the assumption that the rate of exchange was consistent. Furthermore, it must be held that the atmospheric and surface water conditions present at the site of observation were homogenous across the entire water body. With those assumptions made and surface water areas known, estimates of total NH₃ being emitted from or deposited to surface waters can be determined. Here, total annual NH₃ import/export from Coastal Bend estuaries will be estimated by utilizing the monthly water-atmosphere NH₃ fluxes from September 2018 - April 2019.

Due to inconsistent surface areas having been reported for many of the Coastal Bend waters in the literature, it was determined that the measurements used here should all be obtained from a single source. Measurements from Bricker et al. (2007) were utilized as surface areas for all the bays and estuary systems of the region were included in that report. Notably, our totals must be reported by estuary system for Lavaca-Colorado and Mission-Aransas as Bricker et al.

(2007) defined Matagorda Bay as including secondary Lavaca Bay, and Aransas Bay as including Copano Bay in their surface area measurements. Being that the sites of this study included both primary and secondary bays within those estuaries, the two monthly NH₃ flux values from the sites of each system were simply averaged to produce a single monthly value.

Based on the water-atmosphere NH₃ fluxes of this study, it can be estimated that the Coastal Bend estuaries emitted a total of 584 metric tons (mT) NH₃ and received 335 mT NH₃ by deposition between September 2018 and April 2019. Those values produce a net emission of 249 mT NH₃ from the estuaries of the Coastal Bend over the eight-month study (Table 33). With the sites arranged by estuary system and by excluding GM, exactly half of the monthly reported totals were positive and half negative. While this appears to display equity in the water-atmosphere flux process, the comparatively higher magnitude of the NH₃ emissions resulted in an overall greater amount of NH₃ being emitted to the atmosphere.

Table 33. Monthly calculated NH₃ flux totals in mT for Coastal Bend bays and estuaries, September 2018 - April 2019.

(mT) NH ₃	Sept 2018	Oct 2018	Nov 2018	Dec 2018	Jan 2019	Feb 2019	Mar 2019	Apr 2019	8 mo. net NH ₃
Lavaca-Colorado San Antonio Bay	32.8	6.43	-20.5	-6.19	-5.86	-4.72	-20.3	77.3	58.9
Mission-Aransas Corpus Christi Bay	21.8	51.9	-2.46	15.9	-0.56	-1.18	9.32	13.5	108
Upper Laguna M. Baffin Bay	17.5	-10.0	-9.98	-3.06	-6.27	-10.5	-10.9	14.5	-18.8
Lower Laguna M.	37.9	29.7	17.8	-15.1	2.25	-5.39	-15.1	3.34	55.4
All waters net NH₃	7.59	43.2	1.76	-15.5	5.24	-6.11	-4.77	0.13	31.5
	33.5	3.29	15.3	-5.53	-9.44	0.50	5.93	-8.19	35.4
	82.9	-35.9	2.46	-7.50	-51.8	-16.1	-25.7	30.3	-21.4
All waters net NH₃	234	88.6	4.34	-37.0	-66.4	-43.5	-61.5	131	249

Table 34. Monthly calculated NH₃ flux totals in mT for Corpus Christi Bay and the Upper Laguna Madre, May 2018 - April 2019.

	May 2018	June 2018	July 2018	August 2018	September 2018	October 2018
C.C. Bay	-18.4	-36.8	4.87	60.3	37.9	29.7
Up. Laguna	18.2	-21.8	-18.3	46.0	7.59	43.2
<i>All total</i>	<i>-0.19</i>	<i>-58.5</i>	<i>-13.4</i>	<i>106</i>	<i>45.5</i>	<i>72.9</i>
November 2018	December 2018	January 2019	February 2019	March 2019	April 2019	12 mo. net NH ₃
17.8	-15.1	2.25	-5.39	-15.1	3.34	65.4
1.76	-15.5	5.24	-6.11	-4.77	0.13	55.6
19.6	-30.6	7.50	-11.5	-19.9	3.47	121

Twelve months of observation at CCB and UL provided the NH₃ flux data needed to produce annual water-atmosphere NH₃ budgets for the water bodies represented by those sites. Corpus Christi Bay produced a net emission of 65.4 mT NH₃ from its surface over the year, resulting from the balance of 156 mT NH₃ emitted and 90.8 mT NH₃ deposited (Table 34). Likewise, the Upper Laguna Madre featured net NH₃ emission over twelve months (55.6 mT), with a total of 122 mT NH₃ emitted and 66.4 mT NH₃ deposited. To consider the region without contributions from the Gulf of Mexico here, an estimated total of 121 mT NH₃ was emitted from surface waters to the lower atmosphere of the Corpus Christi metropolitan area over one year's time.

The magnitudes of those annual totals of atmospheric NH₃ loading are considerable when compared against previous estimates of N deposition for the area. Meyers et al. (2000) estimated that Corpus Christi Bay receives 210 mT and the Upper Laguna Madre 340 mT of inorganic N deposited to their water surfaces from the atmosphere, annually (Table 35). By their quantification, inorganic N included both the wet and dry deposition of NH₄⁺ and NO₃⁻, and the dry deposition of NH₃. Notably, their NH₃ dry deposition estimates were derived from model predictions which did not factor NH₃ emission (Meyers et al., 2000). When our totals of annual

NH₃ emission for Corpus Christi Bay and the Upper Laguna Madre are factored into the estimates of Meyers et al. (2000), the atmospheric inorganic N totals are reduced by 31.1% and 16.4%, respectively. It is evident here that NH₃ emissions from the water-atmosphere exchange process can total a significant portion of the inorganic N loads received by coastal waters. Furthermore, the quantification of water-atmosphere NH₃ fluxes and the factoring of the process in atmospheric models can effectively refine and improve N deposition estimates.

Table 35. Comparison of annual atmospheric inorganic N loads estimated by Meyers et al. (2000), with values adjusted by this study's annual NH₃ emission estimates for Corpus Christi Bay and the Upper Laguna Madre.

Water body	Annual inorganic N to surface water (mT N)	Annual NH ₃ from surface water (mT N)	Adjusted inorganic N to surface water (mT N)	Meyers et al. (2000) to adjusted (% change)
Corpus Christi Bay	210	65.4	145	-31.1
Upper Laguna Madre	340	55.6	284	-16.4

5. Conclusions

In this study, site-specific measurements were applied to a mathematical model to calculate the water-atmosphere NH₃ fluxes of ten water bodies across the Texas Coastal Bend. Between September 2018 and April 2019, a grand mean water-atmosphere NH₃ flux of $2.52 \pm 3.57 \text{ ng m}^{-2} \text{ s}^{-1}$ was determined, denoting net NH₃ emission across the entire region during that period. From May 2018 to April 2019, sites at Corpus Christi Bay, the Upper Laguna Madre and the Gulf of Mexico produced a mean water-atmosphere NH₃ flux of $2.54 \pm 1.23 \text{ ng m}^{-2} \text{ s}^{-1}$ which denotes net annual NH₃ emission from the surface waters local to Corpus Christi. Seasonal variation in water-atmosphere flux was evident, with regionwide results displaying net NH₃ deposition in winter and NH₃ emission in the fall. Monthly mean NH₃ flux values reflected that seasonality as the monthly minimum was found in December ($-4.03 \pm 6.37 \text{ ng m}^{-2} \text{ s}^{-1}$) and the

maximum in September ($18.39 \pm 15.79 \text{ ng m}^{-2} \text{ s}^{-1}$). Seasonal trends in the water-atmosphere NH_3 fluxes of the sites local to Corpus Christi were likewise evident, however the longer duration of observation yielded additional insights. The late spring to mid-summer months (May, June, July) featured consistently depositional NH_3 fluxes, with the yearlong monthly minimum being produced in June ($-11.57 \pm 14.77 \text{ ng m}^{-2} \text{ s}^{-1}$). Conversely, the late summer to mid-fall period (August, September, October) featured high rates of NH_3 emission, with the monthly maximum NH_3 flux value being reached in August ($24.85 \pm 17.08 \text{ ng m}^{-2} \text{ s}^{-1}$). Spatially, the site mean NH_3 fluxes of SAB ($8.68 \pm 11.41 \text{ ng m}^{-2} \text{ s}^{-1}$) and BB ($7.18 \pm 22.99 \text{ ng m}^{-2} \text{ s}^{-1}$) represent the highest values found regionwide, while the NH_3 flux values of CB ($-2.61 \pm 7.84 \text{ ng m}^{-2} \text{ s}^{-1}$) and AB ($-0.80 \pm 10.68 \text{ ng m}^{-2} \text{ s}^{-1}$) were the lowest. The three sites of the Corpus Christi area featured positive mean NH_3 fluxes of a similar magnitude, with no significant differences between those values as determined by one-way ANOVA ($F(2,33) = 0.134, p = 0.875$).

The total observation period (May 2018 - April 2019) featured regular and at times, severe rain events. Many of the surface waters displayed elevated NH_4^+ concentrations in the days and weeks following substantial rainfall. This response improved the conditions necessary for water-atmosphere NH_3 emission to occur and appears to have driven, amplified and/or prolonged such NH_3 emission events. Various mechanisms were suspected of contributing to increased surface water NH_4^+ concentrations and thus, the likelihood of NH_3 water-atmosphere emission. Among those considered were increased surface water inflows and riverine DOM and NH_4^+ delivery, the wet deposition of NH_4^+ , wind-driven transport of DOM and NH_4^+ -enriched surface waters between water bodies, and the movement of NH_4^+ -enriched benthic porewater into the water column by sediment disturbance and SGD. The site at San Antonio Bay displayed NH_3 flux characteristics unique of nearby bays, with a distinctly high mean surface water NH_4^+

concentration and greater occurrences and magnitudes of NH_3 emissions. In the Corpus Christi area, a water-atmosphere relationship was found between the sites of North Padre Island (UL and GM). Periods of elevated NH_4^+ concentrations in the nearshore Gulf of Mexico caused high-magnitude NH_3 emission events at times when low surface water NH_4^+ and a depositional NH_3 flux were occurring across the barrier island at the Upper Laguna Madre. It is believed that NH_3 emitted from the Gulf of Mexico may be transported across the barrier island by south-southeastern winds and deposited in the Laguna Madre. This could be an important mechanism for supporting biological production in the relatively oligotrophic lagoon.

It is evident that both Corpus Christi Bay and the Upper Laguna Madre were predominantly sources of NH_3 in the late summer and early fall and sinks of atmospheric NH_3 in the mid-summer and winter months. While it is believed that such seasonality could vary with weather patterns and greater shifts in climate, it is important to note that the Corpus Christi metropolitan area is likely receiving substantial amounts of NH_3 supplied to its lower atmosphere at least periodically from surrounding water bodies. Atmospheric NH_3 is a precursor for $\text{PM}_{2.5}$, and although NH_3 is not controlled in the U.S. at this time, may receive regulatory attention in the future. $\text{PM}_{2.5}$ is considered a criteria air pollutant by the U.S. Environmental Protection Agency (EPA) and so is controlled by National Ambient Air Quality Standards (NAAQS) and monitored by the Texas Commission on Environmental Quality (TCEQ) in the state of Texas. As the population of Corpus Christi has been projected to increase, additional urban inputs of DOM and NH_4^+ to area waters will inevitably result. As we have discussed extensively, such enrichments will likely drive NH_3 emission events from local surface waters, possibly increasing those in magnitude and/or duration. If increased levels of atmospheric NH_3 ever become problematic in the urban airshed of Corpus Christi, a thorough understanding and consideration

of the water-atmosphere NH_3 exchange process would be critical for the development of effective mitigation strategies.

REFERENCES

- Asman, W. A. H., Harrison, R. M., and Ottley, C. J. (1994). Estimation of the net air-sea flux of ammonia over the southern bight of the North Sea. *Atmospheric Environment*, 28(22), doi:10.1016/1352-2310(94)00192-n.
- Bange, H. (2008). Gaseous Nitrogen Compounds (NO, N₂O, N₂, NH₃) in the Ocean. *Nitrogen in the Marine Environment*. 51-94. doi:10.1016/B978-0-12-372522-6.00002-5.
- Behera, S. N., Sharma, M., Aneja, V. P., and Balasubramanian, R. (2013). Ammonia in the atmosphere: a review on emission sources, atmospheric chemistry and deposition on terrestrial bodies, *Environ. Sci. Pollut. R. Int.*, 20, 8092–8131, doi:10.1007/s11356-013-2051-9.
- Bell, T.G., Johnson, M.T., Jickells, T.D., Liss, P.S. (2007) Ammonia/ammonium dissociation coefficient in seawater: A significant numerical correction. *Environmental Chemistry* 4, 183-186, doi:10.1071/EN07032
- Berner, A.H., Felix, J.D. (2020). Investigating ammonia emissions in a coastal urban airshed using stable isotope techniques. *Sci. of The Total Env.*, 707, 134952, doi:10.1016/j.scitotenv.2019.134952
- Bricker, S., B. Longstaff, W. Dennison, A. Jones, K. Boicourt, C. Wicks, and Woerner, J. (2007). *Effects of Nutrient Enrichment in the Nation's Estuaries: A Decade of Change*. NOAA Coastal Ocean Program Decision Analysis, Series No. 26. National Centers for Coastal Ocean Science, Silver Spring, MD. 328 pp.
- Brock, D. A. (2001). Nitrogen budget for low and high freshwater inflows, Nueces Estuary, Texas. *Estuaries*, 24:509–521.
- Castro, M.S., Driscoll, C.T., Jordan, T.E. et al. (2003). Sources of nitrogen to estuaries in the United States. *Estuaries*, 26, 803-814, doi:10.1007/BF02711991.
- Davidson, E.A., et al. (2012). Excess nitrogen in the US environment: trends risks and solutions. *ESA Issues in Ecology*, 15pp.
- Dorado, S., Booe, T., Steichen, J., McInnes, A.S., Windham, R., Shepard, A., Lucchese, A.E.B., Preischel, H., Pinckney, J.L., Davis, S.E., Roelke, D.L., and Quigg, A. (2015). Towards an understanding of the interactions between freshwater inflows and phytoplankton communities in a subtropical estuary in the Gulf of Mexico. *PLOS ONE*, 10(7), e0130931, doi:10.1371/journal.pone.0130931.
- Douglas, A., Murgulet, D., Wetz, M.S., Spalt, N. (2017) *Evaluating Groundwater Inflow and Nutrient Transport to Texas Coastal Embayments Phase II*. Texas General Land Office, Texas General Land Office.
- Farmer, J.C. and Dawson, G.A. (1982). Condensation Sampling of Soluble Atmospheric Trace Gases. *Journal of Geophysical Research*, 87(11), 8931-8942.

- Fear, J. M., Paerl, H.W., Braddy, J.S. (2007). Importance of Submarine Groundwater Discharge as a Source of Nutrients for the Neuse River Estuary. North Carolina. *Estuaries and Coasts*, 30(6), 1027-1033.
- Felix, J.D., Campbell, J. (2019). Investigating Reactive Nitrogen Sources that Stimulate Algal Blooms in Baffin Bay. Report submitted to the Coastal Bend Bays & Estuaries Program for project 1818, Publication CBBEP-129; Texas A&M University – Corpus Christi, Corpus Christi, TX, 30 pp.
- Gibb, S. W., Mantoura, R. F. C., and Liss, P. S. (1999). Ocean-atmosphere exchange and atmospheric speciation of ammonia and methylamines in the region of the NW Arabian Sea. *Global Biogeochemical Cycles*, 13(1), doi:10.1029/98gb00743
- Gong, L., Lewicki, R., Griffin, R.J., Flynn, J.H., Lefer, B.L., and Tittel, F.K. (2011). Atmospheric ammonia measurements in Houston, TX using an external-cavity quantum cascade laser-based sensor. *Atmos. Chem. Phys.*, 11, 9721–9733.
- Gruber, N. (2008). The Marine Nitrogen Cycle. *Nitrogen in the Marine Environment*, 1-50, doi:10.1016/b978-0-12-372522-6.00001-3
- Hardebeck, S., Vogel Boze, B., Basilotto, J.P., McGuire, J.M. and Rhi-Perez, P. (1997). Economic Impact of Barge Transportation on the Texas Portion of the Gulf Intracoastal Waterway (GIWW) and Extension of the GIWW into Mexico. College Station, Texas Transportation Institute at The Texas A&M University System Project No. 7-2993, April 1997. Revised March 1999.
- Heald, C. L., Collett Jr., J. L., Lee, T., Benedict, K. B., Schwandner, F. M., et al. (2012). Atmospheric ammonia and particulate inorganic nitrogen over the United States. *Atmospheric Chemistry and Physics, European Geosciences Union*, 12 (21), pp.10295-10312, doi:10.5194/acp-12-10295-2012.hal-00722962
- Hedgpeth, J. W. (1947). The Laguna Madre of Texas. *North American Wildlife Conference* 12, 364-380.
- Holm, S. (1979). A simple sequentially rejective multiple test procedure. *Scandinavian Journal of Statistics*, 6, 65–70.
- Holmes, R.M., Aminot, A., Kerouel, R., Hooker, B.A. and Peterson, B.J. (1999). A simple and precise method for measuring ammonium in marine and freshwater ecosystems. *Canadian Journal of Fisheries and Aquatic Sciences*, 56(10), 1801-1808.
- Hothorn T., Bretz F., Westfall P. (2008). Simultaneous Inference in General Parametric Models. *Biometrical Journal*, 50(3), 346–363.
- Howarth, R.W. (2008). Coastal nitrogen pollution: A review of sources and trends globally and regionally. *Harmful Algae*, 8, 14-20, doi:10.1016/j.hal.2008.08.015.

Islam, M. S., Bonner, J., Page, C., Ojo, T. (2011). An integrated real time monitoring system to investigate the hypoxia in a shallow wind-driven bay. *Journal of Environmental Monitoring and Assessment*, 172(1), 33–50.

Johnson, M. T., Liss, P. S., Bell, T. G., Lesworth, T. J., Baker, A. R., Hind, A. J., and Gibb, S. W. (2008). Field observations of the ocean-atmosphere exchange of ammonia: Fundamental importance of temperature as revealed by a comparison of high and low latitudes. *Global Biogeochemical Cycles*, 22(1), doi:10.1029/2007gb003039

Knee, K.L. and Paytan, A. (2011). Submarine groundwater discharge: A source of nutrients, metals, and pollutants to the coastal ocean, p. 205–233. In Wolanski, E. and McLusky, D.S. [eds.], *Treatise on estuarine and coastal science*. Academic.

Kruskal, W.H., Wallis, W.A. (1952). Use of ranks in one-criterion variance analysis. *J. Am. Stat. Assoc.* 47, 583–621 and errata, *ibid.* 48, 907–911.

Larkin, T.J. and Bomar, G.W. (1983). *Climatic Atlas of Texas*. Austin, TX: Texas Department of Water Resources. Austin, TX: Texas Water Development Board, 141 pp.

Larsen R.K., Steinbacher J.C., Baker, J.E. (2001). Ammonia exchange between the atmosphere and the surface waters at two locations in the Chesapeake Bay. *Environmental Science and Technology*, 35(24), 4731–4738.

Lebreton, B., Beseres Pollack, J., Blomberg, B., Palmer, T.A., Adams, L., Guillou, G., Montagna, P.A. (2016). Origin, composition and quality of suspended particulate organic matter in relation to freshwater inflow in a South Texas estuary. *Estuarine, Coastal and Shelf Sci.*, 170, 70–82.

Lee, D. S., Halliwell, C., Garland, J. A., Dollard, G. J., and Kingdon, R. D. (1998). Exchange of ammonia at the sea surface - a preliminary study. *Atmospheric Environment*, 32(3), doi:10.1016/s1352-2310(97)00277-x.

Li, Y., Schichtel, B.A., Walker, J.T., Schwede, D.B., Chen, X., Lehmann, C.M.B., Puchalski, M.A., Gay, D.A., Collett, J.L. (2016). Increasing importance of deposition of reduced nitrogen in the United States. *Proceedings of the National Academy of Sciences*, 113(21), 5874-5879, doi: 10.1073/pnas.1525736113.

Longley, W.L. (1994). *Freshwater inflows to Texas bays and estuaries: ecological relationships and methods for determination of needs*. Austin, TX: Texas Water Development Board and Texas Parks and Wildlife Department, 386 pp.

MacIntyre, H. L., & Cullen, J. J. (1996). Primary production by suspended and benthic microalgae in a turbid estuary: Timescales of variability in San Antonio Bay, Texas. *Marine Ecology Progress Series*, 145, 245–268.

McKee, C. M. (2001). *Biogeochemical Cycles of Ammonia and Dimehtylsulphide in the Marine Environment*, PhD thesis, University of East Anglia, 2001.

- Mesfioui, R., Abdulla, H. A., Hatcher, P. G. (2015). Photochemical Alterations of Natural and Anthropogenic Dissolved Organic Nitrogen in the York River. *Environmental science & technology*, 49(1), 159–167.
- Meyers, T., Sickles, J., Dennis, R., Russell, K., Galloway, J., Church, T. (2000). Atmospheric nitrogen deposition to coastal estuaries and their watersheds, p. 53–76. In R. M. Valigura, R.B. Alexander, M. S. Castro, H. Greening, T. Meyers, H. Paerl, and R. E. Turner (eds.), *An Assessment of Nitrogen Loads to U.S. Estuaries with an Atmospheric Perspective*. Coastal and Estuarine Studies, American Geophysical Union, Washington, D.C.
- Montagna, P.A., Hu, X., Palmer, T.A., and Wetz, M. (2018). Effect of hydrological variability on the biogeochemistry of estuaries across a regional climatic gradient. *Limnology and Oceanography* 63(6), 2465-2478.
- Mooney, R.F. & McClelland, J.W. (2012). Watershed Export Events and Ecosystem Responses in the Mission–Aransas National Estuarine Research Reserve, South Texas. *Estuaries and Coasts*, 35, 1468-1485.
- NOAA National Weather Service Advanced Hydrologic Prediction Service maps. (2019, March 1). Retrieved from <https://water.weather.gov/precip/>
- Norman, M., and Leck, C. (2005). Distribution of marine boundary layer ammonia over the Atlantic and Indian Oceans during the Aerosols99 cruise. *J. Geophys. Res.*, 110, D16302, doi:10.1029/2005JD005866.
- Paulot, F., Jacob, D. J., Johnson, M. T., Bell, T. G., Baker, A. R., Keene, W. C., and Stock, C. A. (2015). Global oceanic emission of ammonia: Constraints from seawater and atmospheric observations. *Global Biogeochemical Cycles*, 29(8), doi:10.1002/2015gb005106.
- Pennock, J.R., Boyer, J.N., Herrera-Silveira, J.A., Iverson, R.L., Whittedge, T.E., Mortazavi, B., Comin, F.A. (1999). Nutrient behavior and phytoplankton production in Gulf of Mexico estuaries. In: Bianchi, T.S., Pennock, J.R., Twilley, R.R. (Eds.), *Biogeochemistry of Gulf of Mexico Estuaries*. John Wiley & Sons, New York, pp. 109-162.
- Pinheiro J, Bates D, DebRoy S, Sarkar D, R Core Team (2020). nlme: Linear and Nonlinear Mixed Effects Models. R package version 3.1-137, <https://CRAN.R-project.org/package=nlme>.
- Pope, A.C., Dockery, D.W. (2006). 2006 critical review on health effects of fine particulate air pollution: lines that connect. *J. Air Waste Manag. Assoc.* 56, 709e742.
- Quinn, P.K., Barrett, K.J., Dentener, F.J., Lipschultz, F., Six, K.D. (1996). Estimation of the air/sea exchange of ammonia for the North Atlantic basin. *Biogeochemistry*, 35, 275-304.

Quinn, P. K., Bates, T.S., Johnson, J. E., Covert, D. S. and Charlson, R.J. (1990). Interactions between the sulfur and reduced nitrogen cycles over the central Pacific Ocean. *J. Geophys. Res.*, 95, 16,405-16,416.

Quinn, P.K., Charlson, and R.J., Bates, T.S. (1988). Simultaneous observations of ammonia in the atmosphere and ocean. *Nature*, 335, doi: 10.1038/335336a0.

R Core Team (2018). R: A language and environment for statistical computing. R Foundation for Statistical Computing, Vienna, Austria. <https://www.R-project.org/>.

Solis, R.J. and Powell, G.L. (1999). Hydrography, mixing characteristics and residence times of Gulf of Mexico estuaries. p. 29-61. In Bianchi, T.S., Pennock, J.R., Twilley, R.R., (eds.), *Biogeochemistry of Gulf of Mexico Estuaries*. New York, NY: John Wiley and Sons.

Sorensen, L. L., Hertel, O., Skjoth, C. A., Lund, M., and Pedersen, B. (2003). Fluxes of ammonia in the coastal marine boundary layer. *Atmospheric Environment*, 37, doi:10.1016/s1352-2310(03)00247-4.

Tang, M. J., Shiraiwa, M., Pöschl, U., Cox, R. A., and Kalberer, M. (2015) Compilation and evaluation of gas phase diffusion coefficients of reactive trace gases in the atmosphere: Volume 2. Diffusivities of organic compounds, pressure-normalised mean free paths, and average Knudsen numbers for gas uptake calculations. *Atmospheric Chemistry and Physics*, 15, 5585-5598, doi:10.5194/acp-15-5585-2015.

TCEQ Wastewater Outfalls Viewer (2019, September 4). Retrieved from <https://www.tceq.texas.gov/gis/wastewater-outfalls-viewer>

Tucker, W.A. and Nelken, L.H. (1982). Diffusion coefficients in air and water. *Handbook of Chemical Property Estimation Methods: Environmental Behavior of Organic Compounds*, McGraw-Hill, New York, NY.

Tukey, J. (1949). Comparing Individual Means in the Analysis of Variance. *Biometrics*. 5 (2): 99–114. JSTOR 3001913.

Tunnell, J.W. and Jud, F. W. (2002). *The Laguna Madre of Texas and Tamaulipas*. Corpus-Christi, TX: Texas A&M University Press. 372pp.

Turner, E. L., Paudel, B., Montagna, P. A. (2015). Baseline nutrient dynamics in shallow well mixed coastal lagoon with seasonal harmful algal blooms and hypoxia formation. *Marine Pollution Bulletin*, 96(1-2), 456-462.

United States Census Bureau (2019). Quick Facts, Corpus Christi city, Texas. <https://www.census.gov/quickfacts/corpuschristicitytexas>

Wentworth, G.R., Murphy, J.G., Croft, B., Martin, R.V., Pierce, J.R., Côté, JS., Courchesne, I., Tremblay, J.É., Gagnon, J., Thomas, J.L., Sharma, S., Toom-Sauntry, D., Chivulescu, A., Levasseur, M., and Abbatt, J. P. D. (2016). Ammonia in the summertime Arctic marine boundary layer: sources, sinks, and implications. *Atmos. Chem. Phys.*, 16, 1937–1953, doi:10.5194/acp-16-1937-2016, 2016.

- Wetz, M. S., Cira, E.K., Sterba-Boatwright, B., Montagna, P.A., Palmer, T.A., Hayes, K.C. (2017). Exceptionally high organic nitrogen concentrations in a semi-arid South Texas estuary susceptible to brown tide blooms. *Estuarine, Coastal and Shelf Sci.*,188:27–37.
- Wetz M.S., Hayes K.C., Fisher K.V.B., Price L., Sterba-Boatwright B. (2016). Water quality dynamics in an urbanizing subtropical estuary (Oso Bay, Texas). *Marine Pollution Bulletin*, 104: 44–53.
- Whitledge, T. E. (1989). Data synthesis and analysis - Nitrogen process studies (NIPS): Nutrient distributions and dynamics in Lavaca, San Antonio, and Nueces/Corpus Christi Bays in relation to freshwater inflow. Tech. Rep. 89-007, Mar. Sci. Inst. Univ. of Tex., Austin.
- Wood, S.N. (2011). Fast stable restricted maximum likelihood and marginal likelihood estimation of semiparametric generalized linear models. *Journal of the Royal Statistical Society (B)*, 73(1), 3-36.
- Wu, K., Lu, K., Dai, M., Liu, Z. (2019). The bioavailability of riverine dissolved organic matter in coastal marine waters of southern Texas. *Estuarine, Coastal and Shelf Sci.*, 231, 106477.
- Zeng, Y., Tian, S., Pan, Y. (2018). Revealing the Sources of Atmospheric Ammonia: A Review. *Curr. Pollut. Rep.*, 4, 189–197.
- Zhang, L., Jacob, D. J., Knipping, E. M., Kumar, N., Munger, J. W., Carouge, C. C., van Donkelaar, A., Wang, Y. X., and Chen, D. (2012). Nitrogen deposition to the United States: distribution, sources, and processes. *Atmos. Chem. Phys.*, 12, 4539–4554, doi:10.5194/acp-12-4539-2012, 2012
- Zhao, Y., Zhang, L., Pan, Y., Wang, Y., Paulot, F., and Henze, D. K. (2015). Atmospheric nitrogen deposition to the northwestern Pacific: seasonal variation and source attribution. *Atmos. Chem. Phys.*,15, 10905–10924, doi:10.5194/acp-15-10905-2015

LIST OF APPENDICES

APPENDIX	PAGE
Appendix A	99
Appendix B	100
Appendix C	101

Appendix A



Figure 13. Photo of condensate collecting device with ice-filled test tubes and collection vials visible inside modified 5-gallon bucket.

Appendix B

Table 36. Previously reported watershed characteristics data of the Coastal Bend estuary systems.

Estuary system	Watershed land area (km²)	Watershed population	Watershed pop. density (residents per km²)	Watershed land use: (%) urban – agriculture – range – undeveloped			
Lavaca - Colorado	121,762	1,432,800	11.8	4.0	29.8	48.3	17.9
Guadalupe	27,097	1,590,933	58.7	7.2	36.7	10.8	45.3
Mission - Aransas	6,420	76,928	12.0	4.1	34.2	28.4	33.3
Corpus Christi Bay	44,525	424,884	9.5	1.9	17.5	64.3	16.3
Upper Laguna Madre & Baffin Bay	10,582	77,970	7.4	2.1	28.9	64.4	4.6
Lower Laguna Madre	13,165	616,541	46.8	6.1	35.8	51.7	6.4

Data from Bricker et al. (2007)

Appendix C

Table 37. Previously reported meteorological and hydrological measurements of the Coastal Bend estuary systems.

Estuary system	Annual rainfall* (cm/yr)	Annual evapor.* (cm/yr)	Net freshwater inflow* (10 ⁶ m ³ yr)	Annual inflow to estuary volume ratio	Estuary water residence time (yr) ^{†‡}	Estuary water (%) fresh - mixed – marine ^{††}		
Lavaca - Colorado	112	123	3,999	2.54	0.22	0.2	82.3	17.5
Guadalupe	101	128	2,799	8.09	0.10	5.1	78.5	16.4
Mission - Aransas	88	139	345	0.67	0.99 [‡]	0.0	71.0	29.0
Corpus Christi Bay	74	150	323	0.21	0.98 [‡]	0.0	8.2	91.8
Upper Laguna Madre & Baffin Bay	74	150	63	0.19	>1.0	0.0	0.0	100
Lower Laguna Madre	66	158	-452	-0.45	–	0.0	2.1	97.9

* Texas Water Development Board (2018)

† Longley (1994)

‡ Solis and Powell (1999)

†† Bricker et al. (2007)

Table 38. Previously reported surface water and watershed measurements of the Coastal Bend estuary systems.

Estuary system	Estuary area (km ²)	Water volume (10 ⁹ m ³)	Mean depth (m)	Watershed land area (km ²)	Watershed to estuary area ratio
Lavaca - Colorado	1,115	1,572	1.41	121,762	109.2
Guadalupe	587	0,346	0.59	27,097	46.2
Mission - Aransas	524	0,514	0.98	6,420	12.3
Corpus Christi Bay	571	1,536	2.69	44,525	78.0
Upper Laguna Madre & Baffin Bay	830	0,337	0.41	10,582	12.7
Lower Laguna Madre	1,308	0,994	0.76	13,165	10.1

Data from Bricker et al. (2007)